


國立交通大學

環境工程研究所

博士論文

光電廢棄物資源化製備奈米吸附材料及
其應用於二氧化碳捕獲之研究



Optoelectronic industrial waste derived porous
adsorbents and their application for the capture of CO₂
greenhouse gas

研究生：林亮毅

指導教授：白曠綾

中華民國一百零一年六月

光電廢棄物資源化製備奈米吸附材料及
其應用於二氧化碳捕獲之研究

Optoelectronic industrial waste derived porous adsorbents and
their application for the capture of CO₂ greenhouse gas

研究生：林亮毅

Student : Liangyi Lin

指導教授：白曠綾

Advisor : Hsunling Bai



Submitted to Institute of Environmental Engineering
College of Engineering

National Chiao Tung University

in partial Fulfillment of the Requirements
for the Degree of Doctor of Philosophy
in Environmental Engineering

June 2012

Hsinchu, Taiwan, Republic of China

中華民國一百零一年六月

光電廢棄物資源化製備奈米吸附材料及 其應用於二氧化碳捕獲之研究

研究生：林亮毅 指導教授：白曠綾

國立交通大學環境工程研究所

摘要

隨著京都議定書正式生效，同時二氧化碳捕獲及封存技術 (Carbon dioxide Capture and Storage, 簡稱 CCS) 也於 2005 年被聯合國之 IPCC 組織評估為可行方式之一。其中利用固體吸附劑捕獲二氧化碳被視為是現行許多捕獲技術中最具有潛力之一；在眾多吸附劑中，中孔洞二氧化矽因其有高比表面積、可調整之孔徑大小與高抗熱性，目前逐漸被應用至二氧化碳控制。雖然中孔洞二氧化矽藉助於奈米科技的創新與技術上之改良，使其材料製程與發展得以快速進化發展，不過該類型材料價格昂貴且其製造過程亦較費時費能，產物取得較沸石與活性碳困難，目前應用中孔洞二氧化矽於二氧化碳控制之研究不若傳統沸石與活性碳廣泛。此外為解決全球溫室效應問題所需削減之二氧化碳氣體排放量相當龐大，因此若採用 CCS 技術將必須消耗大量之地球資源。另一方面，近年來隨著半導體與光電產業的快速發展，大量含矽之廢棄粉末亦伴隨而生。此類型之廢棄物質輕且體積龐大，需額外花費較多之成本委託廠商進行後續廢棄物處理。相對的，如能有效利用廢棄物，將之加以資源化製成多孔材料，則不僅具有成本效益，且可解決廢棄物處理與處置問題。

本研究旨在利用光電粉末廢棄物做為二氧化矽之前驅物，分別透過液相水熱法以及氣相製程製備中孔洞二氧化矽，並將其應用做為吸附劑進行二氧化碳氣體捕獲之研究。研究中亦探討中孔洞吸附劑孔洞特性對於二氧化碳吸附效能之影響以及利用廢棄粉末製備吸附劑之經濟效益，以評估取代商業吸附劑之可行性。研究結果指出以廢棄粉末做為矽源，透過離子型界面活性劑十六烷基三甲基溴化銨(CTAB)作為模板並加入適量之氫氟酸與氫氧化銨可於常溫下製備出具有高比表面積($788 \text{ m}^2\text{g}^{-1}$)、大孔徑(4.5 nm)以及大孔洞體積($1.1 \text{ cm}^3\text{g}^{-1}$)之中孔材料 MCM-41(DU)-F。為了進一步縮減吸附劑製備所需之成本，本研究亦嘗試利用非離子型之三嵌式界面活性劑 F127 做為模板；相對於陽離子型界面活性劑(CTAB)

不僅在價格上較便宜外，在環境汙染程度上也相對較低。而研究成果顯示，界面活性劑 F127 濃度於再生製備中孔洞材料 MS 上有顯著的影響。當 F127/Si 莫耳比例為 0.001 時，MS 材料為具有籠狀(cage-like)之中孔材料；而當 F127/Si 莫耳比例提升於 0.0023 時，MS 材料則是轉變為具有囊泡狀(cellular foam)之材料，而其孔徑與孔體積亦大幅提升。

另一方面，本研究亦開發出利用常溫鹼萃取法可將廢棄粉末分離為矽酸鹽水溶液與沉澱物；沉澱物之成分經鑑定後主要為高純度之氟化鈉(>90%)。由於氟化鈉是工業上常用之化學品，因此所回收之高純度氟化鈉可提供二次再利用的機會；而經分離所得之矽酸鹽水溶液則可作為合成二氧化矽材料之前驅物。透過此萃取法能夠將廢棄粉末轉變為兩種具有高度經濟價值的物質。而利用矽酸鹽經由水熱法所製造之中孔材料 MCM-41(AF)其物化特性與利用純化學品所製備出 MCM-41(NaSi)之特性相似，顯示由 TFT-LCD 粉末廢棄物所製得之矽酸鹽的確為一具有潛力的二氧化矽來源。本研究亦延伸以粉末廢棄物所製得之矽酸鹽之製備與應用範疇，以無機鹽類做為模板透過連續式氣相製程製備出 MSP(AS)以及 MSS(HNO₃)中孔材料。在價錢成本估算部分中，使用廢棄物粉末合成之中孔材料 MSS(HNO₃)可相較於使用化學品合成 SBA-15 節省約 95 % 的價錢，更為使用化學品合成 MCM-41 僅 2% 的價錢。因此利用廢棄矽酸鹽為前驅物以一步氣膠合成方式預期將可大幅減少化學材料成本以及製造時間，如此本研究所製得之奈米材料即可大量製造，並應用於捕獲 CO₂ 溫室氣體上。

在二氧化碳吸附捕獲測試結果顯示，中孔洞材料其孔徑大小以及孔體積對於二氧化碳捕獲效能有顯著的影響。經迴歸分析，可知孔洞體積為最影響吸附效能之關鍵因子，其次為孔洞大小，比表面積之影響則相對較小。其中中孔材料 MSS(HNO₃)在二氧化碳入流濃度 10%、吸附溫度 60°C 時吸附量可達到 122 mg-CO₂/g-adsorbent，高於利用純化學品所合成之中孔洞材料 MCM-41 與 SBA-15。因此結果顯示利用廢棄物所合成之樣品 MSS(HNO₃)具有價格便宜、高二氧化碳吸附量以及快速之製備時間。本研究所製得之奈米材料因此可大量製造，並應用於捕獲 CO₂ 溫室氣體上。綜合成本考量和後端二氧化碳應用，使用此材料在未來二氧化碳捕捉的應用上具有前瞻性。

關鍵字：廢棄物資源化、光電廢棄粉末、中孔洞矽材料、氟化鈉、二氧化碳、氣膠輔助製程

Optoelectronic industrial waste derived porous adsorbents and their application for the capture of CO₂ greenhouse gas

Student : Liangyi Lin

Advisor : Hsunling Bai

Institute of Environmental Engineering

National Chiao Tung University

Abstract

The carbon dioxide (CO₂) capture and storage (CCS) technologies have received out-breaking concerns after the Kyoto Protocol came into force in 2005. Among capturing technologies, adsorption is regarded as one of the feasible approaches which can limit the CO₂ emission. Mesoporous silica materials with high surface area, large pore size and large pore volume are considered as good candidates for CO₂ capture. However, the requirements of tedious processing time and expensive manufacture costs strongly limited their applications. Furthermore, the global emission quantity of CO₂ is so huge that it may consume tremendous amount of resource materials to capture the CO₂ greenhouse gas. On the other hand, with the evolution of semiconductor and optoelectronic industries, huge amounts of siliceous waste powder are significantly increased. Such waste powders are light-density with bulky volume and are thus difficult to be transported and disposed. Therefore, additional expenses on waste treatment and landfill disposal are needed. So if the captured sorbent can be obtained from product wastes, the cost-effectiveness of the CO₂ capture technology and the waste treatment and disposal problem will be resolved simultaneously.

This study intends to reutilize the waste powder as an alternative resource for the production of mesoporous silica materials via either solution precipitation method or aerosol spray approach. The structural properties and cost-effectiveness of the recycled materials on CO₂ adsorption performance was investigated as well. The

results showed that the waste powder can be directly converted in to mesoporous silica MCM-41(DU)-F with high surface area ($788 \text{ m}^2\text{g}^{-1}$), large pore size (4.5 nm) and large pore volume ($1.1 \text{ cm}^3\text{g}^{-1}$) with the assistance of ionic surfactant of CTAB, hydrofluoric acid as well as ammonium hydroxide. Through similar pathway, silica materials with hierarchically mesocellular structures can be facily prepared by using single F127 surfactant. The concentrations of hydrofluoric acid and F127 were found to strongly affect the structural properties of the recycled materials.

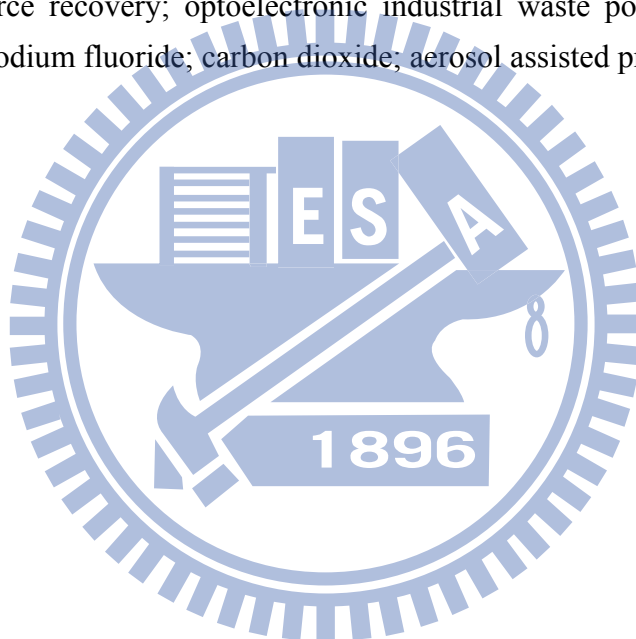
On the other hand, a low-temperature alkali extraction was developed to effectively separate the silicate supernatant and the sediment of sodium fluoride (NaF) from the waste powder. The obtained sediment containing high purity of NaF (>90%), which provides further reuse possibility since NaF is widely applied in chemical industry. The supernatant is a valuable silicate source for synthesizing mesoporous silica material. In other words, the optoelectronic waste powder can be converted into two valuable resources, the supernatant as the silica precursor and the sediment of sodium fluoride. The mesoporous MCM-41 produced from the waste-derived silicate, namely MCM-41(AF), possessed high specific surface areas ($1069 \text{ m}^2/\text{g}$), narrow pore size distributions (3.0 nm) and large pore volumes ($0.97 \text{ cm}^3/\text{g}$), similar with those of the MCM-41(NaSi) fabricated using commercial silica precursors. This clearly suggests that the silicate supernatant from waste powder can be potential silica resource.

This study further extends the preparation of mesoporous materials using waste-derived silicate supernatant as precursors. It was demonstrated that mesoporous MSP(AS) and MSS(HNO_3) materials can be synthesized by employing inorganic salts as templating media. The cost analysis shows that the synthesized material of MSS(HNO_3) is about five percent of the price of SBA-15 and two percent of the MCM-41 made from commercial silica precursors.

Furthermore, the correlation between CO_2 adsorption capacity and the pore structure properties (pore size, pore volume and specific surface area) is studied. The result of the linear regression indicates that the CO_2 adsorption capacity has the

strongest correlation with the total pore volume of the mesoporous materials ($R^2 > 0.9$). The amine-impregnated MSS(HNO_3) can achieve 122 mg/g adsorption capacity, which is superior to that of the original MCM-41(115 mg/g) and SBA-15(117) made from commercial precursors under the same conditions. The MSS(HNO_3) prepared using optoelectronic industrial waste powder as the silica source via salt-templated aerosol spray approach exhibits several important advantages of simple and rapid synthesis, low manufacturing costs and superior CO_2 adsorption performance. Therefore, it could be considered as potential and competitive sorbents for CO_2 capture from flue gas.

Keywords: resource recovery; optoelectronic industrial waste powder; mesoporous silica materials; sodium fluoride; carbon dioxide; aerosol assisted process



誌謝

轉眼間博士班生涯到了尾聲，研究期間承蒙恩師 白曠綾教授對於研究方向與細節的悉心指導，以及董瑞安教授、蔡春進教授、林錕松教授、李壽南博士與張淑閔副教授於論文口試期間對於本文疏漏及謬誤之處費心指正並提供寶貴之學術建議，在此表達萬分感謝。

回首這四年期間實驗室大夥的相處就像是一個大家庭；除了研究上大家能夠互相討論給予協助，日常生活的關心照顧、嘻笑打鬧也讓實驗室生活更加多采多姿。在此也感謝博士班錦德與承業學長對於研究上的討論，以及劉凱、祈緯、瑋婷、建廷、侑霖、祐菖、詩婉、國華、志成、崇瑋、佳錡、紘宇、智傑、世元、玫華、婉婷、太太、Momo 與姥姥等學弟妹的生活相伴與協助，與你們一起度過的日子與點點滴滴都會是未來美好的回憶，也在此致上最深的謝意。

最後要感謝我的家人在背後的支持關心，讓我能夠一路順利完成學業。今日學位的完成，是一個階段的結束更是另一階段的開始，期望自己未來能貢獻所學，取之於社會，還之於社會。

謹誌於 交大環工所

民國一百零一年六月

CONTENTS

CONTENTS	IX
LIST OF FIGURES	XI
LIST OF TABLES	XVII
CHAPTER I INTRODUCTION	1
1.1 Background and Motivation	1
1.2 Objectives and Scope	2
CHAPTER II LITERATUR REVIEW	3
2.1 Mesoporous silica materials	3
2.1.1 MCM-41	3
2.2.1 SBA-15	4
2.3.1 Mesostructured cellular foam (MCF)	4
2.2 Carbon capture and storage (CCS)	8
2.2.1 Amine-functionalized solid sorbent for CO ₂ removal	9
2.2.1.1 Microporous zeolite sorbents	9
2.2.1.2 Mesoporous silica sorbents	14
2.3 Effect of pore structure on CO ₂ adsorption performance	18
2.4 Siliceous solid wastes derived adsorbents for CO ₂ capture	22
CHAPTER III SILICA MATERIALS RECOVERED FROM OPTOELECTROMIC INDUSTRIAL WASTE POWDER: ITS EXTRACTION, MODIFICATION, CHARACTERIZATION AND APPLICATION	26
CHAPTER IV DIRECT CONVERSION OF WASTE POWDER INTO MESOPOROUS SILICA MATERIALS	42
CHAPTER V AEROSOL-ASSISTED SYNTHESIS OF MESOPOROUS SILICA PARTICLES VIA THE USE OF SODIUM METASILICATE PRECURSOR	73

CHAPTER VI AEROSOL PROCESSING OF MESOPOROUS SILICA PARTICLES USING WASTE-DERIVED SILICATE	88
CHAPTER VII COMPARISON OF WASTE-BASED ADSORBENTS FOR THEIR CO₂ CAPTURE PERFORMANCE.....	115
CHAPTER VIII CONCLUSIONS AND RECOMMENDATION.....	121
8.1 Conclusions	121
8.2 Recommendation for future work	122
REFERENCES	124
APPENDIX	139



LIST OF FIGURES

Figure 2.1 A scheme for the formation mechanism of mesoporous MCM-41.	6
Figure 2.2 TEM image of the honeycomb structure of MCM-41 and a schematic representation of the hexagonal shaped one-dimensional pores.....	6
Figure 2. 3 Illustration of mesoporous SBA-15.....	7
Figure 2. 4 Schematic cross section of the strut-like structure exhibited by MCFs.	7
Figure 2.5 Physisorption and chemisorption capacities of 15% CO ₂ on Y60(TEPA) at 30-70 °C	12
Figure 2.6 CO ₂ Reaction Pathways with Primary Amines.	12
Figure 2.7 Morphology of the amine composites prepared based on a) quartz, b) KA zeolite, c) NaA zeolite, d) NaY zeolite, e) as-synthesized MCM-41, and f) calcined MCM-41 loaded with 50 wt% TEPA.	13
Figure 2.8 Schematic diagram of PEI loaded in the mesoporous molecular sieve of MCM-41. (A) MCM-41 support; (B) low PEI loading; (C) high PEI loading; (D) extremely high PEI loading.....	17
Figure 2.9 Schematic diagram illustrating the influence of the template occluded in a channel of MCM-41 on the distribution of TEPA	17
Figure 3.1 (a) EDS spectrum and (b) FTIR spectrum of the optoelectronic waste powder.....	29
Figure 3.2 XRD pattern of the optoelectronic waste powder.....	29
Figure 3.3 (a) TGA analysis and (b) DTG profile of the optoelectronic waste powder.	

.....	31
Figure 3.4 (a) EDS spectrum and (b) XRD pattern of the sediment after silica extraction.....	33
Figure 3.5 (a) TGA analysis and (b) DTG profile of the sediment.....	33
Figure 3.6 (a) EDS spectrum of MCM-41(PWP) sample and (b) XRD patterns of the MCM-41(PWP) and MCM-41(NaSi) samples.....	37
Figure 3.7 N ₂ adsorption-desorption isotherms of the optoelectronic waste powder, calcined MCM-41(NaSi) and MCM-41(PWP) samples.....	38
Figure 3.8 BJH pore diameter distributions of calcined MCM-41(NaSi) and MCM-41(PWP) samples.....	38
Figure 3.9 TEM images of MCM-41(NaSi) and MCM-41(PWP) samples.....	40
Figure 4. 1 CO ₂ adsorption via pack column system.....	44
Figure 4.2 Schematic procedures for (a) conventional alkaline fusion process and (b) direct utilization process for the recovery of mesoporous silica from the optoelectronic waste powder.....	48
Figure 4.3 (a) Low angle XRD patterns of MCM-41(DU), MCM-41(DU)-F as well as MCM-41(AF) and (b) wide angle XRD patterns of MCM-41(DU) and MCM-41(DU)-F samples.....	50
Figure 4.4 N ₂ adsorption-desorption isotherms of raw optoelectronic waste powder, MCM-41(DU), MCM-41(DU)-F and MCM-41(AF) samples.....	52
Figure 4.5 BJH pore size distribution of MCM-41(DU), MCM-41(DU)-F and MCM-41(AF) samples.....	52

Figure 4.6 (a) EDS spectrum of MCM-41(DU)-F; (b) TEM image of MCM-41(DU); (c) TEM image of MCM-41(DU)-F.....	54
Figure 4.7 ²⁹ Si NMR spectrum of MCM-41(DU) and MCM-41(DU)-F samples.....	57
Figure 4.8 SEM images of (a) MCM-41(AF) and (b) MCM-41(DU)-F samples.	57
Figure 4.9 CO ₂ breakthrough curves for TEPA-functionalized adsorbents of MCM-41(NaSi), MCM-41(AF), MCM-41(DU) and MCM-41(DU)-F samples.....	60
Figure 4.10 (a) Relationship between the pore diameter of the mesoporous substrates and CO ₂ uptake and (b) correlation of total pore volume of the mesoporous substrates and CO ₂ uptake at 60 °C.....	60
Figure 4.11 BJH pore size distribution of TEPA-MCM-41(NaSi), TEPA-MCM-41(AF) and TEPA-MCM-41(DU)-F samples.....	61
Figure 4.12 Schematic cartoon of the structure of the recycled MS (0.0023).....	68
Figure 4.13 Representative TEM image of the recycled MS (0.0023).....	68
Figure 4.14 N ₂ adsorption-desorption isotherms of mesoporous silica materials synthesized with various n _{F127} /n _{Si} ratios.	69
Figure 4.15 Pore size distribution of mesoporous silica materials synthesized with various n _{F127} /n _{Si} ratios.	69
Figure 4.16 N ₂ adsorption-desorption isotherms of mesoporous silica materials synthesized with various n _{HF} /n _{Si} ratios.	70
Figure 4.17 Pore size distribution of mesoporous silica materials synthesized with various n _{HF} /n _{Si} ratios.	70

Figure 4.18 Possible mechanism of recycling of mesostructured cellular foam from optoelectronic industrial waste powder.....	71
Figure 4.19 TEM images of the recycled mesoporous silica samples synthesized by using different amounts of F127. a) MS(0.001), b) MS(0.01).....	72
Figure 5.1 Experimental setup for the generation of mesoporous silica spherical particles (MSPs) through aerosol-assisted evaporation induced self-assembly (EISA) process.....	76
Figure 5.2 XRD patterns of calcined MSPs prepared from Na_2SiO_3 (denoted as MSP(NaSi)) and TEOS (denoted as MSP(TEOS)), respectively.	78
Figure 5.3 Nitrogen adsorption-desorption isotherms of calcined MSP(NaSi) and MSP(TEOS), respectively.....	81
Figure 5.4 BJH pore diameter distribution of calcined MSP(NaSi) and MSP(TEOS), respectively.....	82
Figure 5.5 SEM images of calcined MSPs. (a1) MSP(TEOS) with scale bar of 10 μm , (a2) MSP(TEOS) with scale bar of 1 μm (b1) MSP(NaSi)-18 with scale bar of 10 μm , and (b2) MSP(NaSi)-18 with scale bar of 500 nm.....	85
Figure 5.6 TEM images of calcined MSPs. (a) MSP(TEOS), (b) MSP(NaSi)-10, (c) MSP(NaSi)-18 and (d) MSP(NaSi)-22. (The scale bar is 20 nm)	86
Figure 6.1 Experimental setup for the generation of mesoporous silica spherical particles (MSPs) through aerosol spray process.....	91
Figure 6.2 TGA system for the CO_2 adsorption.....	91
Figure 6.3 XRD patterns of as-synthesized MSP, as-synthesized MSP (AS) and	

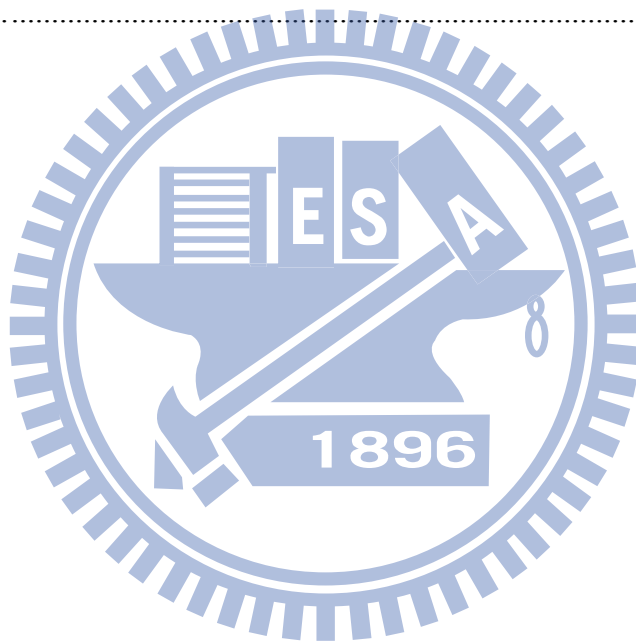
washed MSP (AS) samples.....	94
Figure 6.4 (a) TGA and (b) DTG analyses of the washed MSP (AS).....	94
Figure 6.5 (a) N ₂ adsorption-desorption isotherms and (b) BJH pore diameter distributions of the washed MSP and MSP (AS) samples.....	97
Figure 6.6 Possible pathway for the formation of MSP and MSP (AS) samples through aerosol spray process.....	99
Figure 6.7 SEM images (a) low-magnification, (b) high-magnification of the washed MSP (AS). (c) TEM image and (d) EDS spectrum of the washed MSP (AS).....	101
Figure 6.8 Comparison on CO ₂ uptakes of TEPA loaded on MCM-41, SBA-15, MSP (AS) and NaY zeolite samples.....	104
Figure 6.9 N ₂ adsorption-desorption isotherms (a) parent MCM-41, SBA-15, MSP (AS) and NaY zeolite and (b) TEPA loaded on MCM-41, SBA-15, MSP (AS) and NaY zeolite samples.....	104
Figure 6.10 CO ₂ adsorption performance of TEPA-MSP (AS) with 10% and pure CO ₂ feed gas at 60°C.....	105
Figure 6.11 XRD patterns of the as-synthesized MSS samples.....	110
Figure 6.12 N ₂ adsorption-desorption isotherms of the washed MSS samples.....	111
Figure 6.13 Pore size distribution of the washed MSS samples.....	111
Figure 6.14 SEM images of the washed (a) MSS (H ₂ SO ₄), (b) MSS (HNO ₃) and MSS (HCl) samples; TEM images of the washed (d) MSS (H ₂ SO ₄), (e) MSS (HNO ₃) and (f) MSS (HCl) samples.....	112

Figure 6.15 Comparison on CO₂ uptakes of TEPA loaded on MCM-41, SBA-15, MSS (H₂SO₄), MSS (HNO₃) and MSS (HCl) samples..... 113

Figure 7.1 Correlation of the surface area of the mesoporous substrates and the CO₂ uptake..... 117

Figure 7.2 Correlation of the pore diameter of the mesoporous substrates and the CO₂ uptake..... 117

Figure 7.3 Correlation of total pore volume of the mesoporous substrates and the CO₂ uptake..... 118



LIST OF TABLES

Table 2. 1 Amine-functionalized mesoporous siliceous sorbents for CO ₂ capture.....	16
Table 3.1 Elemental analysis of optoelectronic waste powder and sediment analyzed by the SEM-EDS and ICP-MS analyses.....	35
Table 3.2 Physical properties of optoelectronic waste powder and mesoporous adsorbents	41
Table 4.1 Structural properties of MCM-41(NaSi) silica, waste powder and waste-derived mesoporous siliceous materials.....	62
Table 4.2 Physical parameters of the optoelectronic waste powder and the recycled mesoporous silica samples prepared at different n_{F127}/n_{Si} ratio.	73
Table 4.3 Physical parameters of the recycled mesoporous silica samples prepared at different n_{HF}/n_{Si} ratio.....	73
Table 5.1 Physical properties of the mesoporous adsorbents	87
Table 6.1 Elemental analysis of optoelectronic waste powder and silicate supernatant analyzed by the SEM-EDS and ICP-MS analysis	96
Table 6.2 Structural parameters of the materials.....	96
Table 6.3 Structural parameters of mesoporous and microporous adsorbents.....	114
Table 7.1 TEPA-related adsorbents for CO ₂ capture in this work.	119

CHAPTER I INTRODUCTION

1.1 Background and Motivation

Worldwide issues including energy crisis, global warming and sustainable development are receiving great attention. The carbon dioxide (CO₂) capture and storage (CCS) technologies have attracted out-breaking concerns after the Kyoto Protocol came into force in 2005 [1]. In this regard, various capture technologies, including absorption, adsorption, cryogenics, membrane separation, etc., have been widely investigated [2–4]. Among them, the design of a full-scale adsorption process might be feasible and the development of a promising material that would efficiently adsorb CO₂ with high adsorption capacity and low energy penalty for the regeneration process will undoubtedly enhance the competitiveness of adsorptive separation in a flue gas application. However, the global emission quantity of CO₂ is so huge that it may consume tremendous amount of resource materials to capture the CO₂ greenhouse gas.

Ever since the rises of flat panel industry, especially thin film transistor-liquid crystal display (TFT-LCD), demands on large scale panel display increase rapidly during recent years [5]. However, huge amounts of waste products have been created in the forms of waste solvents, sludge and solid waste, etc. Silicon (Si)-containing waste powder is a common waste product of chemical vapor deposition (CVD) process in TFT-LCD and semiconductor plants. The waste powders have problems of treatment and disposal due to their light-density and bulky volume. Besides, the small particle sizes of such waste powders would induce harmful effects on human beings if not properly treated. Currently, these waste powders have been disposed of without any profit due to the shortage of storage sites and have resulted in severe environmental issues.

Several research studies have attempted to reuse solid wastes for manufacturing mesoporous silica materials. This includes coal fly ash [6] and rice husk ash [7] which are by-products of the coal-fired power plant and agricultural activities. However, most recycling routes are energy-consumed and time-consuming, which would further increase the manufacturing costs. Unlike the coal fly ash or rice husk ash which

contains lots of complicated metal oxides [8,9], the primary components of optoelectronic waste powder might only contain Si-, N- and F- species. So far, the identification of the waste powder from CVD processes of either semiconductor or optoelectronic industry as well as the possibility of waste powder recovery for further environmental applications have not been reported yet.

1.2 Objectives and Scope

The research described in this study was motivated to develop cost-effective CO₂ adsorbents from waste materials through convenient synthetic procedures. This work intends to utilize the waste powder from TFT-LCD plants as the alternative precursor of the mesoporous siliceous adsorbent for CO₂ capture. So if the adsorbent can be obtained from wastes product, the cost-effectiveness of the CO₂ capture technology and the waste treatment and disposal problem will be resolved simultaneously.

The objectives of this study are listed:

1. To identify the chemical composition of the waste powder from CVD processes of optoelectronic industry as well as the possibility of waste powder recovery for further environmental applications.
2. To fabricate cost-effective mesoporous materials by employing waste powder as silica precursor via either solution precipitation method or aerosol spray process as supports of adsorbents for CO₂ capture.
3. To investigate the effect of textural properties of the mesoporous sorbents on the CO₂ adsorption performance.

CHAPTER II LITERATUR REVIEW

2.1 *Mesoporous silica materials*

Porous materials have been intensively applied to the processes of adsorption, separation and catalysis, etc [10–14]. According to the IUPAC definition, porous materials are divided into three classes; microporous (pore size < 2nm), mesoporous (2-50nm), and macroporous (>50nm) materials [15]. In recent years, microporous zeolites have attracted strong attention due to their high specific area, well-define and crystalline pore structure for environmental protection applications [16–18]. However, zeolites have mass transfer limitations when it is being applied for the adsorption of large molecules. Thus attempts have been made to work on enlargement of the pore sizes into mesopores, which can allow large molecules to penetrate into the pore channels.

Mesoporous materials were first discovered by the Mobil Company in 1992. The characteristics of these materials include: (1) large specific surface area ($\sim 1000 \text{ m}^2/\text{g}$) and pore volume ($\sim 1 \text{ cm}^3/\text{g}$), (2) adjustable size and morphology, (3) uniformly distributed pore size, (4) highly ordered mesostructures and (5) controllable chemical composition and unique surface chemistry via functionalization. Typically, surfactant micelles are the structuring-directing template for the mesoporous materials. So far, many families of mesoporous materials have been developed, including M41S [19,20], SBA [21,22], HMS [23], MCF [24–26], and KIT [27,28], etc. These materials were synthesized by using different surfactants, co-surfactants, synthesis conditions and methods.

2.1.1 *MCM-41*

The first-ordered mesoporous material, namely M41S family, was firstly synthesized by Mobile Corporation [29]. These materials were prepared from ionic surfactants, such as quaternary ammonium ions. A liquid crystal templating mechanism was proposed to elucidate the formation of the inorganic-organic composites, which is based on electrostatic interactions between the positively

charged surfactants and the negatively charged silicate species in solution as shown in [Figure 2.1](#) [13]. MCM-41 is the most widely studied M41S material. It is often used as a model to compare with other materials or to study fundamental aspects in sorption, catalysis, etc [30–32]. It consists of an amorphous silicate framework with hexagonal pores. MCM-41 has high surface areas of up to 1200 m²/g and large pore volumes. The pores are very uniform causing narrow pore size distributions [33,34]. The pores are unidirectional and arranged in a honeycomb structure over micrometer length scales as shown in [Figure 2.2](#) [35].

2.2.1 SBA-15

In 1998, a new family of highly ordered mesoporous silica materials has been synthesized in an acid medium by the use of commercially available non-ionic triblock copolymers (EO_nPO_mEO_n) with large polyethyleneoxide (EO)_n and polypropyleneoxide (PO)_m blocks [15]. Different materials with a diversity of periodic arrangements have been prepared and denoted as SBA materials. A wide variety of SBA materials has been reported in the literature, such as SBA-15 (2D hexagonal) and SBA-16 (cubic cage-structured) [36–39]. SBA-15 immediately attracted a lot of attention because of its desirable features and is now the most intensely studied SBA structure.

SBA-15 is a combined micro- and mesoporous material with hexagonally ordered tunable uniform mesopores (4-14 nm) [21,40]. The size of the micropores was found to depend on the synthesis conditions and can vary between 0.5 and 3 nm in size [21,41,42]. It consists of thick microporous silica pore walls (3-6 nm) responsible for the high hydrothermal stability of SBA-15 compared to other mesoporous materials with thin pore walls like MCM-41, MCM-48 and HMS [43–45].

2.3.1 Mesostructured cellular foam (MCF)

Among various mesoporous materials, a new family of mesostructured cellular foam (MCF) material, which consists of uniform spherical cells interconnected by windows with ultra-large mesocellular pores and three-dimensional porous structure

(Figure 2.4) has received increasing attentions recently. MCF material is originally made by addition of a swelling agent such as 1,3,5-trimethylbenzene (TMB) to the synthesis of SBA-15 [26,46,47]. The swelling agent enlarges of the micelle, resulting in a sponge-like foam with three-dimensional structure with large uniform spherical cells (15-50 nm), accessible via large windows (5-20 nm). Therefore, MCF is a very open structure with large uniform pore diameters and large pore volumes. It has thick pore walls resulting in a high hydrothermal stability. The addition of ammonium fluoride can selectively enlarge the windows by 50-80% [48–50].



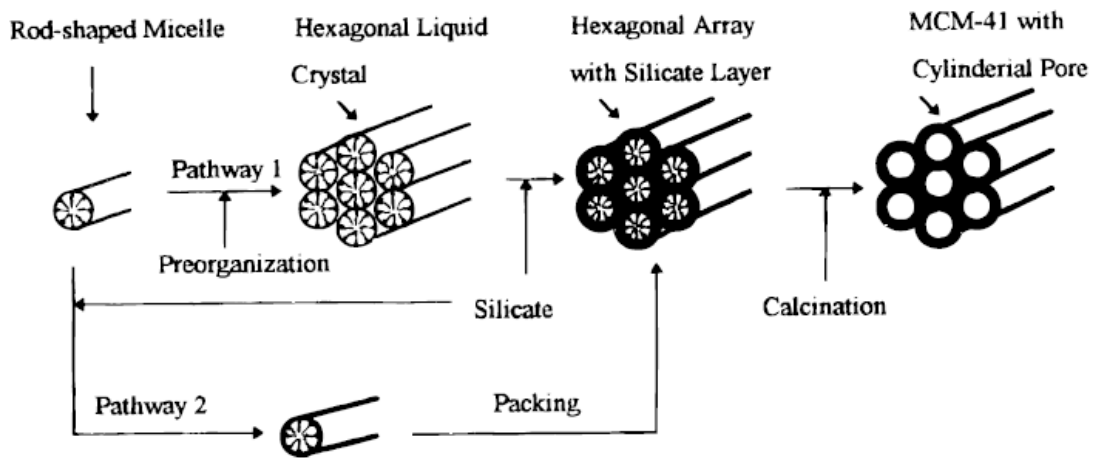


Figure 2.1 A scheme for the formation mechanism of mesoporous MCM-41 [13].

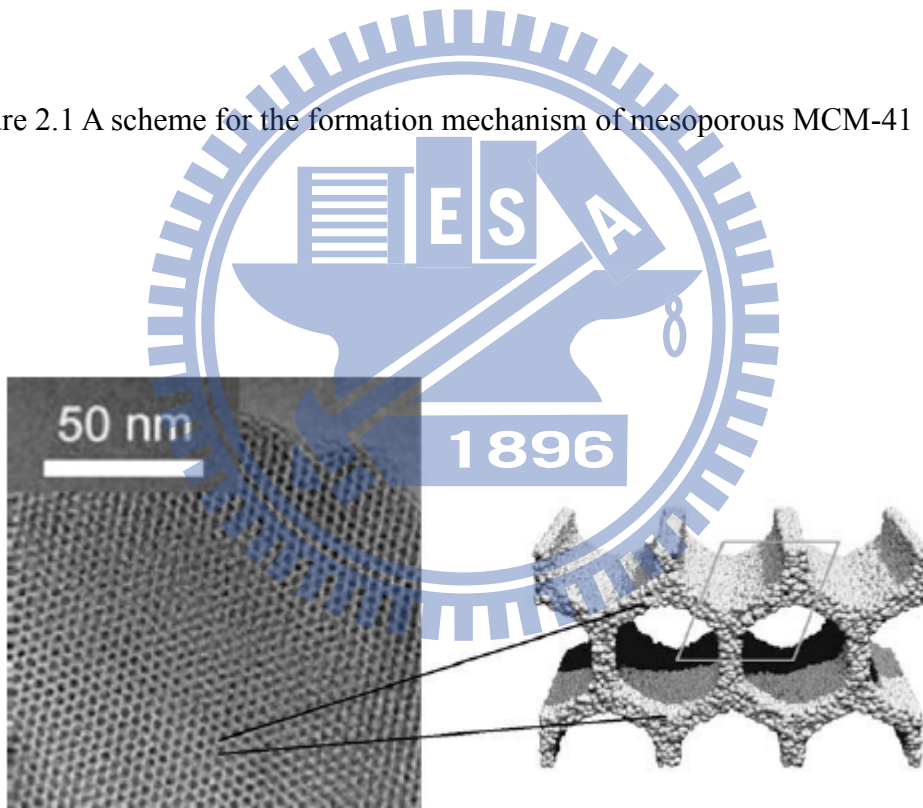


Figure 2.2 TEM image of the honeycomb structure of MCM-41 and a schematic representation of the hexagonal shaped one-dimensional pores [35].

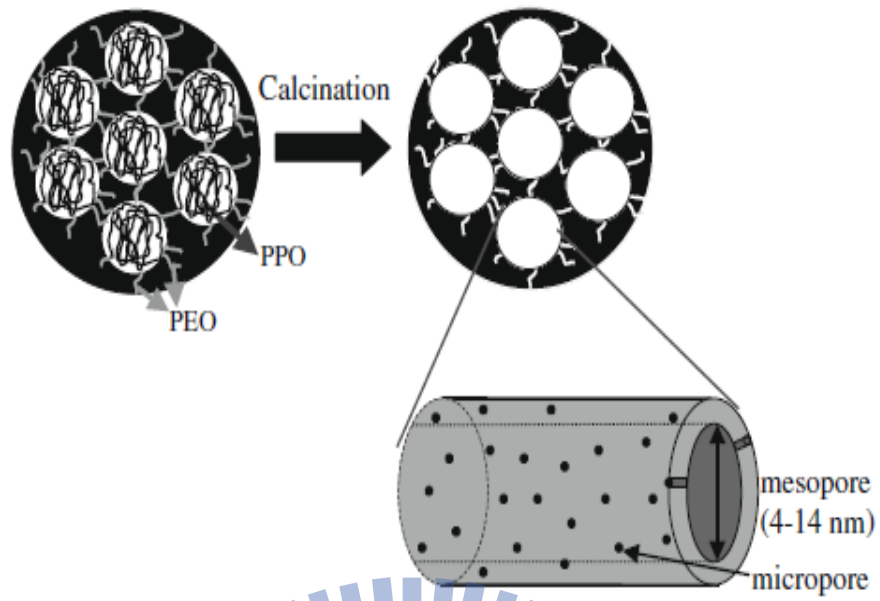


Figure 2. 3 Illustration of mesoporous SBA-15 [35].

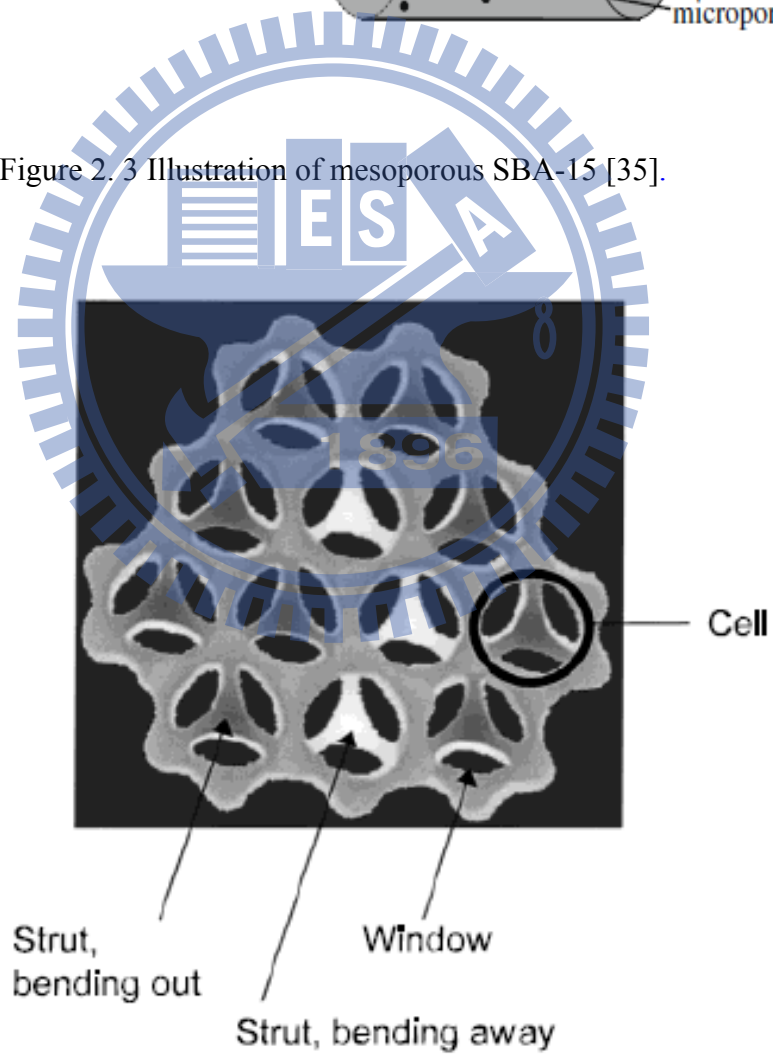


Figure 2. 4 Schematic cross section of the strut-like structure exhibited by MCFs [47].

2.2 Carbon dioxide capture and storage (CCS)

The capture of CO₂ greenhouse gas from industrial and utility plants has become a world issue since the enforcement of Kyoto Protocol [51]. For controlling the emissions of CO₂, several significant efforts have been devoted to develop efficient and low-cost techniques, including the improvement of the efficiency of energy utilization, increasing the use of low-carbon energy sources and CO₂ capture and sequestration. Up to date, Carbon dioxide Capture and Sequestration (CCS) has been identified as the most effective and feasible technique limiting the emissions of CO₂ [51].

Numerous capture processes including adsorption, absorption and membrane separation are proposed to separate and recover CO₂ emitted to the atmosphere [52]. It has been conducted the chemically absorptive removal of CO₂ using ammonia (NH₃) solvent process to replace conventional monoethanolamine (MEA) process. It was found that the potential for removing CO₂ via ammonia scrubbing may be very promising. Although these liquid-phase systems are effective, there are still many drawbacks existing in such systems, such as high energy consumption, limitation of amine concentration in aqueous solutions and corrosion by sulfur oxides [53,54].

Development of a dry-based sorbent in CO₂ post-combustion capture is always desirable when liquid sorbents used in industries are still facing many constraints, such as corrosion, foaming, low removal rate with large-size equipments requirement, etc. Solid sorbents are normally easier for handling and causing fewer issues during the operation. In addition, solid sorbents are expected to be more cost-effective materials over liquid solvents because of its low energy requirement for regeneration.

In this regard, possible dry adsorbents including silica-gel [55], activated carbons [16], carbon nanotubes [56], and zeolite materials [57] have been widely investigated on CO₂ adsorption in terms of adsorption capacity, regeneration ability and tolerance under water-existing environment.

2.2.1 Amine-functionalized solid sorbent for CO₂ removal

2.2.1.1 Microporous zeolite sorbents

Zeolites are the most widely studied adsorbents for CO₂ capture so far [58]. Zeolites are typically employed at ambient temperature and elevated pressure (above 2 bar). [Siriwardane et al.](#) [59] reported that the CO₂ adsorption capacity of zeolite 13X, zeolite 4A and activated carbon was about 160, 135 and 110 mg-CO₂/g-adsorbent, respectively, under 25°C and 1 atm CO₂ partial pressure. However, their adsorption capacity has been confirmed to be significantly influenced by the increasing temperature and the presence of moisture in the gas mixture. Moreover, since all the gases are physically adsorbed on these adsorbents, the separation of various gases is difficult to be achieved. For practical applications, many separation processes were carried out under relatively higher temperatures, i.e., 50°C to 80°C, which is a typical temperature of the exit of flue gas. Therefore, adsorbents with high adsorption capacity and high CO₂ selectivity, which can be operated at relatively higher temperatures, are desired.

In order to enhance the sorption properties of zeolite materials for low pressure applications such as those relevant in flue streams, there have been several reports on development of amine-functionalized zeolite materials as alternative sorbents for CO₂ capture. [Chatti et al.](#) [60] performed the MEA-modified zeolite 13X with enhanced adsorption capacity of 23 mg-CO₂/g-adsorbent, which is 1.4 times higher than the bare 13X at 75°C. Unlike the adsorption process driven by physisorption at lower temperature, the chemical interaction between impregnated amine and CO₂ gas may play an important role in the CO₂ adsorption performance at higher temperatures.

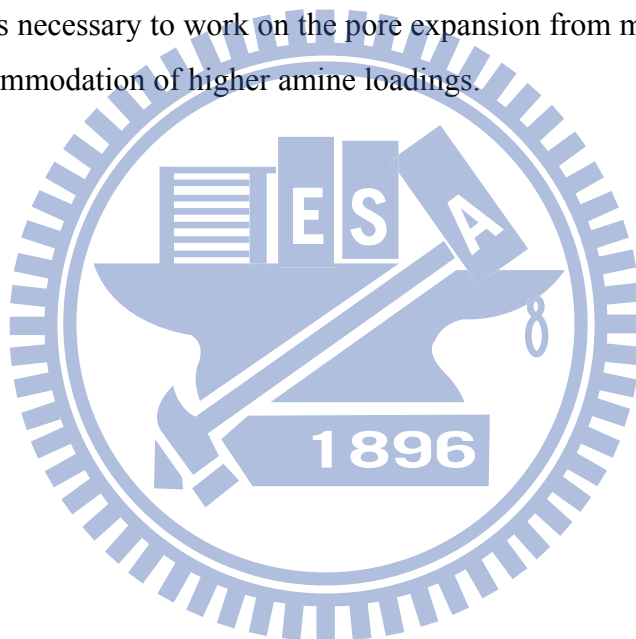
Similar observations were found in the report of [Su et al.](#) [57], who prepared tetraethylenepentamine (TEPA)-modified zeolite Y60 for CO₂ sorption at various temperatures. A comparison of physisorption and chemisorption for CO₂ sorption from 30°C to 70°C was investigated and shown in [Figure 2.5](#). It was found that physisorption mainly determines the CO₂ sorption capacity in raw Y60 material, whereas chemisorption of CO₂ plays a predominant role instead of physisorption in TEPA-functionalized Y60 sorbent and it increased with increasing temperatures. Furthermore, moisture in the stream was found to be beneficial in the enhancement of

CO₂ sorption of TEPA-functionalized Y60 and the sorption capacity could achieve 4.27 mmol g⁻¹ in the presence of 15% CO₂ at 70°C as well as 7% water vapor in the stream. However, the sorption capacity would decrease with further increasing water contents due to the strongly competitive adsorption of water vapor with CO₂ gas. A possible CO₂ reaction scheme with amine solid sorbent is represented in [Figure 2.6](#). It is showed that amine could react with CO₂ molecules to form intermediates of carbamate or bicarbonate under mild temperatures (40~100°C). Besides, this process is reversible; therefore, the CO₂ can be easily desorbed by heating treatment and the adsorbent can be regenerated.

The influence of support on CO₂ capturing performance was studied by [Fisher et al.](#) [55], who demonstrated a comparative study on TEPA-modified silica, alumina and zeolite beta, respectively, for CO₂ capture. The results showed that TEPA-zeolite beta possessed superior sorption capacity of 2.08 mmol g⁻¹ in the presence of 10% CO₂ at 30°C than those of TEPA-SiO₂ and TEPA-Al₂O₃ sorbents. It was suggested that zeolite beta with relatively higher specific surface area could lead to better dispersion of TEPA on support, which would result in higher sorption performance. Besides, [Yue et al.](#) [61–63] employed a series of TEPA-modified porous materials as adsorbent for CO₂ removal and their morphologies are represented in [Figure 2.7](#). Obviously, the amine-containing quartz, KA zeolite and NaA resulted in gel-like composite. It was due to the fact that the lack of pores of quartz and small pore openings of KA zeolite (0.4 nm) and NaA zeolite (0.3 nm), the TEPA could only be loaded on the external surface. In contrary, the amine-supported NaY zeolite, as-synthesized MCM-41 and calcined MCM-41 were in the form of powder instead of gels. This was ascribed to the larger pore diameter and pore volume of the support, which allowed the amines penetrated insides the channels freely.

From the above studies, it is clear that zeolite materials provides advantages of high specific area and well-defined porous structures, which may be considered as candidates of supports for loading amines for efficient removal of CO₂. There have been studies showing that TEPA-functionalized zeolites can achieve the CO₂ bench mark of 2 mmol g⁻¹; however, since TEPA is thermally unstable, these TEPA-containing sorbent composites would suffer from continuous decay of CO₂ sorption during cyclic adsorption/desorption tests.

To develop thermally stable amine-supported sorbents, numerous reports on various types of amines such as TEPA [64], ethylenediamine (EDA) [65], polyethyleneimine (PEI) [66] and 3-aminopropyltriethoxysilane (APTES) [56], etc., have been investigated in terms of their molecular structure, adsorption capability and thermal stability on CO₂ adsorption. The results showed that most amines like EDA-supported zeolites could not contribute capacity of 2 mmol g⁻¹; despite they are more thermally stable than those of TEPA-containing sorbents during cyclic tests. Thus, it is necessary to prepare such amine-modified sorbents with higher loadings to achieve the bench mark value for commercialization (2 mmol g⁻¹). However, zeolite supports with small pore diameters and small pore volumes may not provide sufficient spaces to accommodate high amounts of amines as shown previously in Yue et al. [62]. Consequently, it is necessary to work on the pore expansion from micropores to larger pores for the accommodation of higher amine loadings.



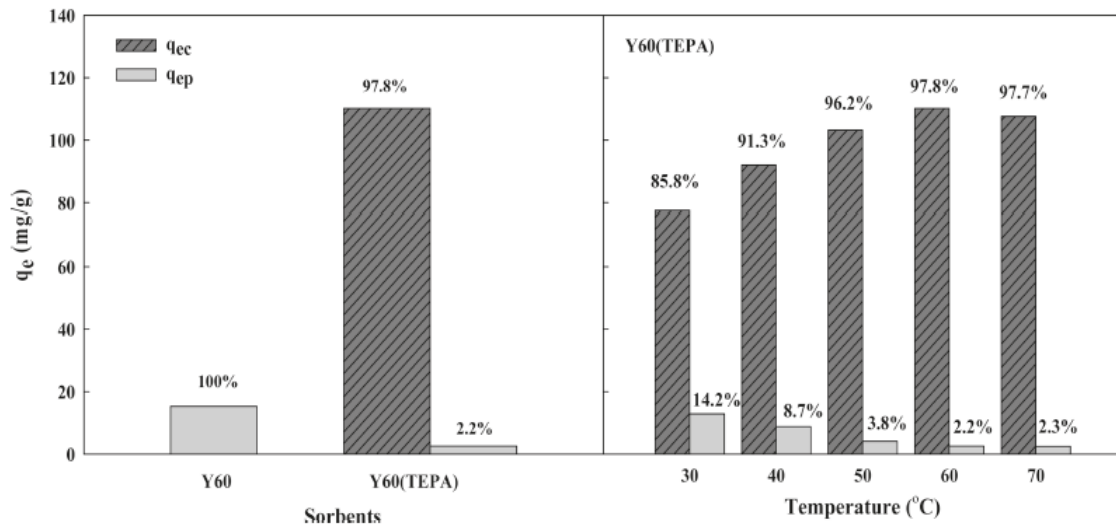


Figure 2.5 Physisorption and chemisorption capacities of 15% CO₂ on Y60(TEPA) at 30-70 °C [57].

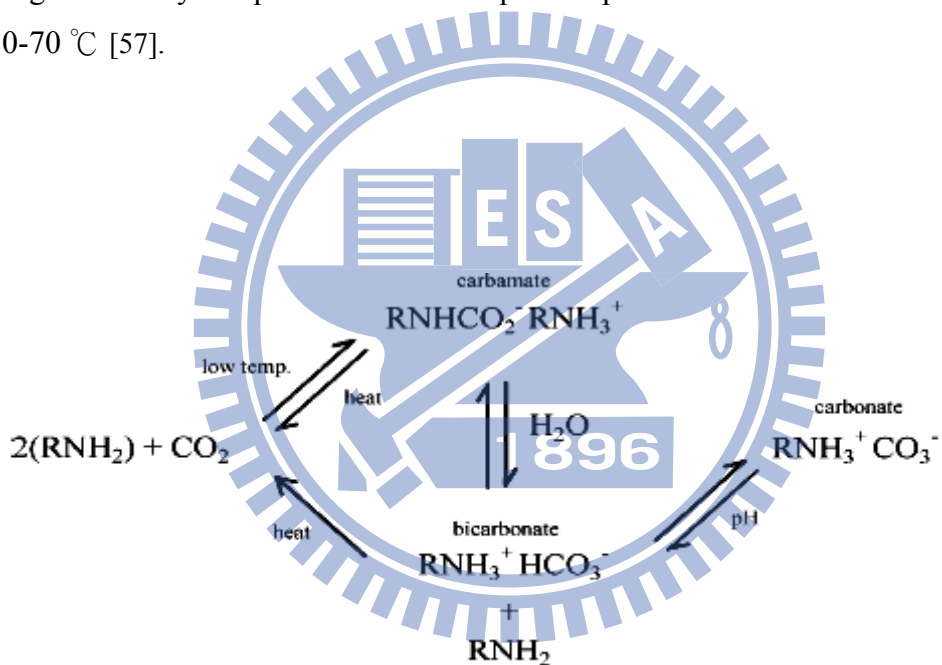


Figure 2.6 CO₂ Reaction Pathways with Primary Amines [67].

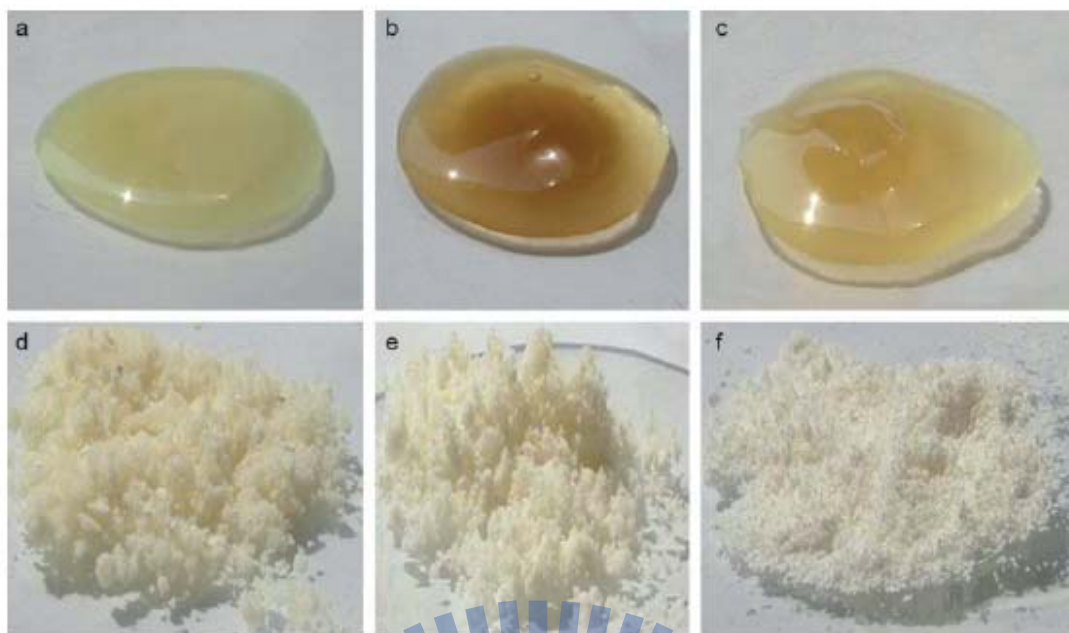
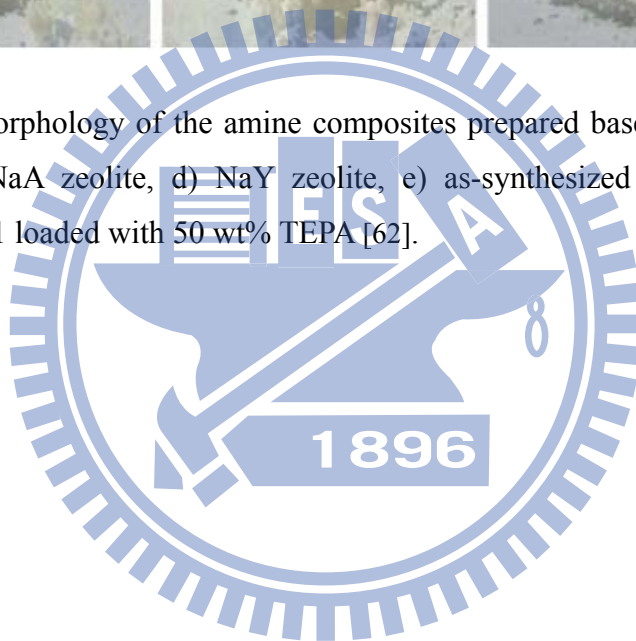


Figure 2.7 Morphology of the amine composites prepared based on a) quartz, b) KA zeolite, c) NaA zeolite, d) NaY zeolite, e) as-synthesized MCM-41, and f) calcined MCM-41 loaded with 50 wt% TEPA [62].



2.2.1.2 Mesoporous silica sorbents

Recent advances in the development of efficient amine-functionalized adsorbents revealed that amine molecules can be introduced and stabilized inside the pore channels of the mesoporous silica materials, leading to high adsorption performance [68]. A new concept called “molecular basket” was firstly proposed by Xu and colleagues [69], who impregnated PEI onto mesoporous silica MCM-41 and it has high specific surface area ($1486 \text{ cm}^2 \text{ g}^{-1}$), large pore diameter (2.8 nm) and large pore volume ($1 \text{ cm}^3 \text{ g}^{-1}$) which can serve as a good sorbent for CO_2 adsorption. It was demonstrated that there is a synergetic effect of MCM-41 on the PEI for the adsorption of CO_2 . The 75 wt% PEI-supported MCM-41 could achieve capacity of 3.02 mmol g^{-1} in the presence of pure CO_2 at 75°C , which is much higher than unmodified MCM-41 (0.2 mmol g^{-1}) and pure PEI (2.47 mmol g^{-1}) under the same conditions. This clearly reveals that the addition of MCM-41 as support for loading PEI can significantly enhance the sorption performance and this could be due to the fact that high surface area and uniform mesoporous channel of MCM-41 increase the dispersion of PEI.

The synergetic effect between MCM-41 and the PEI was further studied by altering the PEI loadings on MCM-41 [70] and the schematic illustrations are presented in Figure 2.8. As the bare MCM-41 was employed alone for CO_2 adsorption (Figure 2.8A), physical adsorption driven by capillary condensation was almost negligible (0.14 mmol g^{-1}). As the PEI loading increases, higher sorption capacity was obtained (Figure 2.8B), and the highest synergetic effect adsorption gain was obtained when MCM-41 was loaded with 50wt% PEI as shown in Figure 2.8C. With PEI loading higher than 50wt%, parts of PEI were coated on the external surface of the MCM-41, which resulted in the blockage of pores and active adsorption sites (Figure 2.8D), and the sorption capacity tended to decrease.

Later on, various types of mesoporous silica materials including MCM-48 [71], SBA-15 [72], SBA-16 [73], HMS [23], KIT-6 [28], etc were utilized as supports of adsorbents in terms of CO_2 adsorption. Huang and Yang [74] employed the amine-modified MCM-48 for acid gas removal from natural gas. It was demonstrated that APTES-modified MCM-48 shows superior selective adsorption of CO_2 from the $\text{CO}_2\text{-H}_2\text{S}$ gas mixture. Chen et al. [75] conducted the CO_2 adsorption tests by using

novel TEPA-impregnated silica monolith materials, which exhibited 5.80 mmol g^{-1} sorption capacity in the presence of pure CO_2 at $75 \text{ }^\circ\text{C}$. Very recently, mesocellular silica foam (MCF) with large pore volume ($1.82 \text{ cm}^3 \text{ g}^{-1}$) were found to be efficient CO_2 sorbents, which can achieve 3.45 mmol g^{-1} sorption capacity in the presence of 15% CO_2 at $75 \text{ }^\circ\text{C}$ [76]. Until now, there have been numerous works on the development of novel amine-functionalized mesoporous silica sorbents for the capture of CO_2 as summarized in Table 2.1 in terms of their starting precursors, amine types, operational conditions as well as CO_2 adsorption capacities.

Besides having good CO_2 capture ability, cost is another important issue to be considered in the development of any potential adsorbent. Specifically, the most enormous barrier for CCS application is its relatively high costs for the capture and separation of CO_2 from flue gas. In terms of the costs of CCS, the capture of CO_2 represents over 80% of the total costs associated with the CO_2 capture, transport and storage cycle [77]. As seen from Table 2.1, most amine-supported mesoporous materials can exhibit superior performance over the benchmark value for commercialization (2 mmol g^{-1}). However, the utilization of expensive precursors including the preferred silica sources and organic additives would lead to the high manufacturing costs of the adsorbents. This would prevent cost-effective and large-scale production of the mesoporous materials to replace industrially manufactured zeolite materials [34,78]. The use of cheaper starting precursors in the manufacturing process would be a great contribution to industrial applications, especially for the capture of abundant CO_2 greenhouse gas where massive quantities of adsorbents are required. However, so far, information on manufacturing cost of adsorbents is rarely discussed.

Table 2.1 Amine-functionalized mesoporous siliceous sorbents for CO₂ capture

Support	Si source	Amine type	Temp(°C)	Ce (mg/g)	CO ₂ conc.(%)	Ref.
MCM-41	Colloid silica+CTAB	PEI	75	111	>99	[66]
MCM-41	Fumed silica+CTAB	PEI	75	133	>99	[69]
MCM-41	Fumed silica+CTAB	DEA	25	55	>99	[79]
PE-MCM-41	Fumed silica+CTAB+TMB	DEA	25	104	>99	[79]
As-syn MCM-41	Silica aerosol+CTAB	TEPA	75	237	>99	[62]
Al-MCM-41-100	Fumed silica+CTAB	PEI	75	127	>99	[70]
MCM-48	RHA+CTAB	TREN	25	70	>99	[71]
MCM-48	Colloid silica+CTAB	PEI	75	119	>99	[66]
KIT-6	TEOS+F127	TEPA	60	129	10	[27]
KIT-6	TEOS+F127	PEI	75	135	>99	[66]
SBA-15	TEOS+P123	EDA	22	86	>99	[65]
SBA-15	TEOS+P123	PEI	75	127	>99	[66]
SBA-15	RHA+P123	TREN	25	80	>99	[72]
SBA-15	TEOS+P123	PEI	75	105.2	15	[80]
As-syn SBA-15	TEOS+P123	TEPA	75	173	>99	[61]
SBA-16	TEOS+F127	PEI	75	129	>99	[66]
SBA-16	TMOS+F127	AEAPS	60	32	15	[73]
HMS	TEOS+DDA	PEI	75	128	>99	[23]
As-syn MSU-1	Sodium silicate	TEPA	75	170	10	[81]
MCF	TEOS+P123+TMB	PIE	105	151	15	[82]
MCF	TEOS+P123+TMB	PEI	75	152	15	[76]
MCF	Sodium silicate+P123	PEI	75	255	80	[83]
MC400/10	TEOS+CTAB	TEPA	75	347.6	10	[64]

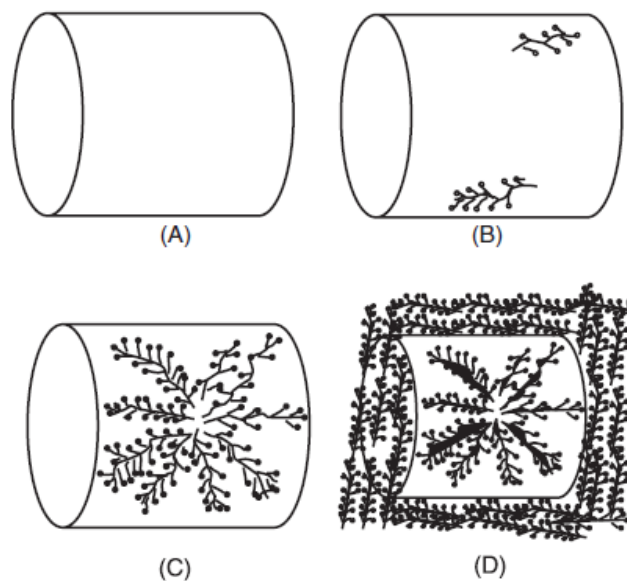


Figure 2.8 Schematic diagram of PEI loaded in the mesoporous molecular sieve of MCM-41. (A) MCM-41 support; (B) low PEI loading; (C) high PEI loading; (D) extremely high PEI loading [70].

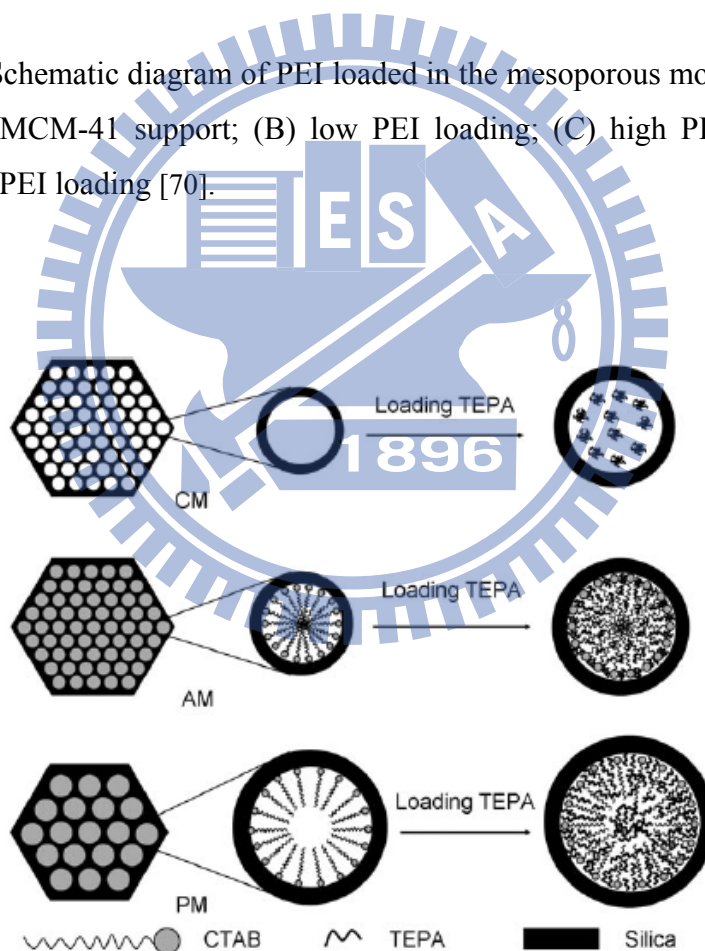


Figure 2.9 Schematic diagram illustrating the influence of the template occluded in a channel of MCM-41 on the distribution of TEPA [62].

2.3 Effect of pore structure on CO₂ adsorption performance

As described previously, mesoporous materials provides several advantages of high specific surface area ($>1000 \text{ m}^2\text{g}^{-1}$), large pore size (2-50 nm) and large pore volume ($\sim 1 \text{ cm}^3\text{g}^{-1}$) in the enhancement of CO₂ adsorption performance. Xu et al. [69,70,84] clearly suggested the synergic effect between the impregnated amines and mesoporous supports. In other words, the structural properties of the supports might strongly influence the behaviors of the impregnated amines and the CO₂ adsorption performance. Fisher et al. [55] conducted the CO₂ adsorption tests by employing three different supports of alumina, silica and beta zeolite as adsorbents. They claimed that when the TEPA was loaded on the materials with high surface area, more CO₂ affinity sites were exposed to the adsorbate and thus the adsorption capacity increased. This is in line with the work reported by Xu et al. [69], who synthesized PEI-impregnated MCM-41 for the adsorptive removal of CO₂.

Zelenák et al. [85] studied the effect of textural properties of the mesoporous supports including MCM-41, SBA-12 as well as SBA-15 on CO₂ capture. They claimed that the sorption capacity was in the subsequence of pore size of support and follow the order of SBA-15 > SBA-12 > MCM-41. As SBA-15 with larger pore size (7.1 nm) could promote more amines into the channel easier and avoid the blockage of accessible adsorption sites for CO₂ gas, higher capacity can be obtained. Their results are in agreement with the works of Son et al. [86], who employed a series of PEI-functionalized mesoporous silica of MCM-41, MCM-48, SBA-15, SBA-16, and KIT-6 with different textural properties to evaluate their CO₂ sorption performance. The CO₂ capacities were found to be in the following order: MCM-41 (2.8 nm, 1D) < MCM-48 (3.1 nm, 3D) < SBA-15 (5.5 nm, 1D) \approx SBA-16 (4.1 nm, 3D) < KIT-6 (6.5 nm, 3D).

Moreover, PEI-impregnated SBA-15 materials with different pore diameters and pore volumes were developed by Yan and his groups [80]. It was reported that 50wt% PEI-SBA-15 can perform 2.39 mmol g^{-1} sorption capacity in the presence of 15% CO₂ at 75 °C. They intended to address the effect of textural properties of the SBA-15 on CO₂ sorption performance. It was demonstrated that the total pore volume of the raw SBA-15 support plays an important role instead of pore diameter on CO₂ sorption. In their subsequent study, it was also suggested that the pore size and the pore volume of

the PEI-impregnated mesocellular silica foams largely influenced the adsorption performance. Besides, similar observations were also found in a recent report by Qi et al. [64], who prepared the PEI-impregnated mesoporous hollow spheres as CO₂ adsorbents. The results revealed that larger particle size and higher interior void volume of the mesoporous hollow spheres all improved the CO₂ capacity of the sorbents.

Table 2.2 summarizes the studies on the CO₂ adsorbents in terms of their adsorption capacities, test conditions and structural properties. Based on the above observations, it could conclude that the adsorption performance could be affected by the pore structure of the substrates; however, most research works were carried out by using different porous supports and lack of systematical and quantitative information on the correlations between the adsorption performance and the structural properties of the supports. Consequently, we intend to address the relationship between the adsorption performance and the structural properties of the supports by using the same mesoporous substrate with different surface area, pore size as well as pore volume as supports. Subsequently, comparison on various substrates on CO₂ adsorption was also carried out.

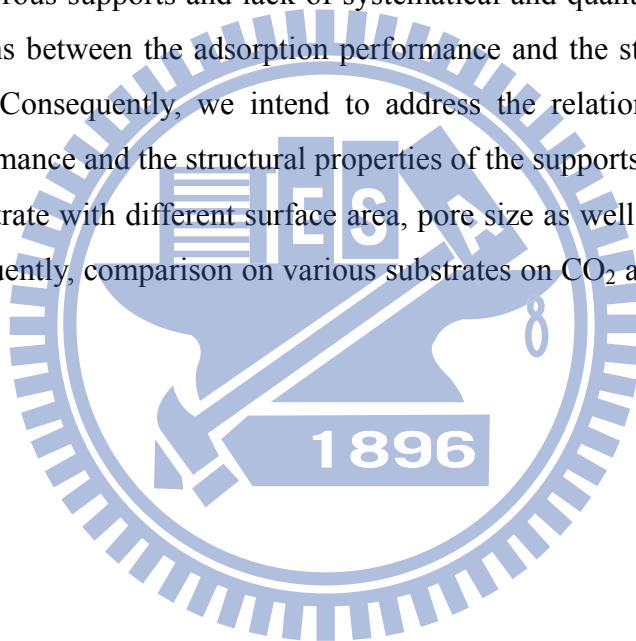
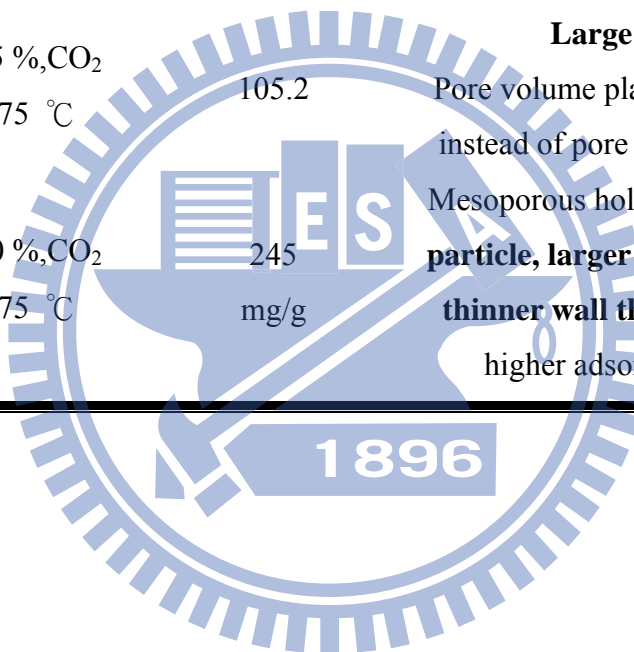


Table 2.2 Studies on the effect of pore structure on CO₂ capture.

Materials	^a S _{BET} (m ² /g) ^b d _{BJH} (nm) ^c V _p (cm ³ /g)	Condition	Capacity	Note: (key factors)	Reference
Al ₂ O ₃ , SiO ₂ , Beta zeolite	^a 680 ^b - ^c -	10%,CO ₂ 30 °C	91	High surface area: Beta zeolite with high surface area can lead to better dispersion of amines, which can enhance the performance.	[55]
MCM-41 (Amine: 50wt. %PEI)	^a 1480 ^b 2.75 ^c 1.0	>99%,CO ₂ 75 °C	133	High surface area and uniform pore structure: MCM-41 with high surface area can lead to better dispersion of amines, which can enhance the performance.	[69]
KIT-6 (Amine: 50wt. %PEI)	^a 895 ^b 6.0 ^c 1.22	>99%,CO ₂ 75 °C	135	Large pore size: KIT-6>SBA-16=SBA-15> MCM-48>MCM-41. Pore size is the main parameter determining the performance.	[66,87-89]

MCF(Amine: 50wt. %PEI)	^a 532 ^b 11.3 ^c 1.82	15 %,CO ₂ 75 °C	177.8	Large window size: & large pore volume: Both Window size and pore volume resulted in increasing CO ₂ adsorption	[76]
SBA-15 (Amine: 50wt. %PEI)	^a 802.9 ^b 8.6 ^c 1.14	15 %,CO ₂ 75 °C	105.2	Large pore volume: Pore volume plays an predominant role instead of pore size on CO ₂ adsorption	[80]
MC400/10 (Amine: 83wt. %TEPA)	^a 725 ^b 3.1 ^c 0.73	10 %,CO ₂ 75 °C	245 mg/g	Mesoporous hollow particle with larger particle, larger pore volume as well as thinner wall thickness prefer to have higher adsorption performance.	[64]



2.4 Siliceous solid wastes derived adsorbents for CO₂ capture

Current concerns of increasing generation of various waste residues have initiated extensive efforts toward the more efficient disposal of these waste materials. In particular, the development of processes for converting waste by-products into high value-added materials is highly desirable for global resource conservation and sustainable environment. Previously, intensive efforts have been made to promote the recycling of waste materials such as municipal sewage sludge [90], coal fly ash [91] and blast-furnace slag [92] into heterogeneous catalyst, adsorbent and catalyst support, and these all target a recycling-beneficial use of the residues to set-off part of the resources depletion problem. This would be expected to be economically beneficial in industrial manufacture of huge amount of adsorbents, especially for the environmental protection applications which require massive quantity of adsorbents or catalysts.

There have been numerous reports on the reutilization of siliceous wastes for the production of mesoporous silica materials as supports of adsorbents for CO₂ removal as listed in [Table 2.3](#). Siliceous solid wastes including coal fly ash, rice husk ash and bottom ash, which are rich of silica and alumina, are confirmed to be potential resources for the production of silica-based sorbents [9,71,78]. However, the procedures in such recycling routes usually require complex preparation steps including high energy-consuming fusion or hydrothermal treatment for the pre-extraction of silica. Besides, the need of expensive organic additives such as CTAB and TMB would also significantly lead to the high manufacturing costs. Considering the mass production of adsorbents for potential commercialization, the synthesis of mesoporous adsorbents by avoiding costly surfactants seems highly desirable.

On the other hand, the development of flat panel display, especially thin film transistor-liquid crystal display (TFT-LCD), has been continuously increased and it is second only to the semiconductor industry over past decade [5]. According to statistics from Industrial Economics & Knowledge Center (IEK) of Taiwan's Industrial Technology Research Institute (ITRI), the production value of the global display panel industry reached \$104.90 billion in 2007; the production value of large-area TFT-LCD constituted the majority of global LCD industry production value, making up almost 70% of total LCD production value. The production value of Taiwanese

large-area TFT-LCD was \$32.73 billion, making Taiwan the world leader in TFT-LCD production and representing the first time that a single industry in Taiwan had exceeded 1 trillion in production value [93].

However, large quantity of sub-micrometer waste powders produced during the chemical vapor deposition (CVD) process has increased annually due to the growing markets. In a typical CVD process, gaseous reagents of silane (SiH_4) and ammonia (NH_3) are introduced and silicon derived compounds such as silica and/or silicon nitride (SiN_x) thin films are formed on the substrates. The cleaning agent of nitrogen trifluoride (NF_3) is subsequently introduced to clean up the accumulative particles formed on the wall of the reaction chamber. The waste powders are then collected by baghouses located in the exhaust of the CVD process. Such waste powders are light-density with bulky volume and are thus difficult to be transported and disposed of. Therefore, additional expenses on waste treatment and landfill disposal are needed. To date, these waste powders have been disposed of without any profit due to the shortage of storage sites and could result in environmental concerned issues, such as leaching of toxic compounds into the groundwater and harmful effects on human beings through direct inhalation. It is, therefore, essential to develop new technologies exploiting the nature of these waste powders so that they can be reutilized instead of being wasted.

If the adsorbent can be produced from the TFT-LCD waste powder, it could be expected that the cost-effectiveness of the CO_2 capture technology and the waste treatment and disposal problem will be resolved simultaneously. Therefore, we aim to develop convenient synthetic procedures for recycling of TFT-LCD waste powder into valuable mesoporous silica materials as supports of adsorbents for the capture of CO_2 from flue gas stream.

Table 2.3 Waste-based CO₂ adsorbent for low temperatures.

Raw material	Sample	Manufacture process	^a S _{BET} (m ² /g)	^b d _{BJH} (nm)	^c V _p (cm ³ /g)	Conditions	Amine type	CO ₂ capacity (mg/g)	Reference
Coal fly ash	MCM-41	Alkali fusion extraction & hydrothermal treatment (100 °C, 48h) Additives: CTAB	^a 610	^b 6.29	^c 1.03	10%, CO ₂ 75 °C	PEI	112	[94]
	SBA-15	Alkali fusion extraction (550°C, 1 h) & hydrothermal treatment (100 °C, 72h) Additives: CTAB	^a 407	^b 7.2	^c 0.7	>99%, CO ₂ 75 °C	PEI	110	[95]
Bottom fly ash	MS	Alkali fusion extraction (600°C, 1 h) & hydrothermal treatment (100 °C, 72h) Additives: P123	^a 847	^b 10.7	^c 1.08	>99%, CO ₂ 75 °C	PEI	118	[96]
	MS-b	Alkali fusion extraction (600°C, 1 h) & hydrothermal treatment (100 °C, 72h) Additives: 1-butanol	^a 785	^b 24.4	^c 1.33	>99%, CO ₂ 75 °C	PEI	153	[96]
	MS-m	Alkali fusion extraction (600°C, 1 h) & hydrothermal treatment (100 °C, 72h) Additives: TMB	^a 986	^b 37.4	^c 2.40	>99%, CO ₂ 75 °C	PEI	178	[96]

	Alkali fusion extraction (550°C, 1 h) &	^a 645	>99%,CO ₂			
SBA-15	hydrothermal treatment (100 °C, 72h)	^b 10.1	75 °C	PEI	169	[97]
	Additives: P123	^c 1.47				
	Alkali extraction (70°C, 24 h) &	^a 1101	>99%,CO ₂			
MCM-41	hydrothermal treatment (100 °C, 72h)	^b 0.96	25 °C	TEPA	40	[98]
	Additives: CTAB	^c 3.54				
	Alkali extraction (70°C, 24 h) &	^a 1099	15%,CO ₂			
MCM-41	hydrothermal treatment (100 °C, 72h)	^b 0.96	75 °C	3-CPA	57	[71]
	Additives: CTAB	^c 3.51				
	Alkali extraction (70°C, 24 h) &	^a 1124	>99%,CO ₂			
Rice husk ash	MCM-48	^b 3.89	25 °C	TEPA	30	[98]
	hydrothermal treatment (100 °C, 48h)	^c 0.98				
	Additives: CTAB	^c 0.98				
	Alkali extraction (77°C) &	^a 1024	1%,CO ₂			
	MCM-48	^b 2.58	25 °C	APTS	28	[78]
	hydrothermal treatment (100 °C,48h)	^c 4.02				
	Additives: CTAB, PLE	^c 4.02				
	Alkali extraction (70°C, 24 h) &	^a 712	>99%,CO ₂			
SBA-15	hydrothermal treatment (40 °C, 24h)	^b 5.82	25 °C	TEPA	30	[98]
	Additives: P123	^c 0.68				

Note: PLE: lauryl ether; 3-CPA: 3-chloropropyl amine hydrochloride; APTS: 3-aminopropyltriethoxysilane

CHAPTER III SILICA MATERIALS RECOVERED FROM OPTOELECTRONIC INDUSTRIAL WASTE POWDER: ITS EXTRACTION, MODIFICATION, CHARACTERIZATION AND APPLICATION

3.1 Motivation

Unlike the coal fly ash or rice husk ash which contains lots of complicated metal oxides [8,9], the primary components of optoelectronic waste powder might only contain Si-, N- and F- species. Thus it would be more facile to be utilized as the silica source since high purity of silica could be obtained. In the present investigation, attempts have been made to evaluate the chemical composition of the optoelectronic waste powder as well as to recover the supernatant and the sediment into valuable resources. The supernatant is used as the silica source for the synthesis of MCM-41.

3.2 Experimental

3.2.1 Alkali extraction of silicate supernatant from optoelectronic waste powder

The extraction of silica was carried out through alkali fusion treatment [99]. In a typical process, the waste powder and NaOH powder were thoroughly mixed at a weight ratio of 1:1.2 and fused at 550 °C for 1 h. The received fused product was then mixed with DI water at a weight ratio of 1:5 with continuous stirring for 24 h. The resulting mixture was then centrifuged to separate the sediment for further characterization of its components. And the supernatant was also analyzed by ICP-MS (SCIEX ELAN 5000- Inductively Coupled Plasma-Mass Spectrometer) and utilized for the synthesis of MCM-41.

3.2.2 Hydrothermal synthesis of MCM-41(PWP) using waste silicate supernatant

Mesoporous silica materials of MCM-41 were synthesized by hydrothermal treatment method using either waste derived silica or pure silica source as the precursor solutions. Cetyltrimethylammonium bromide (CTAB) was employed as the

structure-directing template in the synthesis. For the optoelectronic waste derived MCM-41, the molar composition of the gel mixture was 1 SiO₂ : 0.2 CTAB : 0.89 H₂SO₄ : 120 H₂O, where the SiO₂ precursor source was obtained from the supernatant of optoelectronic waste powder extraction process. In a typical synthesis procedure, 50 ml of supernatant was firstly stirred vigorously for 30 min. Then, the pH of the solution was brought down to 10.5 using 4N H₂SO₄ followed by further stirring to form a gel. After that 4.6 g of CTAB (dissolved in 16 ml of DI water) was added drop by drop into the above mixture and the combined mixture was stirred for three additional hours. The resulting gel mixture was transferred into a Teflon coated autoclave and kept in an oven at 145°C for 36 h. After cooling to room temperature, the resultant solid was recovered by filtration, washed with DI water and dried in an oven at 110°C for 6 h. Finally, the organic template was removed via a muffle furnace in air at 550°C for 6 h. The MCM-41 material synthesized from optoelectronic waste powder (PWP) was named as MCM-41(PWP).

3.2.3 Analysis and characterization

Powder X-ray diffraction patterns of calcined mesoporous adsorbents were recorded by X-ray diffractometer (Bruker D8 SSS) equipped with nickel-filtered CuK α ($\lambda = 1.5405 \text{ \AA}$) radiation. The diffractograms of the mesoporous samples were recorded in the 2θ range of 1-50° with a scanning speed of 1 degree per minute. The specific surface area, pore volume and average pore diameter (BJH method) of the samples were measured by N₂ adsorption-desorption isotherms at -196 °C using a surface area analyzer (Micromeritics, ASAP 2000). All the samples were degassed for 6 hours at 350 °C under vacuum (10⁻⁶ mbar) prior to the adsorption experiments. The ²⁹Si MAS-NMR spectra of the as-synthesized mesoporous silica were recorded at room temperature using a BRUKER DSX 400 WB NMR spectrometer. The elemental analysis and morphologies of the materials was observed by energy-dispersive X-ray spectroscopy in a scanning electron microscope (SEM/EDS, HITACHI-S4700). And transmission electron microscopy (TEM) images of the samples were observed with a JEOL JEM 1210 TEM instrument operated at 120 keV, with the samples (5-10 mg) ultrasonicated in ethanol and then dispersed on carbon film supported by copper grids (200 mesh).

3.3 Results and discussion

3.3.1 Characterization of optoelectronic waste powder

The results of EDS and FTIR analyses for the optoelectronic waste powder are shown in [Figure 3.1](#), and the weight percentages of each element in the optoelectronic waste powder are listed in [Table 3.1](#). As can be seen from [Figure 3.1\(a\)](#), the four observed elements of Si, O, N and F in the optoelectronic waste powder were expected since the solid waste was derived from the CVD process in which the three gaseous reactants were SiH₄, NF₃ and NH₃. Furthermore, the FTIR spectrum of optoelectronic waste powder shown in [Figure 3.1\(b\)](#) exhibited significant absorption bands at 3336, 3139, 1400, 1080, 960, 742 and 482 cm⁻¹. The bands at 3336 and 3139 cm⁻¹ are related to N-H stretching, while 742 and 482 cm⁻¹ can be assigned to SiF₆²⁻ [100]. Besides, the bands at 1400, 1080 and 960 cm⁻¹ can be assigned to the NH₄⁺ [100], Si-O-Si and Si-OH stretching vibrations, respectively [101]. Considering the above results, the primary components in optoelectronic waste powder could be the admixture of (NH₄)₂SiF₆ and SiO₂.

The XRD analysis was then carried out to further identify the crystalline components in the optoelectronic waste powder with the result depicted in [Figure 3.2](#). Strong (NH₄)₂SiF₆ diffraction peaks were identified [102]. In contrast, the diffraction peak of silica was not observed from the XRD pattern, suggesting that SiO₂ was only present in little amount and it might be trapped in the (NH₄)₂SiF₆ lattice. However the precise weight percentages of (NH₄)₂SiF₆ and SiO₂ could not be obtained from [Table 3.1](#) since the EDS data only provided a rough estimate of the elemental content, while the ICP-MS could only detect the Si content in the optoelectronic waste powder.

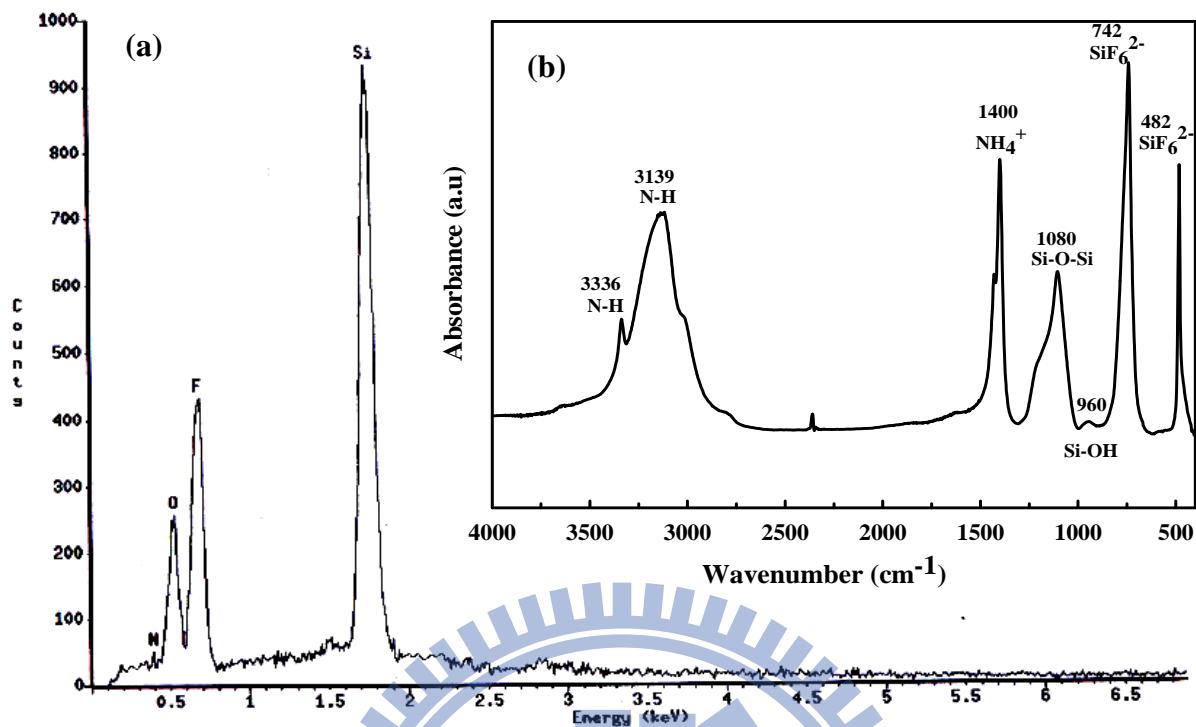


Figure 3.1 (a) EDS spectrum and (b) FTIR spectrum of the optoelectronic waste powder.

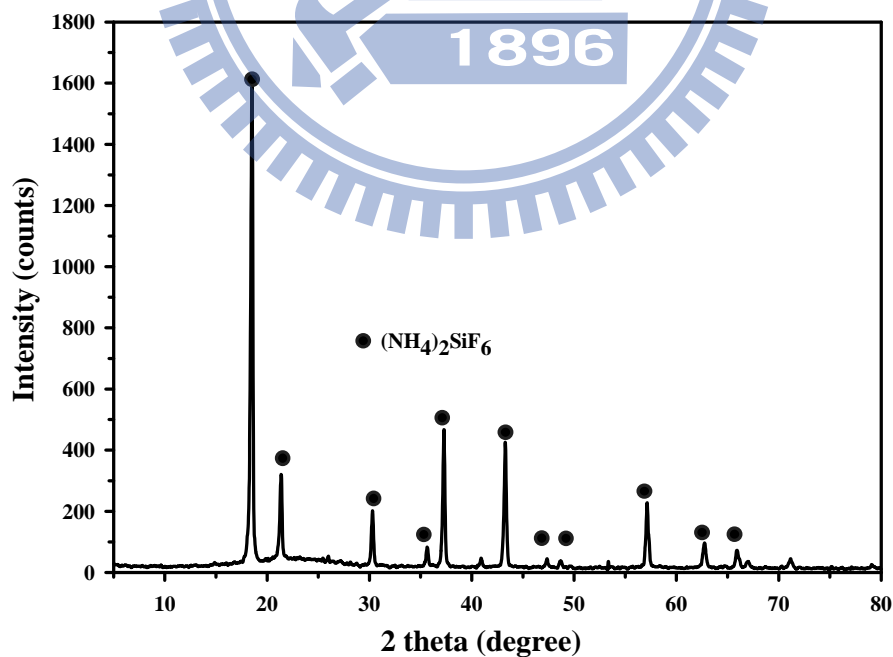


Figure 3.2 XRD pattern of the optoelectronic waste powder.

The weight percentages of $(\text{NH}_4)_2\text{SiF}_6$ and SiO_2 presented in the optoelectronic waste powder were determined using TGA weight loss and differential thermo-gravimetric (DTG) analyses. It can be seen from [Figure 3.3\(a\)](#) that the optoelectronic waste powder sample showed an initial weight loss at $<150^\circ\text{C}$, which could be ascribed to the evaporation of the physically adsorbed water on the surface of the materials. As the temperature exceeded 150°C , there was a significant weight loss for the optoelectronic waste powder at around 237°C as clearly observed from [Figure 3.3\(b\)](#). Mel'nichenko et al. [103] investigated the mechanism of the solid-phase reaction between $(\text{NH}_4)_2\text{SiF}_6$ and SiO_2 , and proposed that $(\text{NH}_4)_2\text{SiF}_6$ could be thermally decomposed between $220\text{-}300^\circ\text{C}$ in the presence of SiO_2 . Generally, the following chemical reactions are expected to take place when $(\text{NH}_4)_2\text{SiF}_6$ was heated up to 900°C [102]:



Considering the above reactions, $(\text{NH}_4)_2\text{SiF}_6$ would be completely decomposed during the thermal treatment up to 900°C . However, it is noted that there was still 15 wt. % of residues remained after heating up the optoelectronic waste powder to 900°C . This is probably due to the presence of SiO_2 since it is thermally stable up to 900°C . The total Si weight fraction (from $(\text{NH}_4)_2\text{SiF}_6$ and SiO_2) of 20.4% calculated by the TGA/DTG result was very close to the Si mass fraction of 22.4% detected by the ICP-MS result shown in [Table 3.1](#). Therefore, the primary components in optoelectronic waste powder were determined to be around 85% of $(\text{NH}_4)_2\text{SiF}_6$ and 15% of SiO_2 from the results of TGA, FTIR and SEM-EDS analysis.

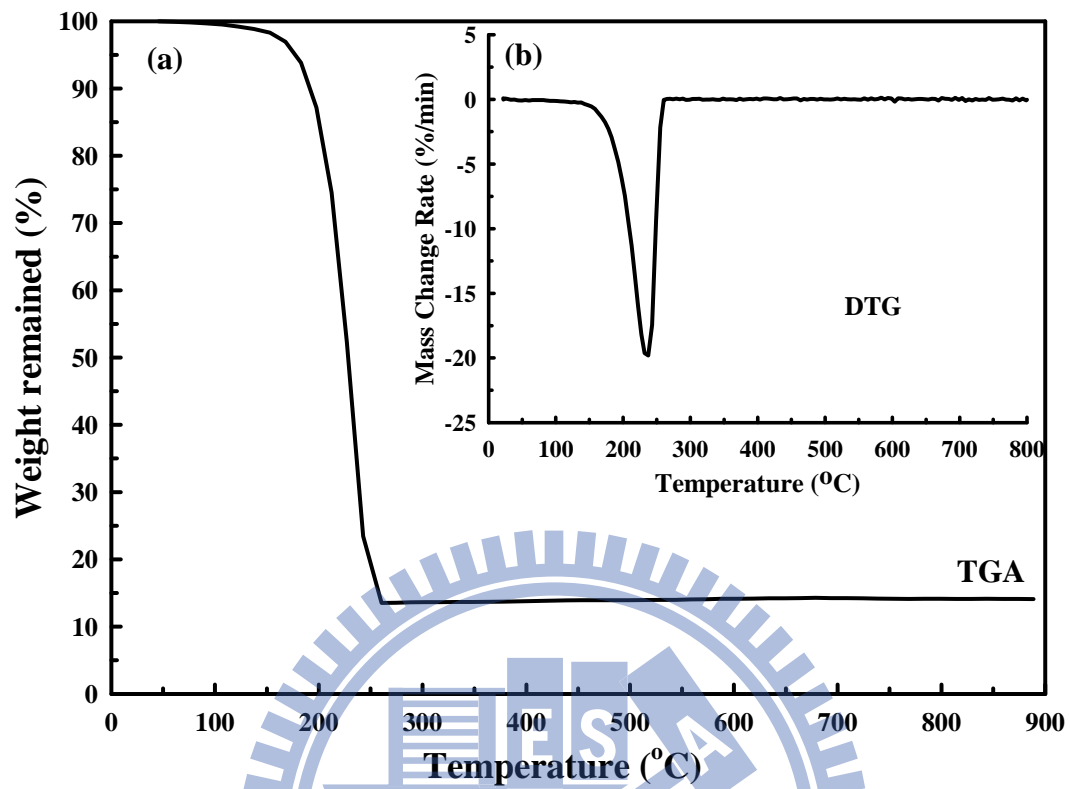


Figure 3.3 (a) TGA analysis and (b) DTG profile of the optoelectronic waste powder.

3.3.2 Characterization of sediment and supernatant liquid after extraction

Figure 3.4 shows the EDS spectrum of the sediment and its corresponding XRD pattern. It can be found from Figure 3.4(a) that Na and F were the primary elements in the sediment, with negligible Si and O species, which was also confirmed by the result of EDS analysis shown in Table 3.1. The residual SiO₂ could be due to insufficient NaOH amounts applied in the extraction process. The major component of NaF presented in the sediment was also demonstrated by Figure 3.4(b). The five sharp diffraction peaks located at 34, 39, 56, 67 and 70.5° were in agreement with the NaF standard XRD peaks [104,105]. Besides, there was a broad peak centering at 22° as observed from Figure 3.4(b), which can be ascribed to the amorphous SiO₂ [106]. This result is consistent with the EDS spectrum which showed that Si and O species were also presented in minor amounts.

The thermal behavior of the sediment was subsequently investigated using TGA and DTG analyses. It can be seen from Figure 3.5(a) that there was only around 5% weight loss for the sediment during the thermal treatment up to 900 °C. The DTG curve showed three distinguished peaks from room temperature to 900 °C (Figure 3.5(b)). The first step (<150 °C) is due to the loss of physically adsorbed water on the surface of the sediment and the second step (150-600°C) is attributed to the loss of chemically adsorbed water bonded to Si-OH through hydrogen bond [107] since the sediment contained only a little amount of SiO₂. From 600 to 900 °C, the weight loss is expected to be associated with the further condensation of the Si-OH groups from the amorphous SiO₂ [106].

As a result, one can conclude that F was effectively captured by NaOH and the sodium fluoride (NaF) sediments were formed after the extraction process. The NaF purity was quite high (>90%) in the sediment as observed from the TGA/DTG data, which provides further possibility for reuse. Sodium fluoride is one of the well-known chemical compounds which are widely utilized in industries as the source of fluoride ion in diverse applications. In other words, the optoelectronic waste powder can be converted into two valuable resources, the supernatant as the silica precursor and the sediment of sodium fluoride.

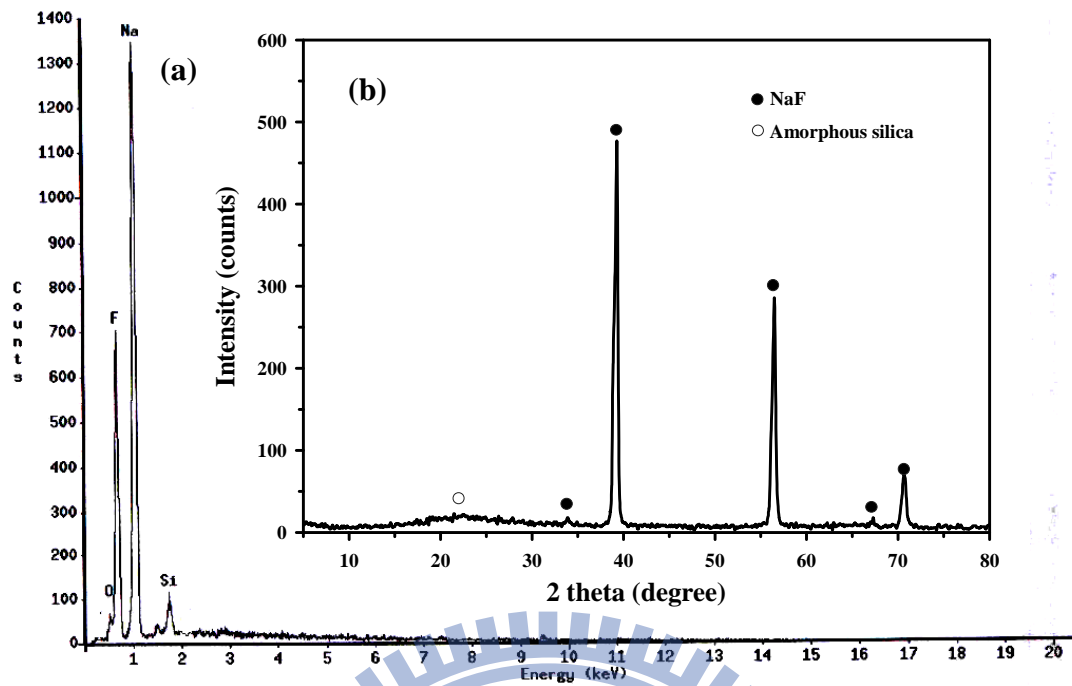


Figure 3.4 (a) EDS spectrum and (b) XRD pattern of the sediment after silica extraction.

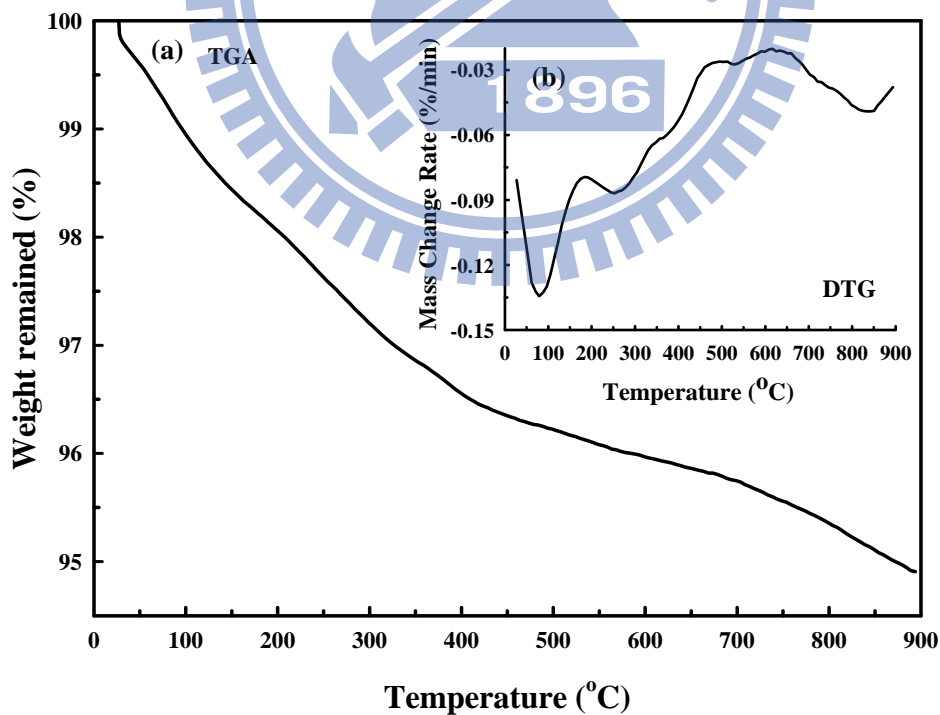


Figure 3.5 (a) TGA analysis and (b) DTG profile of the sediment.

The composition of the supernatant was also analyzed by ICP-MS in order to investigate the concentrations of Si and Na ions. [Table 3.1](#) shows that the concentrations of Si and Na ions were 13080 and 33180 ppm, respectively. The concentration ratio between Na and Si is 2.54 in this study. It is lower than the Na/Si ratio of silica supernatant recovered from fly ash [99] in which the Si and Na concentrations were 572 and 12000 ppm, respectively. [Chang et al.](#) [108] stated that the high concentration ratio of Na/Si in the precursor tended to hinder the mesostructure and thus the MCM-41 obtained from fly ash supernatant could not exceed 1000 m²/g. In comparison, the silica supernatant obtained from the optoelectronic waste powder could be a better source for producing high quality waste-derived MCM-41.

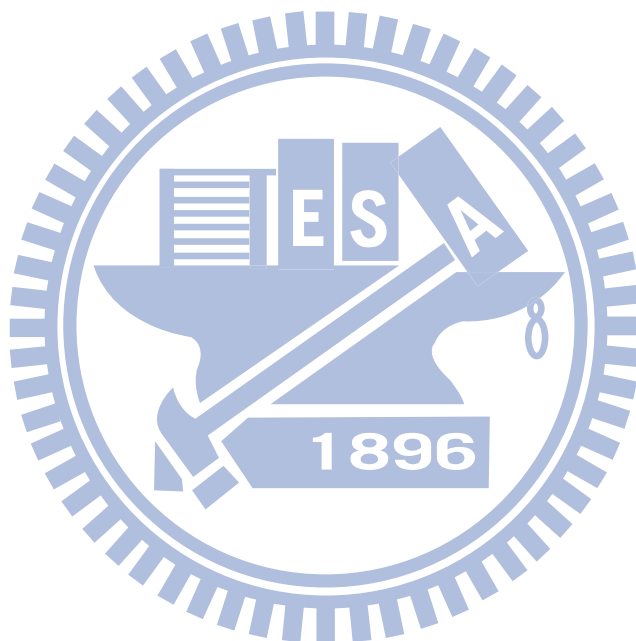


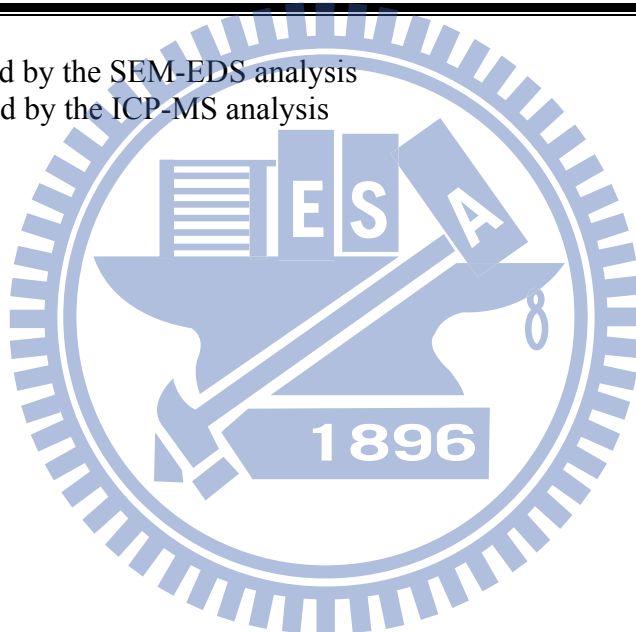
Table 3.1 Elemental analysis of optoelectronic waste powder and sediment analyzed by the SEM-EDS and ICP-MS analyses

Element	Si	F	O	N	Na
^a Optoelectronic waste powder (wt%)	28.82	47.82	17.54	5.82	-
^a Sediment (wt%)	5.22	33.34	2.99	- ^c	58.45
^b Optoelectronic waste powder (wt%)	22.35	-	-	-	-
^b Supernatant (ppm)	13080	-	-	-	33180

a: sample analyzed by the SEM-EDS analysis

b: sample analyzed by the ICP-MS analysis

c: not detected.



3.3.3 Characterization of MCM-41(PWP)

Figure 3.6(a) shows the EDS spectrum of the MCM-41 sample synthesized from the optoelectronic waste powder. It can be seen that only Si and O elements were present in MCM-41(PWP) indicating that alkali fusion treatment is a viable process to effectively separate silicate species from the PWP derived silica. Figure 3.6(b) illustrates the powder XRD patterns of the MCM-41(PWP) and MCM-41(NaSi) samples. One can see that MCM-41(NaSi) sample exhibited a well-defined (100) diffraction peak located at 2θ of $2.3\text{--}2.6^\circ$ and three reflections of (110), (200) and (210) at 4.2 , 4.7 and 6.2° , respectively, which could be indexed on a hexagonal lattice of mesoporous silica materials [109–111]. Similar observation was also seen for the MCM-41(PWP) sample, thus indicating that highly ordered mesostructure was obtained using the supernatant extracted from optoelectronic waste powder as the silica source.

The N_2 adsorption-desorption isotherms of optoelectronic waste powder, MCM-41(NaSi) and MCM-41(PWP) are shown in Figure 3.7. It is clear that optoelectronic waste powder exhibited a typical type II isotherm of non-porous materials according to the IUPAC classification. On the other hand, both MCM-41(NaSi) and MCM-41(PWP) possessed type IV isotherms which are the characteristic of mesoporous materials, featuring a narrow step due to capillary condensation of N_2 within the primary mesopores [112,113]. The isotherms of the MCM-41(NaSi) and MCM-41(PWP) also showed the type H1 hysteresis loop associated with well-arranged cylindrical channels with uniform shape and pore size [114]. However, the less steep condensation step for MCM-41(PWP) sample indicates a lesser degree of uniform mesostructure as compared to that of MCM-41(NaSi) sample. This was expected since the silica precursor of MCM-41(PWP) could not be in such a high purity as the pure chemical of Na_2SiO_3 for producing MCM-41(NaSi).

Figure 3.8 displays the BJH pore size distributions of MCM-41(NaSi) and MCM-41(PWP) samples. It is clear that MCM-41(NaSi) sample showed a narrow pore size distribution with the peak pore size at 2.7 nm, suggesting the uniform porosity of the obtained materials. The MCM-41(PWP) also showed a narrow pore size distribution with the peak size at around 3.0 nm. But a small peak located at around 4 nm was also observed. The bimodal mesoporosity would result in less uniformity of mesostructure of MCM-41(PWP).

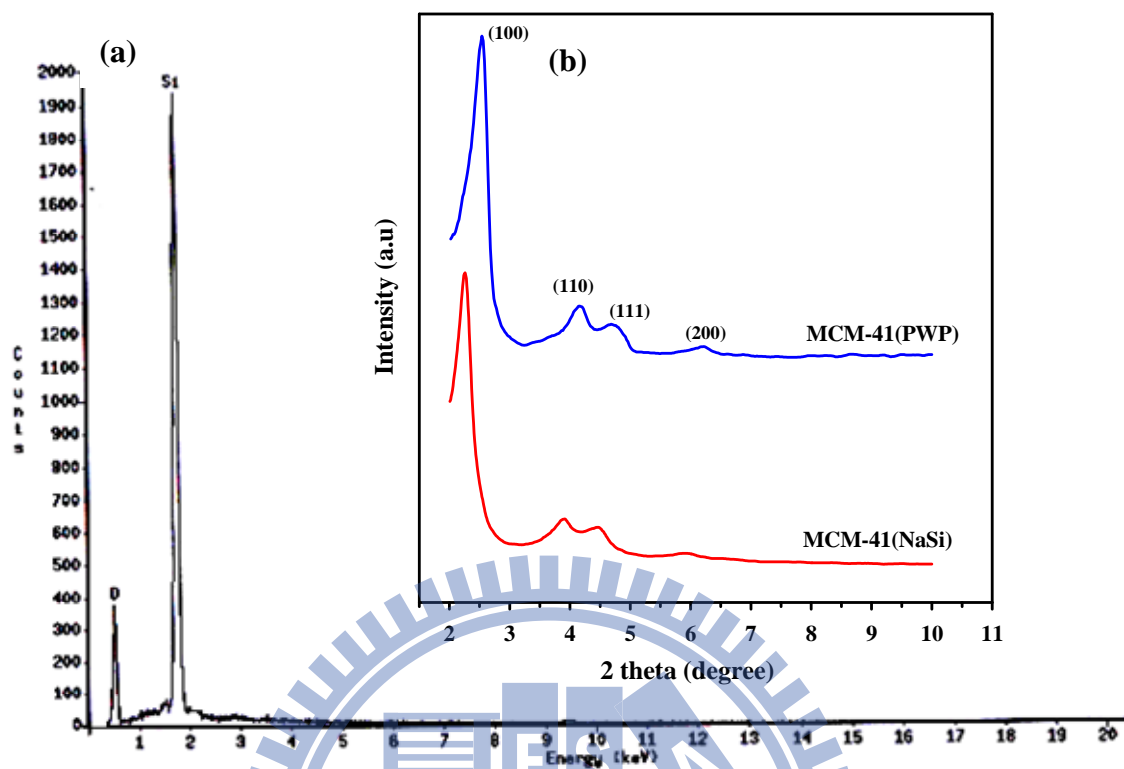


Figure 3.6 (a) EDS spectrum of MCM-41(PWP) sample and (b) XRD patterns of the MCM-41(PWP) and MCM-41(NaSi) samples.

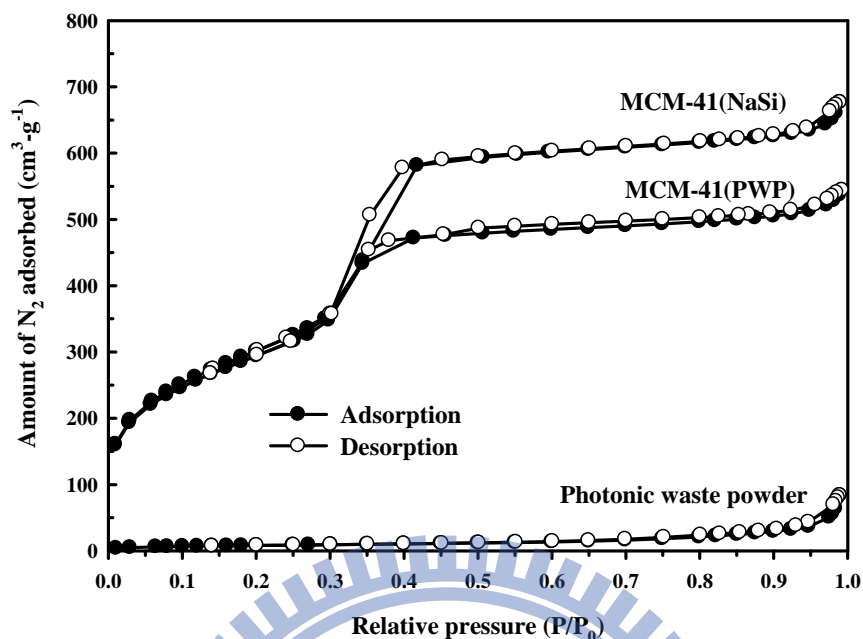


Figure 3.7 N_2 adsorption-desorption isotherms of the optoelectronic waste powder, calcined MCM-41(NaSi) and MCM-41(PWP) samples.

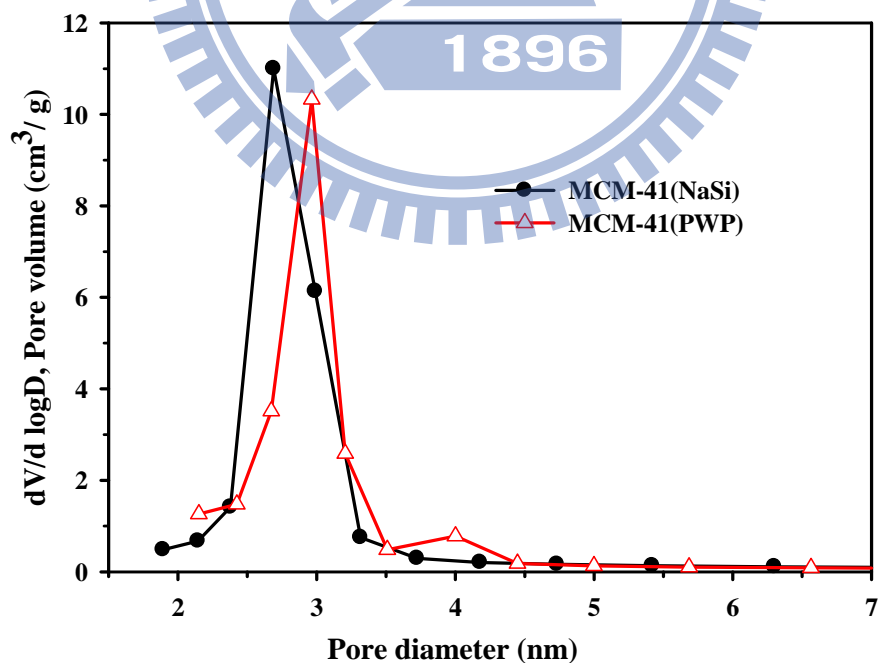


Figure 3.8 BJH pore diameter distributions of calcined MCM-41(NaSi) and MCM-41(PWP) samples.

The physicochemical properties of BET specific surface area, specific pore volume and average pore diameter derived from the N₂ adsorption-desorption measurements are summarized in [Table 3.2](#). To check the stability of using the optoelectronic waste powder for preparing the MCM-41(PWP), duplicate experiments were performed and the BET characterization of the two MCM-41(PWP) samples prepared from two different batches of waste powder showed that there was negligible effect on the sample pore structure. This could be attributed to the fact that the solid waste powder was obtained from the same TFT-LCD plant, which controls their process precisely and stably. It can be observed that MCM-41(PWP) possessed high specific surface area (1082 m²/g), narrow pore size distribution (2.95 nm) and large pore volume (0.99 cm³/g) which are fairly closed to the properties of MCM-41(NaSi). The slight shrinkage in the pore volume of MCM-41(PWP) could be due to the higher amounts of Na ions in the supernatant [99]. However, the effect of the higher Na concentration was very minor which could be attributed to precise pH-controls during the synthesis of the MCM-41(PWP).

The textural mesostructure of the MCM-41(NaSi) and MCM-41(PWP) samples were further revealed by TEM images shown in [Figure 3.9\(a\)](#) and [Figure 3.9\(b\)](#), respectively. The TEM image of MCM-41(PWP) material ([Figure 3.9\(b\)](#)) clearly shows a well ordered long range hexagonal array of mesopores similar to that of the MCM-41(NaSi) material ([Figure 3.9\(a\)](#)), and these long range crystallographic features are consistent with the results of XRD and BET analyses. The pore diameter observed in [Figure 3.9\(b\)](#) was ca. 3.2 nm which was fairly close to the narrow pore size distribution (BJH) determined by N₂ adsorption-desorption measurements, indicating that the pore structure of MCM-41(PWP) is highly ordered.

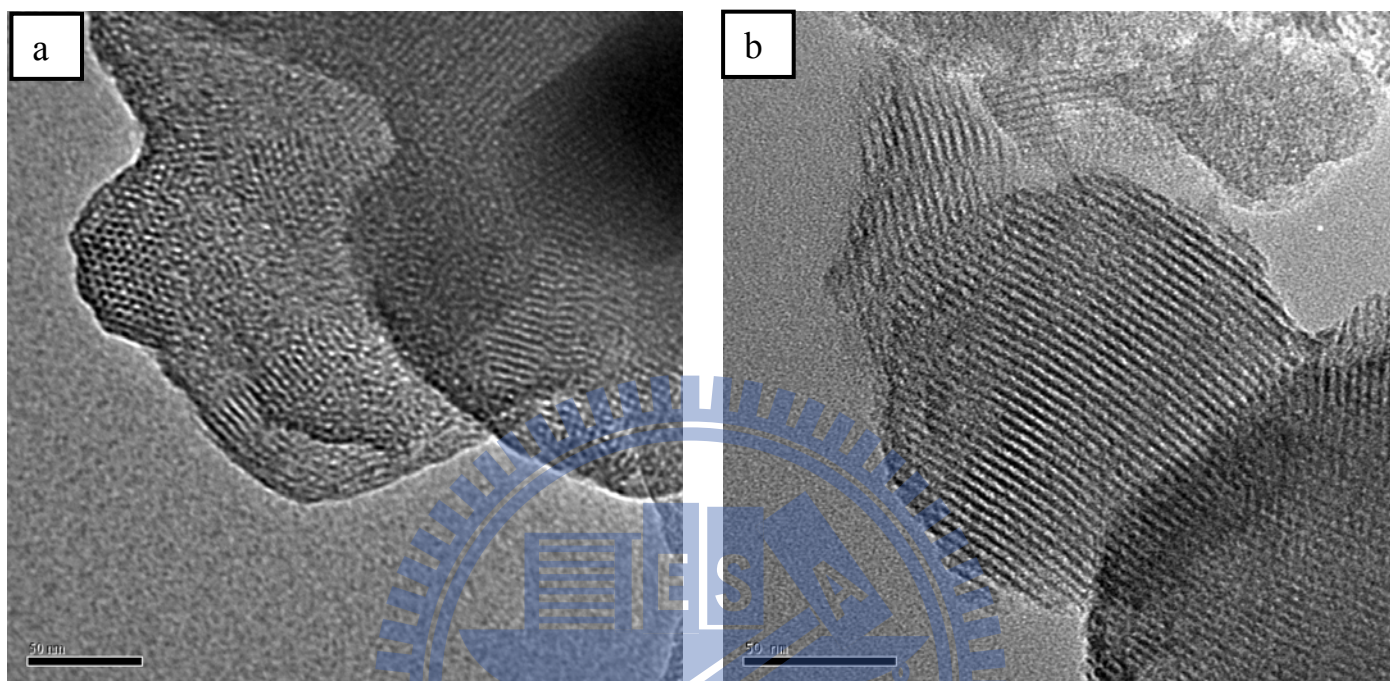


Figure 3.9 TEM images of MCM-41(NaSi) and MCM-41(PWP) samples.

Table 3.2 Physical properties of optoelectronic waste powder and mesoporous adsorbents

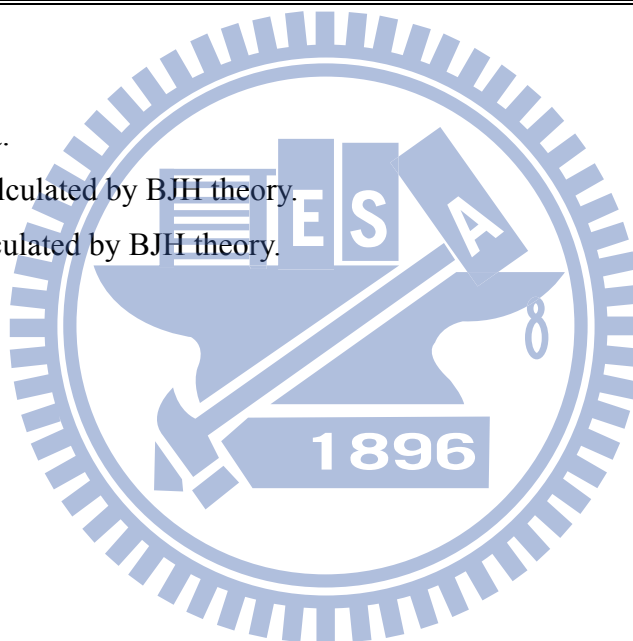
Sample name	^a S _{BET} (m ² /g)	^b D _p (nm)	^c V _p (cm ³ /g)
Optoelectronic waste powder	30	-	0.07
MCM-41(NaSi)	1102	3.0	1.13
MCM-41(PWP)	1082±13	2.95±0.05	0.99±0.02

NOTE:

^aBET surface area.

^bPore diameter calculated by BJH theory.

^cPore volume calculated by BJH theory.



CHAPTER IV DIRECT CONVERSION OF WASTE POWDER INTO MESOPOROUS SILICA MATERIALS

4.1 Direct synthesis of MCM-41-like materials from optoelectronic waste powder

4.1.1 Motivation

Our prior study demonstrated the possibility of extracting silicate supernatant from optoelectronic waste powder which was obtained from the exhaust of CVD process in TFT-LCD plants. The alkaline fusion method was employed in our prior study and the obtained supernatant was further utilized for manufacturing silica materials. However, the disadvantages of alkaline fusion method for extracting the silicon from solid wastes are the long processing period (~24 h) and the low silicon recovery yield (20-33 %) [6,114]. Thus the industrial application of this fusion process would have certain limitations. An efficient and low energy method for the total recycling of optoelectronic waste powder into valuable mesoporous silica must be developed. In this part, a fast and low energy-consumed approach on the direct use of optoelectronic waste powder for complete recycling into silica resources is proposed. Detailed characterization and formation mechanism of silica materials via the direct usage of waste powder were investigated and discussed.

4.1.2 Synthesis

Mesoporous silica was synthesized via the direct utilization of waste powder as the silica source and cetyltrimethylammonium bromide (CTAB) was employed as the structure-directing template. The molar composition of the gel mixture was 1 SiO₂ : 0.2 CTAB : xHF : 12 NH₄OH : 120 H₂O (x varies with molar ratio of HF/Si). In a typical procedure, 9.35 g of waste powder was firstly dissolved in 137 ml of DI water. Subsequently, a given amount of hydrofluoric acid was added into the above solution. Meanwhile, 7.28 g of CTAB was dissolved in 25 ml of DI water and then it was added dropwise into the above solution. Then, 32.06 g of ammonium hydroxide solution was slowly added to promote the hydrolytic condensation of silica-surfactant mixture. All the above procedures were performed under continuous stirring. The resulting gel

mixture was aged at room temperature for 8 h; the resultant solid was recovered by filtration, washed with DI water and dried in an oven at 110°C for 6 h. Finally, the organic template was removed by using a muffle furnace in air at 550°C for 6 h. The mesoporous MCM-41 synthesized by direct usage of waste powder as the silica source in the absence of hydrofluoric acid was denoted as MCM-41(DU), while the MCM-41 sample synthesized by direct usage of waste powder in the presence of hydrofluoric acid was denoted as MCM-41(DU)-F.

4.1.3 CO₂ adsorption measurement

Tetraethylenepentamine (TEPA) was selected as the amine agent to enhance the adsorption performance of the mesoporous materials on capturing CO₂ gas. Mesoporous adsorbents were mixed with TEPA at a weight ratio of 1:1 in ethanol by the wet impregnation method. The mesoporous adsorbents were preheated at 120 °C for 1 h. And then TEPA was mixed with ethanol and the resulting solution was stirred for 30 min. After pretreatment, the mesoporous adsorbents were dispersed into the flask containing TEPA solution and the mixture was then refluxed at 80 °C for 2 h. After cooling to room temperature, the obtained materials were dried at 60 °C.

To obtain the adsorption capacity and breakthrough curve of the adsorbents, CO₂ adsorption experiment was carried out in a packed column with an internal diameter of 0.75 cm. The adsorption column was packed with 1.0 g of adsorbents (packing height = ~ 5 cm) and placed in a temperature-controlled oven. In a typical process, adsorbents were pretreated under a N₂ flow of 0.1 L/min at 110 °C for 1 h, and then cooled to 60 °C. Subsequently, the gas flow was switched to 10% (v/v) CO₂ gas stream (balanced with N₂) under a flow rate of 0.1 L/min. The concentration of CO₂ was continuously measured by a CO₂ analyzer (Molecular Analytics AGM 4000 Gas Analyzer). The CO₂ adsorption capacity (q, mg/g) at a certain time (t, time) was estimated as

$$q = \frac{1}{m} \int_0^t Q \times (C_{in} - C_{eff}) dt \quad (1)$$

where m is the weight of adsorbent (g), Q is the gas flow rate (L/min), and C_{in} and C_{eff} are the influent and effluent CO₂ concentrations (mg/L), respectively, which are expressed in terms of percent in volume (%). The adsorption capacity of zero gas (N₂

only) was deducted from the adsorption capacities of adsorbents.

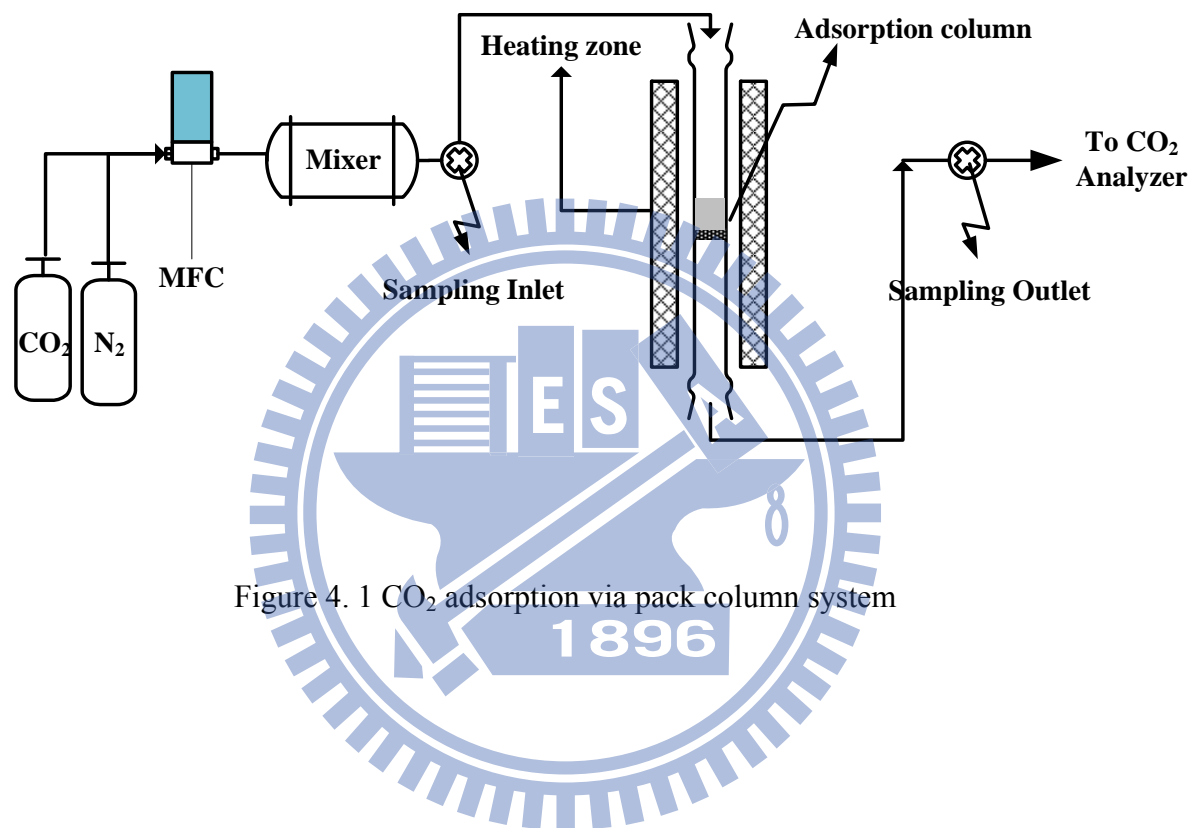
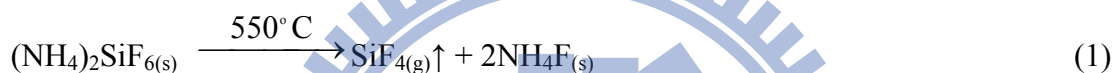


Figure 4. 1 CO₂ adsorption via pack column system

4.1.4 Results and discussion

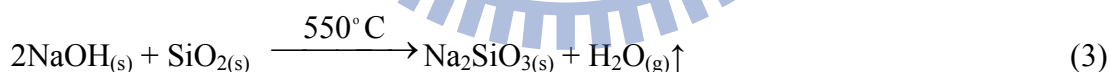
Figure 4.2(a) and Figure 4.2(b) respectively depicts the alkaline fusion process and the direct utilization process for the recovery of silica materials from the optoelectronic waste powder. For alkaline fusion process, the formation mechanism of silica materials from optoelectronic waste powder can be explained by considering the chemical reactions presented in Equations (1)-(3). In brief, optoelectronic waste powder consisting of $(\text{NH}_4)_2\text{SiF}_6$ and SiO_2 was decomposed into gaseous silicon tetrafluoride (SiF_4) and ammonium fluoride (NH_4F) solid residue when the temperature was above $220\text{ }^\circ\text{C}$ [115]:



Subsequently, the remaining NH_4F which is thermally stable up to $850\text{ }^\circ\text{C}$ would react with sodium hydroxide to produce gaseous ammonia and sodium fluoride solid residue:



Meanwhile, the SiO_2 presented in optoelectronic waste powder would also react with sodium hydroxide to produce sodium silicate:



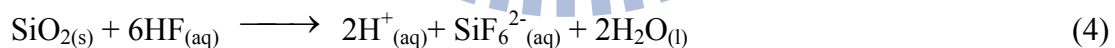
The obtained sodium silicate was then utilized as the silica source to synthesize mesoporous MCM-41 in the presence of cationic surfactant of CTAB via hydrothermal treatment at $145\text{ }^\circ\text{C}$ for 36 h as shown in Figure 4.2(a). Therefore, the gaseous pollutants of SiF_4 and NH_3 tend to be formed during the alkaline fusion process for waste recovery.

The optoelectronic waste powder is mainly composed of 85% of $(\text{NH}_4)_2\text{SiF}_6$ and 15% of SiO_2 and the total Si mass fraction (from $(\text{NH}_4)_2\text{SiF}_6$ and SiO_2) detected by ICP-MS analysis is 22.4% as obtained from our prior study. Silicon recovery yield was determined by the weight ratios of silicon contents in the raw waste powder and the silicon contents in the obtained mesoporous silica materials. It is noted from

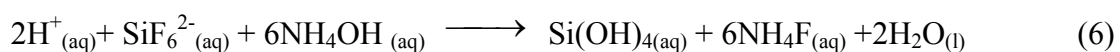
Figure 4.2(a) that there is only 28% of silicon recovery yield for the MCM-41(AF) obtained via the alkaline fusion process. This is similar with the report by Chang and colleagues, who employed the alkaline fusion method for extracting silicon from coal fly ash and the silicon recovery yield was ca. 32% [108]. They stated that sufficient amount of sodium hydroxide and activation time are required for effective converting silica in the form of quartz and mullite phases into more soluble form of sodium silicate during the fusion process.

In the present study, the decomposition of $(\text{NH}_4)_2\text{SiF}_6$ at 550 °C results in losing silicon species from the release of gaseous silicon tetrafluoride. It is reasonable that the silicon recovery yield would be significantly affected by the loss of silicon species from gaseous silicon tetrafluoride since the optoelectronic waste powder is mainly composed of 85% of $(\text{NH}_4)_2\text{SiF}_6$ and 15% of SiO_2 . Therefore, even though the MCM-41(AF) with very high specific surface area can be manufactured, the alkaline fusion process might not be considered as an economic and energy effective approach due to its low silicon recovery yield, long processing time, gaseous pollution formation and high operational temperature.

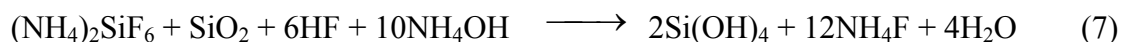
Figure 4.2(b) reveals the direct utilization process proposed in this study. In a typical process, the optoelectronic waste powder was first treated with hydrofluoric acid. It is expected that the SiO_2 presented in optoelectronic waste powder would react with hydrofluoric acid to produce hexafluorosilicic acid (H_2SiF_6) and the chemical reaction is presented as follows:



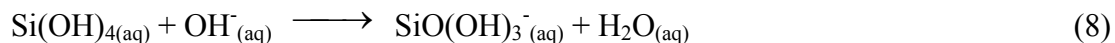
Subsequently, the hydrolysis of $(\text{NH}_4)_2\text{SiF}_6$ and SiF_6^{2-} can be accelerated by the addition of ammonium hydroxide:



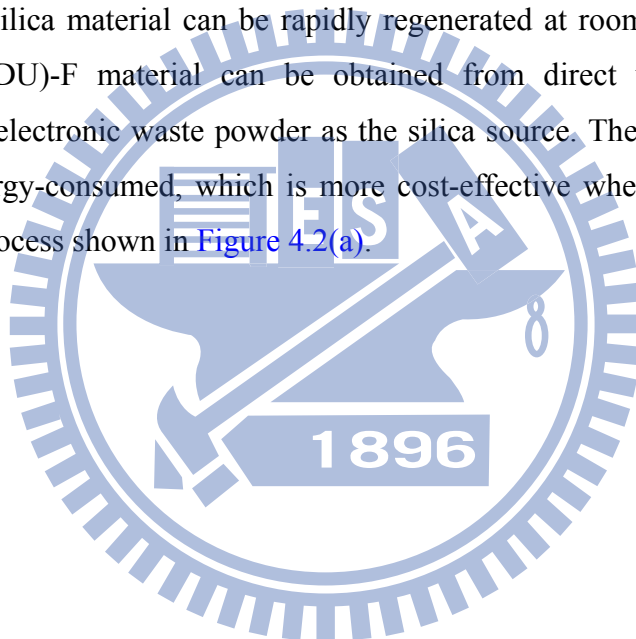
Therefore, the overall reactions for the recovery of silica materials from optoelectronic waste powder in the presence of hydrofluoric acid and ammonium hydroxide can be summarized as follows:



Also it is well-known that the ionization of the $\text{Si}(\text{OH})_4$ produces anion silicate such as $\text{SiO}(\text{OH})_3^-$ and the condensation rate can be greatly enhanced using basic catalyst:



The ionization of the $\text{Si}(\text{OH})_4$ makes silanol more electrophilic and thus more susceptible to react with the cationic surfactants of CTAB by electrostatic force. Finally, the cooperative assembly between the anionic silicate hydrolyzed from SiF_6^{2-} and free charged micelles undergo extensive condensation and polymerization, thus the mesoporous silica material can be rapidly regenerated at room temperature. The novel MCM-41(DU)-F material can be obtained from direct use and complete recycling of optoelectronic waste powder as the silica source. The process is simple, fast and low energy-consumed, which is more cost-effective when compared to the alkaline fusion process shown in [Figure 4.2\(a\)](#).



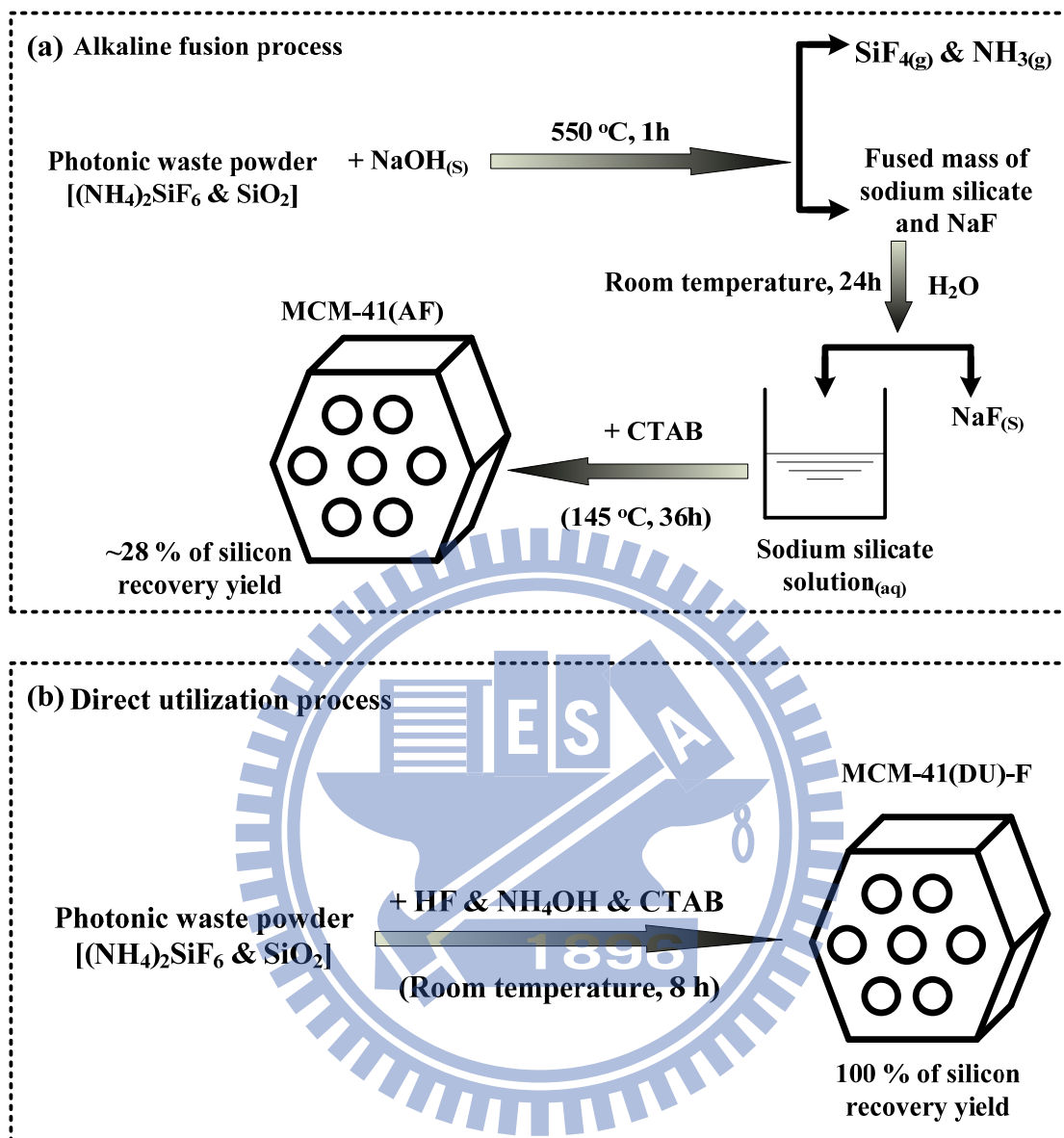
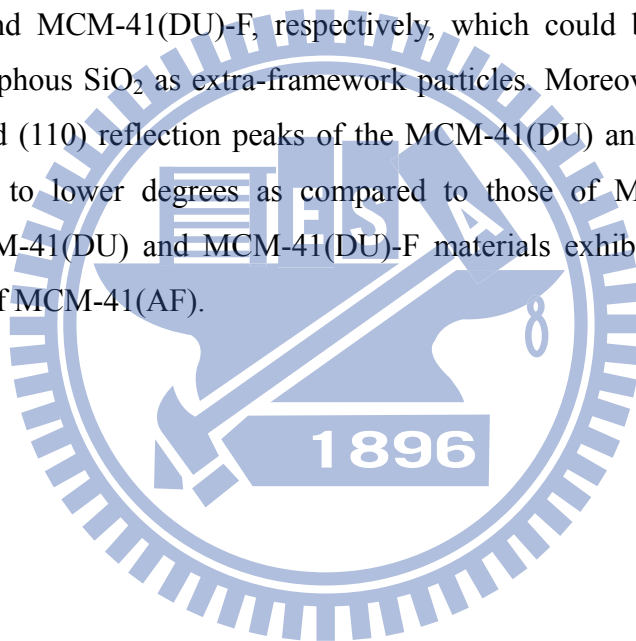


Figure 4.2 Schematic procedures for (a) conventional alkaline fusion process and (b) direct utilization process for the recovery of mesoporous silica from the optoelectronic waste powder.

Low angle powder X-ray diffraction patterns of MCM-41(DU), MCM-41(DU)-F and MCM-41(AF) are shown in [Figure 4.3\(a\)](#). The results reveal the presence of the hexagonal lattice of the MCM-41(AF) material prepared via alkaline fusion process, where two well-defined diffraction peaks of (100) and (110) located at 2θ of 2.5° and 4.1° were observed [19]. Similarly, MCM-41(DU) and MCM-41(DU)-F materials also exhibit two diffraction peaks of (100) and (110) located at 2θ of 1.7° and 3.5° , indicating that the silica materials with hexagonal mesostructure can be obtained by direct usage of optoelectronic waste powder as the silica source. It can be observed that MCM-41(DU)-F shows higher intensity of (100) reflection than that of MCM-41(DU), which suggests better pore arrangement of the MCM-41(DU)-F. On the other hand, there is a broad peak centering at 22° observed in [Figure 4.3\(b\)](#) for the MCM-41(DU) and MCM-41(DU)-F, respectively, which could be ascribed to the presence of amorphous SiO_2 as extra-framework particles. Moreover, it is noticeable that the (100) and (110) reflection peaks of the MCM-41(DU) and MCM-41(DU)-F materials shifted to lower degrees as compared to those of MCM-41(AF). This implies that MCM-41(DU) and MCM-41(DU)-F materials exhibit larger d-spacing values than that of MCM-41(AF).



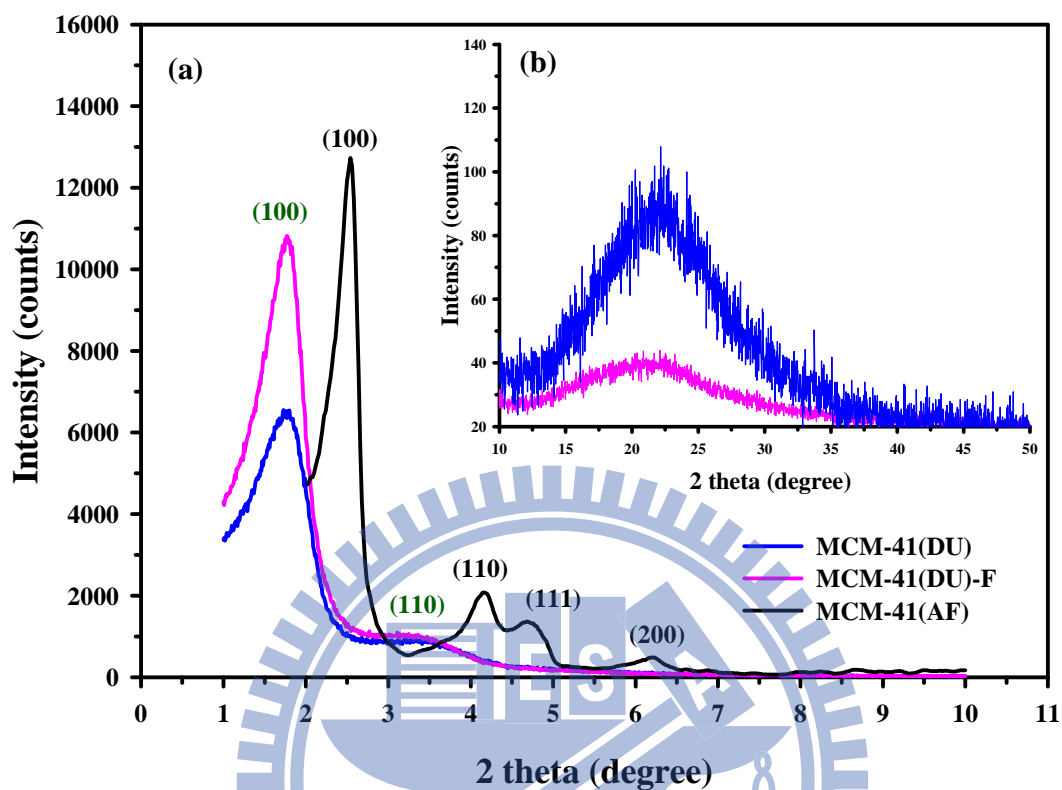


Figure 4.3 (a) Low angle XRD patterns of MCM-41(DU), MCM-41(DU)-F as well as MCM-41(AF) and (b) wide angle XRD patterns of MCM-41(DU) and MCM-41(DU)-F samples.

The N₂ adsorption-desorption isotherms of the waste powder, MCM-41(AF), MCM-41(DU) and MCM-41(DU)-F samples are plotted in [Figure 4.4](#). Apparently, the optoelectronic waste powder revealed a typical type II isotherm of non-porous materials according to the IUPAC classification. On the other hand, MCM-41(AF), MCM-41(DU) and MCM-41(DU)-F samples clearly show capillary condensation steps with H1 hysteresis loops at a relative pressure of $p/p_0 = 0.25 \sim 0.45$, which is attributed to the textural mesoporosity and corresponded to capillary condensation of N₂ molecules within the interparticle pores [34]. The less steep condensation for MCM-41(DU) sample indicates a less degree of uniform mesostructure as compared to that of MCM-41(AF) and MCM-41(DU)-F samples.

Furthermore, the capillary condensation steps of MCM-41(DU) and MCM-41(DU)-F samples tend to shift toward higher values of relative pressure, indicating that MCM-41(DU) and MCM-41(DU)-F samples possess larger pore diameter. This result is further confirmed by the BJH pore size distribution shown in [Figure 4.5](#). It is clear to see that all samples show narrow pore size distribution, suggesting the uniform porosity of the obtained materials, while the sequence of pore diameter is in the order of MCM-41(DU)-F > MCM-41(DU) > MCM-41(AF). This is probably attributed to the formation of soluble NH₄F in the process, which could be easily dissociated and the released fluorine ions are beneficial for the enlargement of the surfactant micelles.

The physical properties such as BET specific surface area, specific pore volume and average pore diameter derived from N₂ adsorption-desorption measurements are summarized in [Table 4.1](#). One can see that the specific surface area and the total pore volume of MCM-41(DU)-F are higher than those of MCM-41(DU), revealing that MCM-41(DU)-F possesses superior quality of the mesostructure and this result is in agreement with the XRD results shown in [Figure 4.3](#). It is noticed that MCM-41(DU) and MCM-41(DU)-F exhibit similar wall thickness and they are thicker than that of MCM-41(AF), suggesting that MCM-41(DU) and MCM-41(DU)-F possess higher hydrothermal stability.

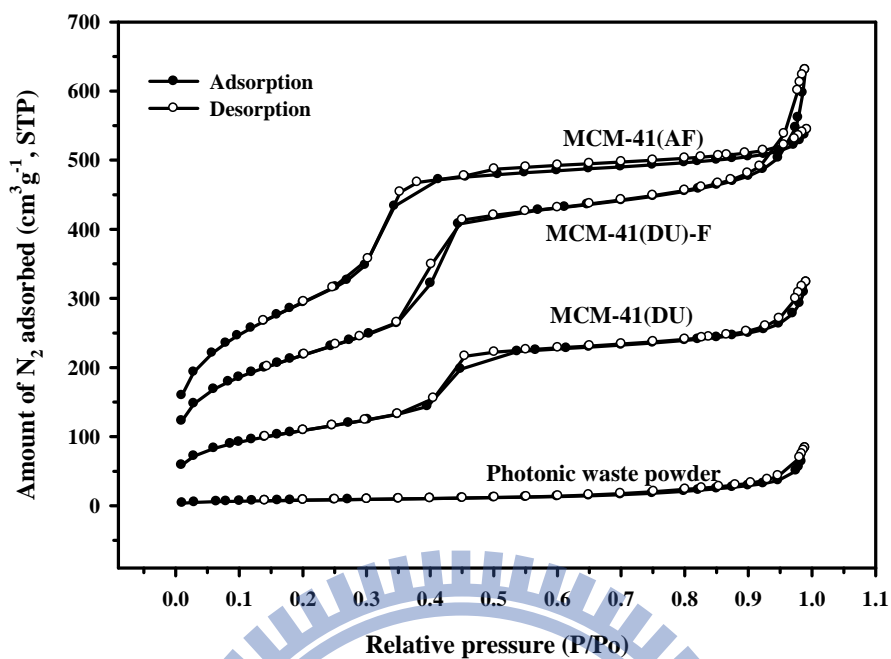


Figure 4.4 N_2 adsorption-desorption isotherms of raw optoelectronic waste powder, MCM-41(DU), MCM-41(DU)-F and MCM-41(AF) samples.

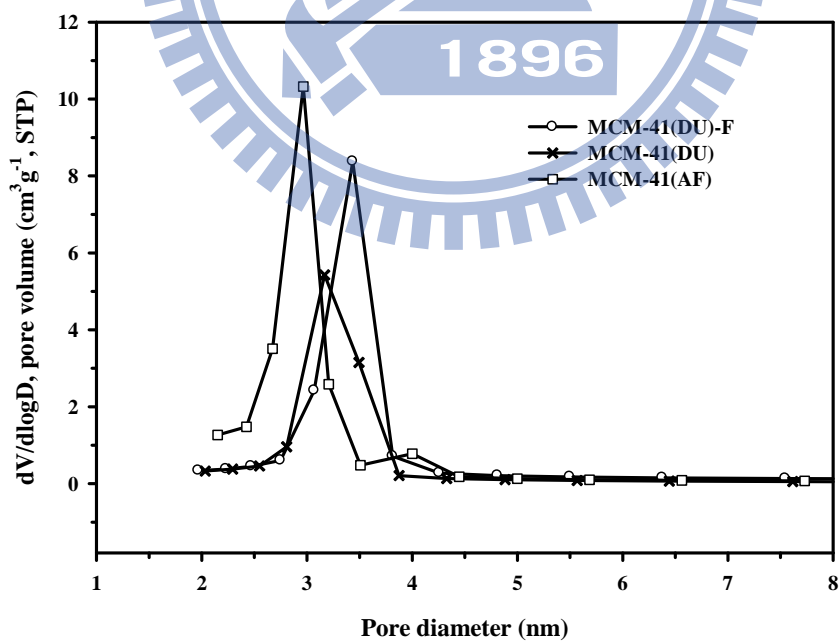
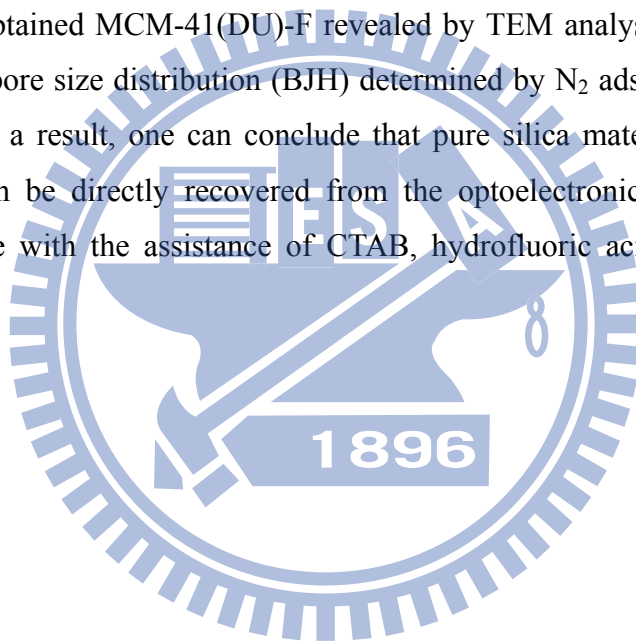


Figure 4.5 BJH pore size distribution of MCM-41(DU), MCM-41(DU)-F and MCM-41(AF) samples.

The chemical composition of the obtained MCM-41(DU)-F sample was investigated by EDS analysis and the result is presented in [Figure 4.6\(a\)](#). As seen from the spectrum that the obtained silica materials contain silicon and oxygen elements and there are no impurities observed at all, suggesting that highly purified siliceous materials can be obtained by the proposed method in this study. The textural structure was obtained from transmission electron microscopy (TEM) analysis as shown in [Figure 4.6\(b\)](#) and [Figure 4.6\(c\)](#). It can be observed that MCM-41(DU) material shows poor organized mesostructure whereas MCM-41(DU)-F exhibits well-organized hexagonal pore arrangement, implying that the addition of hydrofluoric acid is beneficial for the formation of well-organized mesoporous silica from waste powder. This is consistent with the results of XRD and BET analyses. In addition, the uniform porosity of the obtained MCM-41(DU)-F revealed by TEM analysis is in agreement with the narrow pore size distribution (BJH) determined by N₂ adsorption-desorption measurement. As a result, one can conclude that pure silica materials with ordered mesostructure can be directly recovered from the optoelectronic waste powder at room temperature with the assistance of CTAB, hydrofluoric acid and ammonium hydroxide.



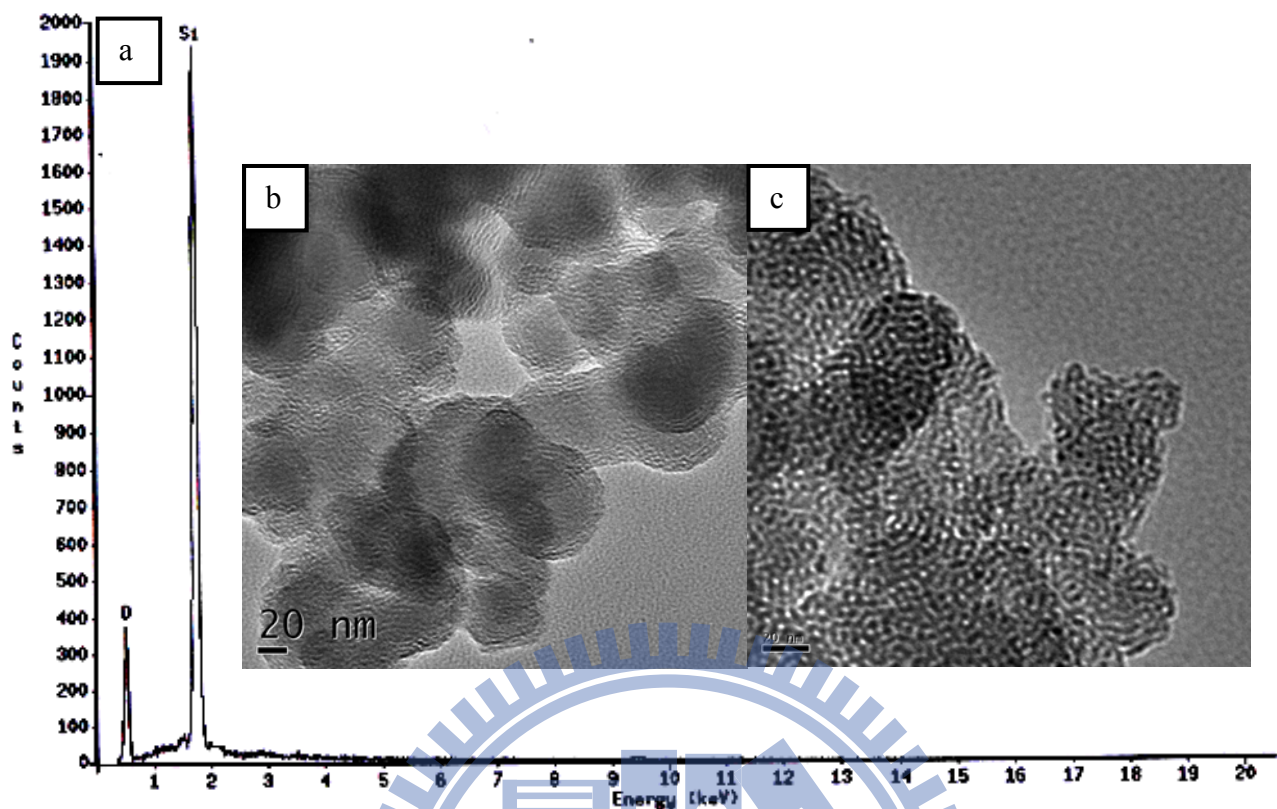


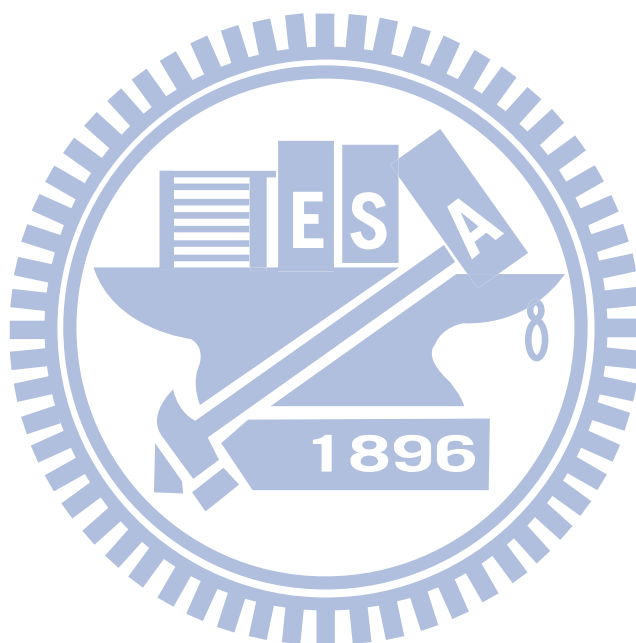
Figure 4.6 (a) EDS spectrum of MCM-41(DU)-F; (b) TEM image of MCM-41(DU);
(c) TEM image of MCM-41(DU)-F.

It could be speculated from the previous results of XRD, BET and TEM that silica materials with well-organized mesostructure can only be formed when all silicon species were firstly pre-activated by hydrofluoric acid. It was proposed by the reaction Equations (4)-(8) that the addition of hydrofluoric acid in the system can firstly induce the reactive fluorine ions with the non-reactive SiO_2 in the waste powder and form more SiF_6^{2-} species, which can be rapidly hydrolyzed to more reactive $\text{Si}(\text{OH})_4$ and/or $\text{SiO}(\text{OH})_3^-$ anions by adding ammonium hydroxide. Then, well-ordered MCM-41(DU)-F can be obtained via the strong electrostatic force between silicate species and CTAB molecules. On the other hand, if hydrofluoric acid was not added then the bulk SiO_2 particles could not be dissolved and further hydrolyzed into reactive $\text{Si}(\text{OH})_4$ and/or $\text{SiO}(\text{OH})_3^-$ anions. Thus, fewer amounts of reactive silicate anions present in the mixture would result in lower specific surface area and pore volume of MCM-41(DU). Besides, the presence of undissolved SiO_2 particles as extra-framework particles would also disrupt the uniformity of the mesostructure. This is confirmed by the XRD analysis shown in Figure 4.3, where MCM-41(DU) shows stronger amorphous SiO_2 crystallinity than that of MCM-41(DU)-F.

It is well-known that fluorine ions are beneficial for enhancing the silanol condensation of the silica materials. Therefore, it is expected that MCM-41(DU)-F should exhibit higher degree of silanol groups condensation. This hypothesis is further supported by the result of ^{29}Si NMR analysis shown in Figure 4.7. The sharp peak centering at -112 ppm was observed for both as-synthesized materials of MCM-41(DU) and MCM-41(DU)-F, which can be assigned to the highly polymerized Q^4 Si sites [$\text{Si}(\text{OSi})_4$] [116]. On the other hand, two distinguished peaks locating at -102 and -90 ppm, respectively, were observed as well. The former peak represents Q^3 Si sites [$\text{Si}(\text{OSi})_3\text{OH}$] while the latter one represents Q^2 Si sites [$\text{Si}(\text{OSi})_2\text{OH}_2$] species [117]. It is noticeable that MCM-41(DU)-F showed higher Q^4/Q^3 ratio, implying that MCM-41(DU)-F possessed higher degree of condensation of the silanol groups. This is probably due to the fact that the presence of fluorine ions which greatly enhanced the condensation reaction of the silanol groups. Generally, it is recognized that higher Q^4/Q^3 ratio of the silica materials represents higher hydrothermal stability [118]. Consequently, it can conclude that hydrofluoric acid in the system is not only favorable to the production of more reactive silicate species, but also beneficial for the enlargement of the pore diameter and it promotes higher degree of silanol

condensation.

The scanning electron microscopy (SEM) images of MCM-41(AF) and MCM-41(DU)-F samples are depicted in [Figure 4.8](#). It can be clearly observed that the MCM-41(AF) prepared via alkaline fusion method was in tubular shape with length of ca. 1-2 μm and diameter of ~ 200 nm. On the contrary, MCM-41(DU)-F was in spherical shape with sizes of around 100-150 nm, which size was much smaller than that of MCM-41(AF). In direct utilization process, the pH value of synthetic medium is 6.9-7.0 and the silica condensation rate is a maximum at around pH value of 6-7 [119]. Therefore, the fast hydrolytic condensation of silica-surfactant mixture results in the formation of small-sized mesostructured particles.



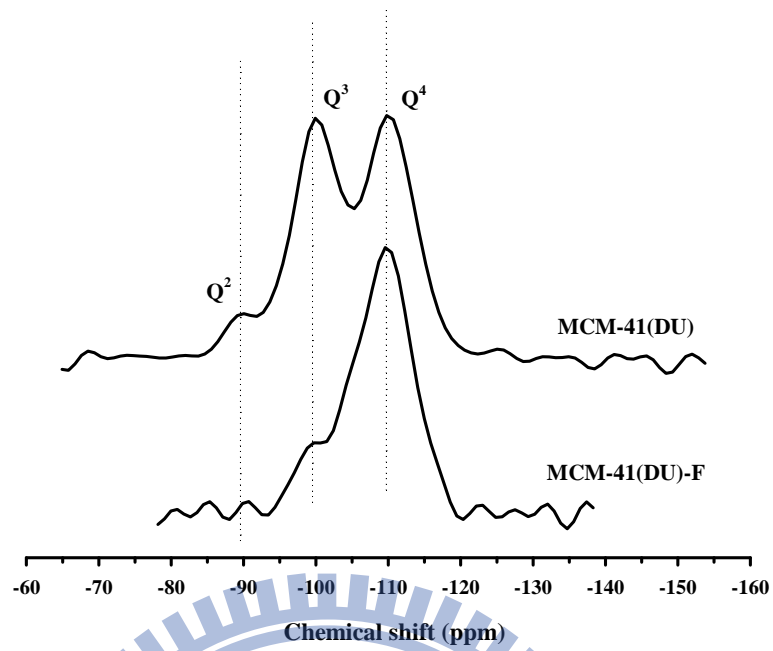


Figure 4.7 ^{29}Si NMR spectrum of MCM-41(DU) and MCM-41(DU)-F samples.

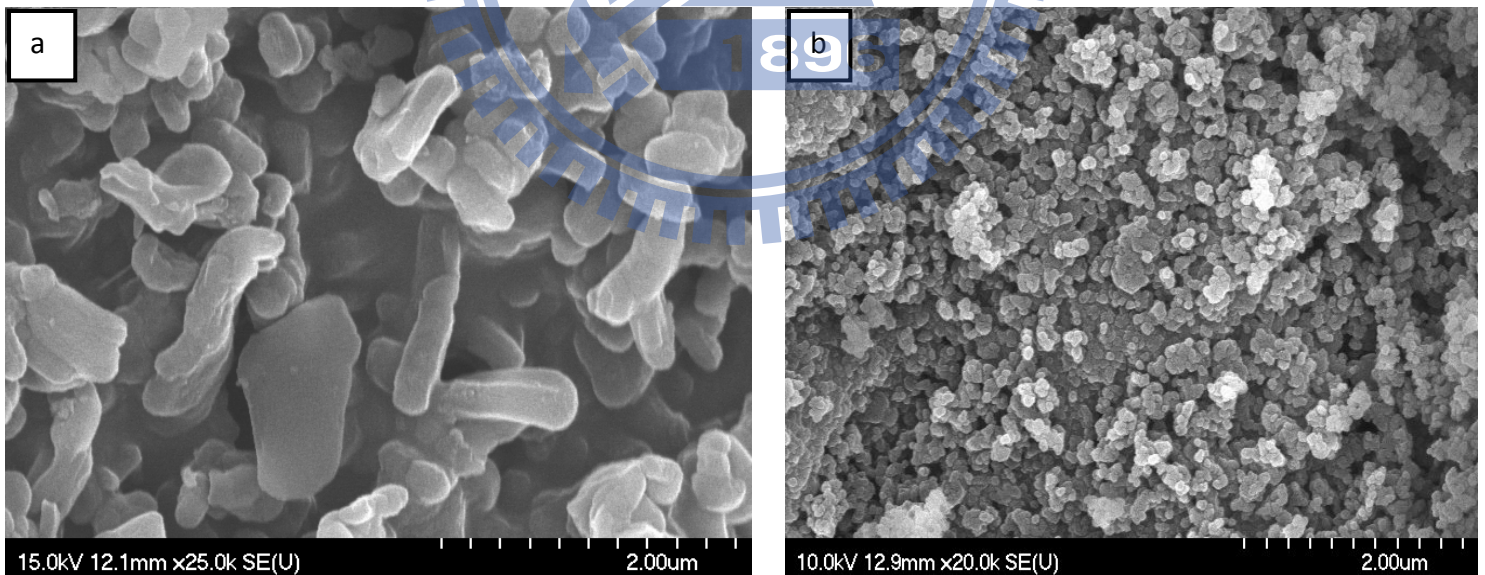


Figure 4.8 SEM images of (a) MCM-41(AF) and (b) MCM-41(DU)-F samples.

The uniform mesostructure with large pore diameter and large pore volume of waste-derived mesoporous silica materials may imply them as potential adsorbents for CO₂ capture. Figure 4.9 displays the breakthrough curves of 10% CO₂ adsorption on three TEPA-functionalized waste-derived mesoporous silica adsorbents at 60 °C via packed column reactor, including MCM-41(AF), MCM-41(DU) and MCM-41(DU)-F samples. Furthermore, MCM-41(NaSi) sample synthesized using pure chemical reagent of sodium silicate was also tested as support of adsorbent for its adsorption capacity. It is seen that initially the CO₂ gas can be efficiently adsorbed on all adsorbents with capture efficiencies greater than 98%. The CO₂ adsorption capacities of all adsorbents shown in Table 4.1 were in a range of 100-121 mg/g-adsorbent and follow the order of TEPA-MCM-41(DU) < TEPA-MCM-41(AF) ≈ TEPA-MCM-41(NaSi) < TEPA-MCM-41(DU)-F. This may be due to the fact that the textural properties of the supports play important roles in CO₂ adsorption performance.

In a related work, Son et al. [66] employed a series of amine-functionalized mesoporous silica materials as support of adsorbent for CO₂ adsorption. They found that the adsorption capacity was a function of the pore diameter of the support and followed the order of MCM-41 (2.8 nm, 1D) < MCM-48 (3.1 nm, 3D) < SBA-15 (5.5 nm, 1D) ≈ SBA-16 (4.1 nm, 3D) < KIT-6 (6.5 nm, 3D). However, in this study MCM-41(DU) with relatively larger pore diameter (4.4 nm) appears to have lower CO₂ uptakes compared to those of MCM-41(AF) (3.0 nm), MCM-41(NaSi) (3.1 nm) and MCM-41(DU)-F (4.5 nm) (Figure 4.10(a)). On the other hand, it is noted from Figure 4.10(b) that a linear relationship with correlation coefficient R² = 0.95 was observed between the total pore volume of the parent silica substrates and the CO₂ adsorption capacity. This may suggest that the total pore volume of the parent support plays a predominant role instead of the pore diameter in CO₂ capture.

The density of TEPA is 0.99 cm³ /g and the total pore volume of MCM-41(NaSi), MCM-41(AF), MCM-41(DU) and MCM-41(DU)-F is 1.00 cm³ /g, 0.99 cm³ /g, 0.52 cm³ /g as well as 1.10 cm³ /g, respectively. Thus the maximum TEPA amount theoretically loaded inside the pore channels was calculated to be 50%, 50%, 34% and 53%, for the MCM-41(NaSi), MCM-41(AF), MCM-41(DU) and MCM-41(DU)-F, respectively. It can be seen from Table 4.1 that TEPA-MCM-41(DU) exhibits tiny pore volume which reveals that the pores of MCM-41(DU) were nearly filled by

TEPA. It is reported that more efficient contact between the CO₂ gas and the impregnated amines could be achieved when a small space is still left inside the pores of the mesoporous silica after amine reagents loading [80]. As a result, the MCM-41(DU) had lower CO₂ adsorption capacity due to the fact that it had smaller pore volumes, which may result in more constricted or blocked pores in the adsorbents.

In addition, the adsorption capacity appears to increase with an increase in pore diameter and follow the order of TEPA-MCM-41(AF) (3.0 nm) \approx TEPA-MCM-41(NaSi) (3.1 nm) < TEPA-MCM-41(DU)-F (4.5 nm). This might be because larger pore diameter of the support could facilitate more TEPA into the pore channels more easily, leading to higher CO₂ adsorption performance. As shown in [Table 4.1](#), the pore volume of MCM-41(DU)-F and TEPA-MCM-41(DU)-F is 1.10 cm³ /g and 0.16 cm³ /g, respectively. Therefore, the amount of TEPA loaded into the pores of MCM-41(DU)-F was calculated to be 49%, while there was only 46% TEPA loaded into the pore channels of the MCM-41(NaSi) and MCM-41(AF), respectively. In addition, the BJH pore size distribution shown in [Figure 4.11](#) shows that the pore sizes of MCM-41(AF) and MCM-41(NaSi) are diminished to less than 2 nm after TEPA loading. In comparison, parts of pores still remain larger than 2 nm in TEPA-MCM-41(DU)-F. This could make the gas flow into TEPA-MCM-41(DU)-F to be easier, which is beneficial for CO₂ adsorption. Consequently, it could be concluded that the large pore diameter and pore volume of MCM-41(DU)-F resulted in the highest CO₂ capacity among all adsorbents.

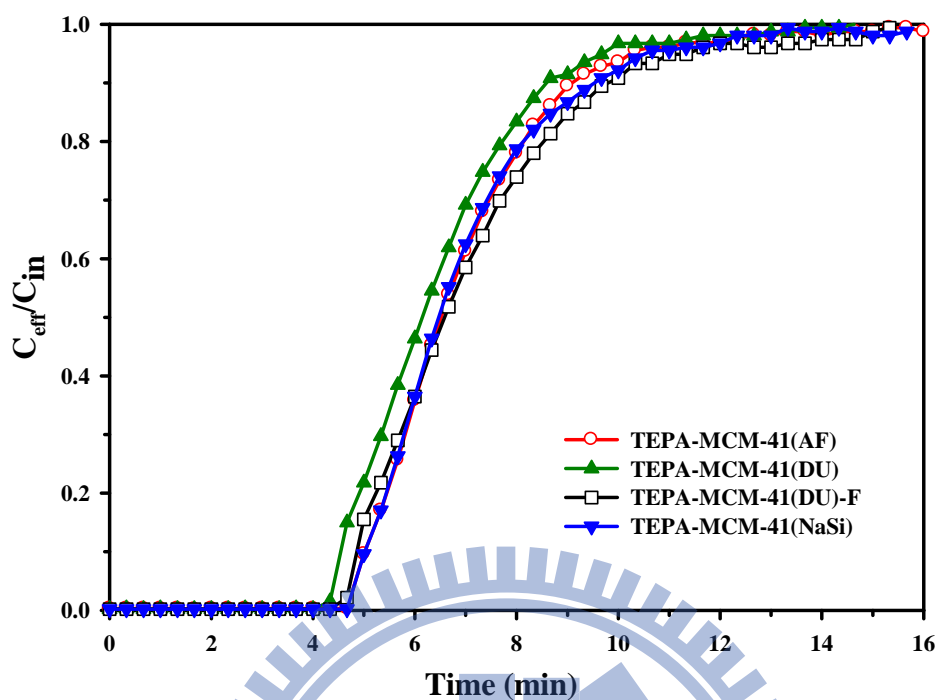


Figure 4.9 CO₂ breakthrough curves for TEPA-functionalized adsorbents of MCM-41(NaSi), MCM-41(AF), MCM-41(DU) and MCM-41(DU)-F samples.

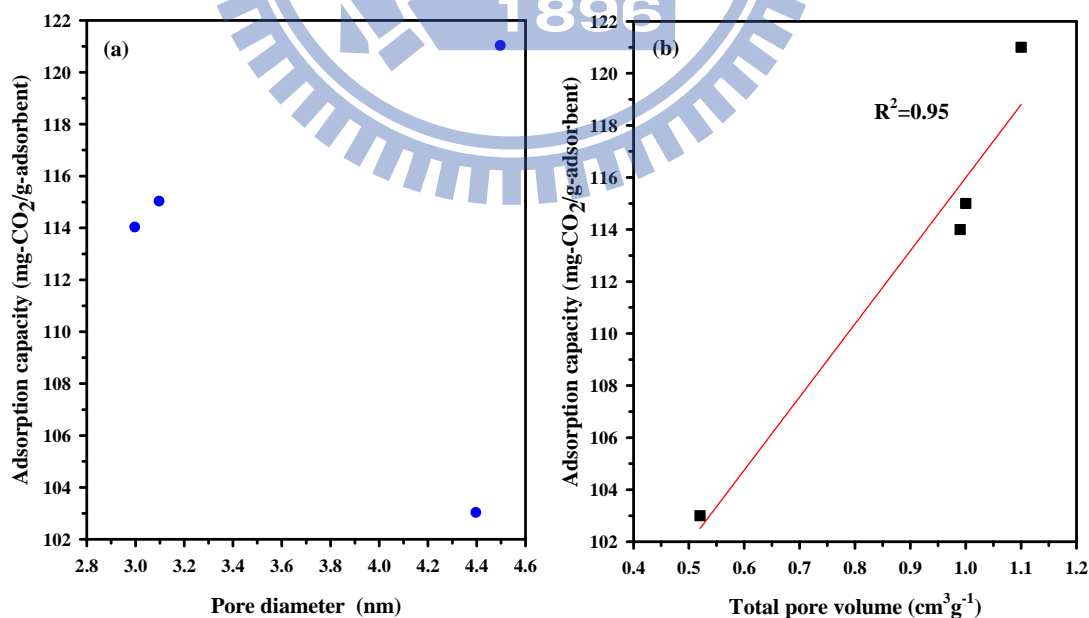


Figure 4.10 (a) Relationship between the pore diameter of the mesoporous substrates and CO₂ uptake and (b) correlation of total pore volume of the mesoporous substrates and CO₂ uptake at 60 °C.

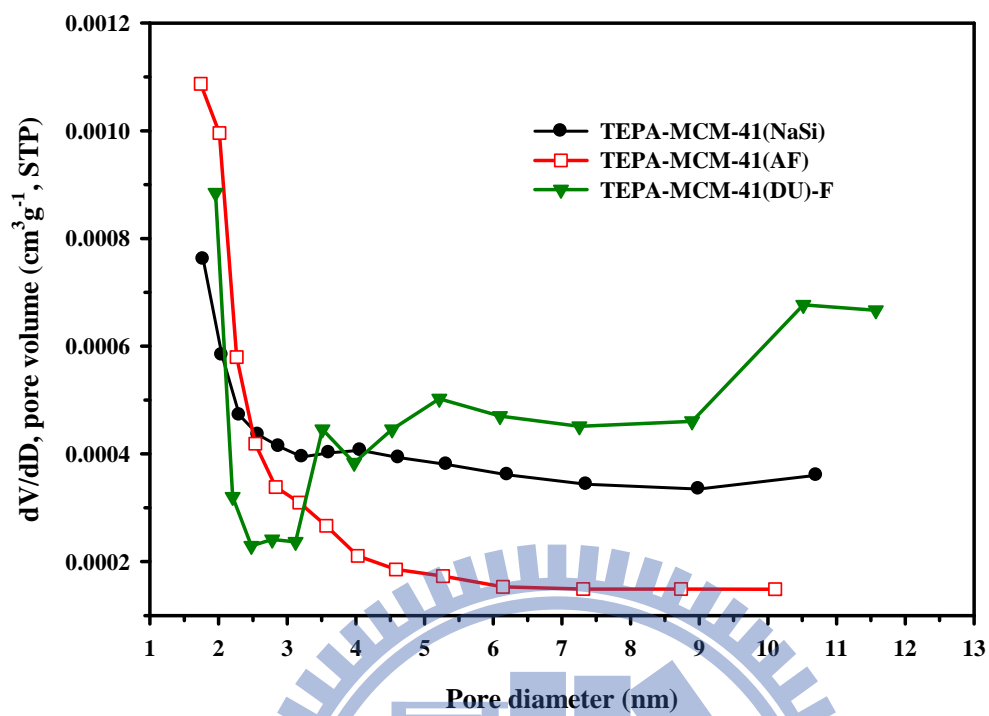


Figure 4.11 BJH pore size distribution of TEPA-MCM-41(NaSi), TEPA-MCM-41(AF) and TEPA-MCM-41(DU)-F samples.

Table 4.1 Structural properties of MCM-41(NaSi) silica, waste powder and waste-derived mesoporous siliceous materials

Sample name	^a S _{BET} (m ² /g)	^b d _{BJH} (nm)	^c V _p (cm ³ /g)	^d d ₁₀₀ (nm)	^e a ₀ (nm)	^f Tw (nm)	^g Silicon recovery	Capacity (mg-CO ₂ /g-adsorbent)
Waste powder	30	-	0.07	-	-	-	-	-
MCM-41(AF)	1082	3.0	0.99	3.47	4.01	1.01	28	7
MCM-41(DU)	396	4.4	0.5	5.1	5.89	1.49	100	5
MCM-41(DU)-F	788	4.5	1.10	5.07	5.86	1.44	100	6
MCM-41(NaSi)	1102	3.1	1.00	-	-	-	-	7
TEPA-MCM-41(AF)	55	-	0.14	-	-	-	-	114
TEPA-MCM-41(DU)	9	3.1	0.02	-	-	-	-	103
TEPA-MCM-41(DU)-F	36	4.0	0.16	-	-	-	-	121
TEPA-MCM-41(NaSi)	53	-	0.15	-	-	-	-	115

NOTE: ^aBET surface area; ^bPore diameter calculated by BJH theory; ^cPore volume calculated by BJH theory; ^dd-spacing between (100) planes. ^eHexagonal unit cell ($a_0 = 2 d_{100} / \sqrt{3}$); ^fPore wall thickness ($Tw = a_0 - d_{BJH}$); ^gSilicon recovery yield=weight ratios of silicon contents in raw waste powder to silicon contents in mesoporous silica.

4.2 Direct synthesis of silica materials with hierarchically mesocellular structures from waste powder

4.2.1 Motivation

It is found from our previous results that amine-impregnated mesoporous substrates with larger pore volume are favorable for achieving superior CO₂ adsorption performance. Among various kinds of mesoporous silica materials, mesostructured cellular foam (MCF) material, has received increasing attention due to their fast mass transfer, good accessibility for large molecules and their large pore volume that are beneficial in various process. They are believed to be more resistant to pore blockage and provide more efficient mass transfer kinetics than mesoporous materials having hexagonal structure with uni-dimensional array of pores. The MCF material is general synthesized using microemulsion approach with the aid of NH₄F and 1, 3, 5-trimethylbenzene (TMB) as swelling agents. However, their industrial development is mainly restricted to the high producing costs by preferred silica sources and swelling agents. Thus, taking into account the potential scale involved in the production of MCF, the use of renewable sources for fabricating these materials would seem highly desirable.

4.2.2 Direct synthesis of mesoporous siliceous materials from waste powder

Directly synthesized mesoporous material was processed by employing optoelectronic industrial waste powder as the silica source, along with triblock copolymer Pluronic F127 (EO₁₀₆PO₇₀EO₁₀₆, MW=12600) as the structure-directing template. The molar composition of the gel mixture was 1 SiO₂: x HF: y F127: 12 NH₄OH: 120 H₂O (x and y varies with the molar ratio of n_{HF}/n_{Si} and n_{F127}/n_{Si}, respectively). In a typical procedure, 9.4 g of waste powder was firstly dissolved in 100 ml of DI water, followed by the addition of the desired amounts of HF solution with stirring for 30 minutes. Subsequently, given amounts of F127 (dissolved in 61 ml of DI water) was added dropwise followed by the addition of 35 ml of NH₄OH solution. The resulting gel mixture was then stirred for 1 h at ambient temperature and aged at 100 °C for 0.5 h. The resultant solid was recovered by filtration, washed with DI water and dried in an oven at 100 °C for 6 h. Finally, the organic template was removed by using a muffle furnace in air at 550 °C for 6 h.

4.2.3 Results and discussion

The structure of the recycled MS(0.0023) sample is presented in [Figure 4.12](#), which is composed of large cells and connecting windows, similar with the structure of mesocellular silica foam materials. Typically, oil-in-water microemulsions were used as structuring-directing agent to prepare MCF materials. Ordered mesoporous silica with hexagonal arrangement is synthesized using block copolymer of P123 (EO₂₀-PO₇₀-EO₂₀) as the template. The addition of 1, 3, 5-trimethylbenzene (TMB) to the P123 solution as a swelling agent converts hexagonally ordered structures to mesocellular structures, which exhibit spherical pores. In this study, the recycled MS(0.0023) sample with mesocellular structure was synthesized using only one F127 template. A representative TEM image ([Figure 4.13](#)) shows that three-dimensional MS(0.0023) can be clearly seen.

As described, single structure-directing agent of F127 was employed for structure assembly; therefore, it is expected that the concentration of F127 surfactant would strongly influence the textural properties of the recycled materials. [Figure 4.14](#) shows the N₂ physisorption isotherms of the recycled MS samples synthesized with various F127 concentrations. The sample obtained with n_{F127}/n_{Si} ratio of 0.001 exhibits typical type IV isotherm with a capillary condensation step at relative pressure of 0.35-0.7 and H2-type hysteresis loop. These characteristics are indicative of cage-like mesopores with an entrance much narrower than the diameter of the cage itself, which is similar with conventional SBA-16 reported in the literatures [120]. In contrast, the samples synthesized with increasing F127 concentrations (0.0023-0.01) show H1-type hysteresis loop, which implies that the entrance sizes of MS samples have been enlarged, compared with MS(0.001). Interestingly, when the n_{F127}/n_{Si} ratio is increased from 0.001 to 0.0023, the hysteresis loop in the isotherm is obviously shifted to the high relative pressure. However, the hysteresis loops tend to shift to lower relative pressure with further increasing F127 concentrations from 0.0023 to 0.01.

Pore size distribution of various samples ([Figure 4.15](#)), estimated from the BJH model, confirms these trends. It can be seen that a significant peak located at ca. 4 nm was observed for all performed MS sample; in contrast, corresponding pore size distribution curves of MS samples with n_{F127}/n_{Si} ratio from 0.0023 to 0.01 showed another emerging peak. It is worth noting that the pore size distribution for MS(0.0023) is relatively broad, compared with MS(0.001). This is possibly related to

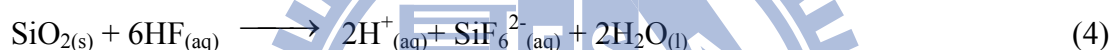
the gradual pore expansion, which decrease the mesostructure ordering. With higher amounts of F127, the pore diameters of MS(0.003) and MS(0.01) decrease subsequently. Generally, mesostructured materials were obtained by the kinetically controlled competitive assembly of organic and inorganic species into nanostructured domains [87]. It is likely that the formation of mesophases can therefore be governed more kinetically as the F127 concentration increases.

In addition, the effect of hydrofluoric acid in the precursors on structural properties of the recycled the MS materials was investigated as well. It can be observed from Figure 4.16 that the MS(0F) materials clearly shows type IV isotherm with a capillary condensation step at relative pressure of 0.5-0.8 and H2-type hysteresis loop, which are indicative of mesoporous materials with cage-like shapes. As the hydrofluoric acid was applied in the synthesis, the hysteresis loops at relative pressure of 0.85-1.0 significantly increased, whereas the capillary condensation step at relative pressure of 0.5-0.8 was still retained. This clearly indicates that parts of pores were enlarged. With increasing amounts of hydrofluoric acid, the hysteresis loops tend to shift to lower relative pressure. This is similar with the trends observed on the physical properties of the resulting materials with various amounts of F127. As seen from Figure 4.17, pore enlargement was clearly observed in the recycled MS materials synthesized with the aid of hydrofluoric acid, as compared with the MS(0F) sample produced without hydrofluoric acid. It has been reported that fluorine ions are beneficial for the formation and growth of micelles, leading to the formation of high quality mesoporous materials [122]. It is seen from Table 4.2 that the MS(10F) possesses much higher specific surface area ($938 \text{ m}^2/\text{g}$) than that of MS(0F) ($239 \text{ m}^2/\text{g}$) fabricated without adding hydrofluoric acid. Furthermore, it is also noted that the HF-assisted recycled MS materials exhibit higher peak intensities than that of MS(0F), which implies that the mesostructures of the MS materials can be significantly enhanced with the addition of hydrofluoric acid. Thus, the introduction of hydrofluoric acid in the synthesis can not only enlarge the pore diameter of the recycled MS materials, but also enhance the capability of F127 micellization, leading to formation high quality mesoporous materials.

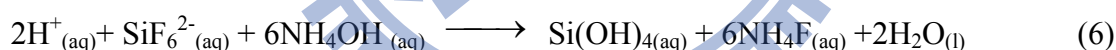
Table 4.2 and Table 4.3 summarize the structural properties of the recycled MS materials prepared at different $n_{\text{F127}}/n_{\text{Si}}$ and $n_{\text{HF}}/n_{\text{Si}}$ ratios. Interestingly, the porosity of these recycled materials can be easily designed by simply modifying the amounts of

F127 and hydrofluoric acid. In the present conditions, HF-induced recycling of mesostructured silica materials with hierarchically meso-structural properties can be facily controlled using extremely low n_{F127}/n_{Si} ratio. This would be expected to be a great contribution to potential mass production of materials because of their low manufacturing costs by reducing surfactant amount. Moreover, it is worth mentioning that, if the pore characteristics of these recycled materials are properly designed, they could be potentially applicable in wide applications as sorbents and/or supports.

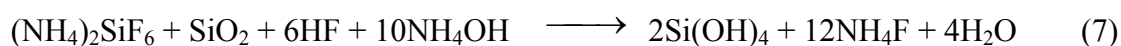
A possible mechanism for recycling of mesoporous silica materials from optoelectronic industrial waste powder is illustrated in [Figure 4.18](#). In the present synthesis, the optoelectronic waste powder was first treated with hydrofluoric acid. It is expected that the SiO_2 presented in optoelectronic waste powder would react with hydrofluoric acid to produce hexafluorosilicic acid (H_2SiF_6) and the chemical reaction is presented as follows:



Subsequently, the hydrolysis of $(NH_4)_2SiF_6$ and SiF_6^{2-} can be accelerated by the addition of ammonium hydroxide:



Therefore, the overall reactions for the recovery of silica materials from optoelectronic waste powder in the presence of hydrofluoric acid and ammonium hydroxide can be summarized as follows:



The pH value of synthetic medium is 6.9-7.0 and the silica condensation rate is a maximum at around pH value of 6-7 [119]. The interaction between F127 surfactant and the silica source is mainly based on hydrogen bonding under neutral conditions. The fast hydrolytic condensation of silica-surfactant mixture results in the formation of small-sized mesostructured particles. Thus, small-sized MS(0.001) materials with mesopores templated by F127 can be formed. TEM analysis in [Figure 4.19\(a\)](#) clearly shows that the MS(0.001) consists of mesopores of ca. 3.8 nm, which is similar with

the result of pore size distribution shown in [Figure 4.15](#).

On the other hand, when the amount of F127 was increased, the mesoporous silica materials with mesocellular structure were obtained ([Figure 4.19\(b\)](#)). Due to the fast SiF_6^{2-} /F127 hydrolytic condensation process, the small-sized mesostructured silica building blocks with large amounts of hydroxyl groups were initially formed. The residual F127 would be expected to be adsorbed on to the hydrophilic surface and self-assemble into large spherical micelles, resulting in the formation of mesocellular pores. Similar pathway was recently proposed by Hsu and colleagues [123], who prepared MCF materials without using swelling agents. Those synthetic procedures, however, are generally conducted using pure silica chemicals of either tetraethylorthosilicate or sodium silicate under strong acid conditions.

Very recently, [An et al.](#) [124] reported the synthesis of MCF materials by employing industrial waste of steel slag as the silica source with the aid of organic swelling agent of TMB. However, the use of expensive TMB significantly increases the production costs of MCF material and this would be an important issue for field applications. In the present study, silica materials with controllable mesocellular structures can be directly recovered from optoelectronic waste powder using single surfactant with extremely low amount. To our knowledge, there have been reports on the synthesis of this type of materials using solid wastes with single surfactant. The process is simple, fast, cost-effective and environmental-friendly because the synthetic procedures were conducted using industrial solid wastes as alternative resource under neutral conditions. Therefore, this process will offer novel solutions not only to waste management problems but also significantly reduce the manufacturing costs for the production of MCF-like materials.

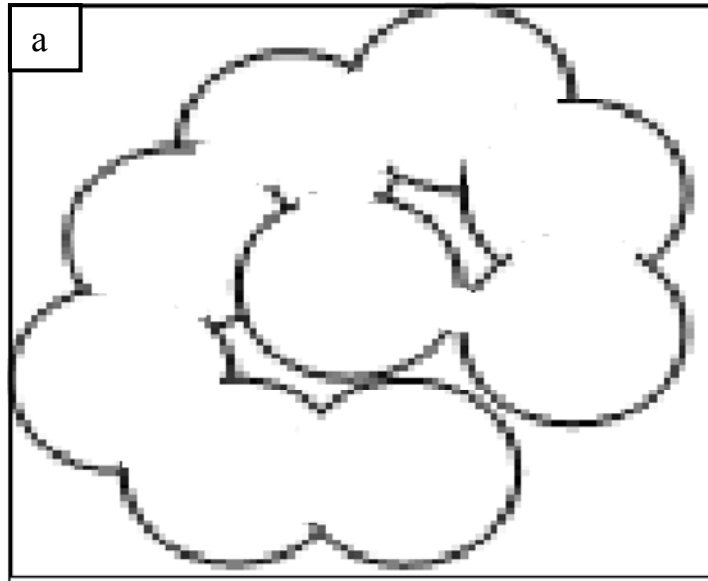


Figure 4.12 Schematic cartoon of the structure of the recycled MS (0.0023).

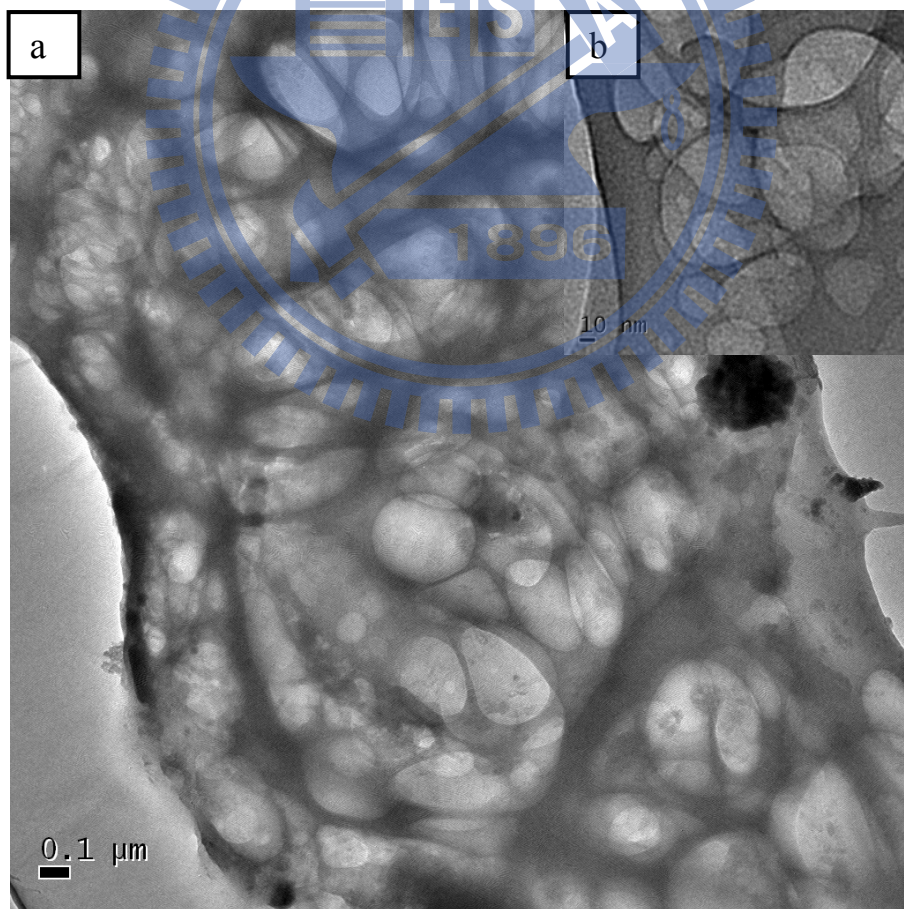


Figure 4.13 Representative TEM image of the recycled MS (0.0023).

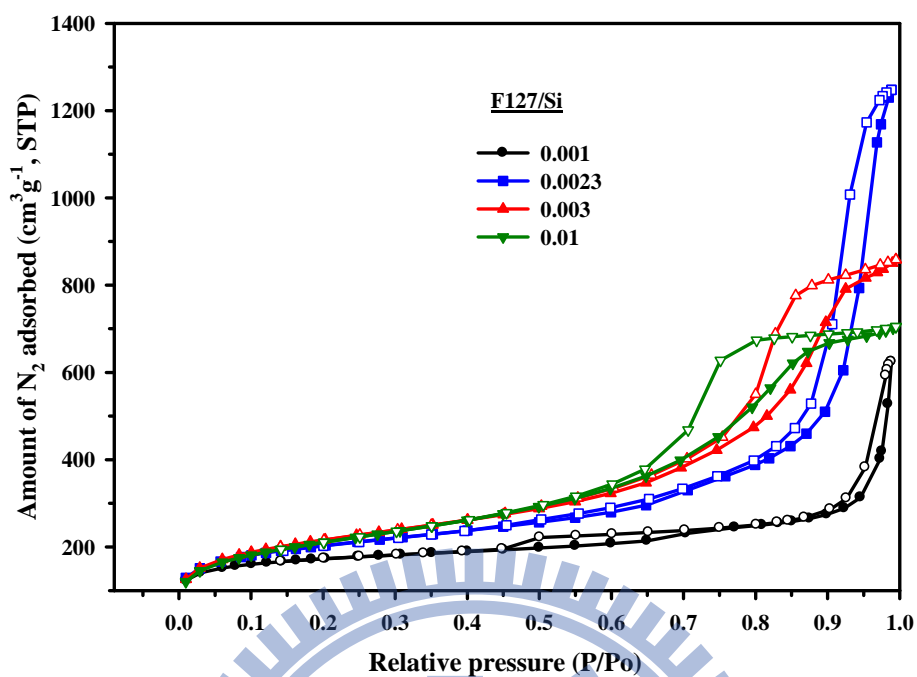


Figure 4.14 N₂ adsorption-desorption isotherms of mesoporous silica materials synthesized with various n_{F127}/n_{Si} ratios.

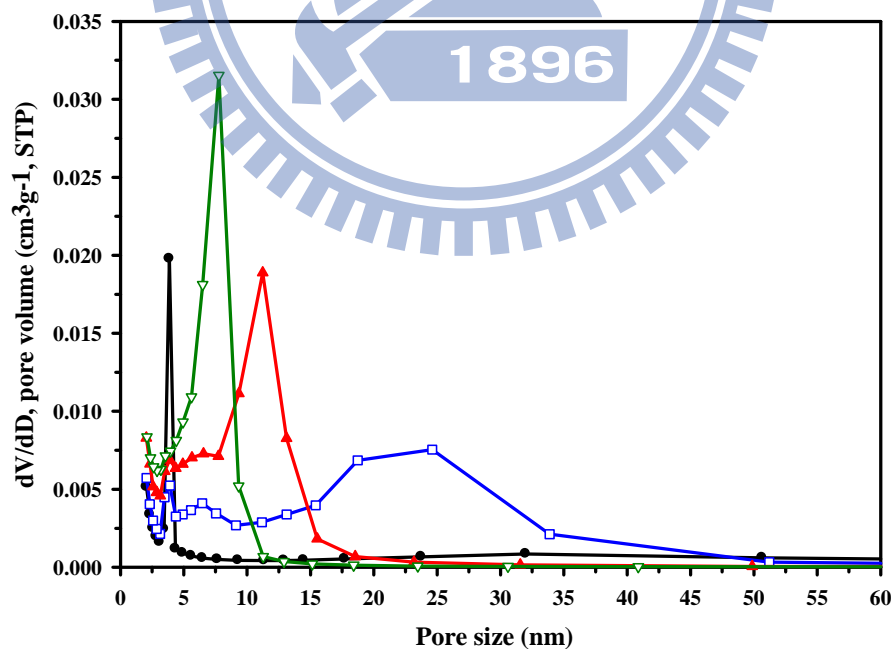


Figure 4.15 Pore size distribution of mesoporous silica materials synthesized with various n_{F127}/n_{Si} ratios.

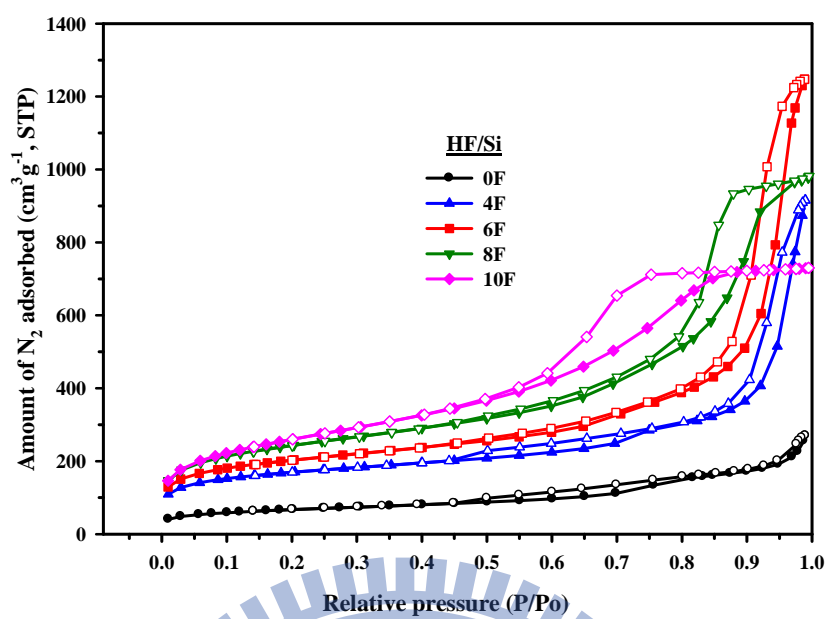


Figure 4.16 N₂ adsorption-desorption isotherms of mesoporous silica materials synthesized with various n_{HF}/n_{Si} ratios.

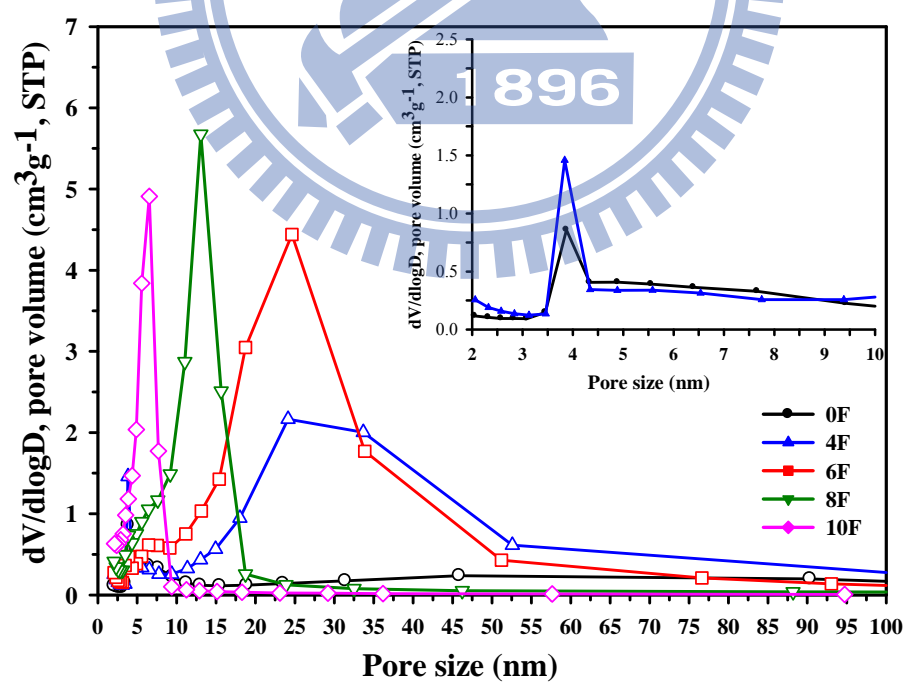


Figure 4.17 Pore size distribution of mesoporous silica materials synthesized with various n_{HF}/n_{Si} ratios.

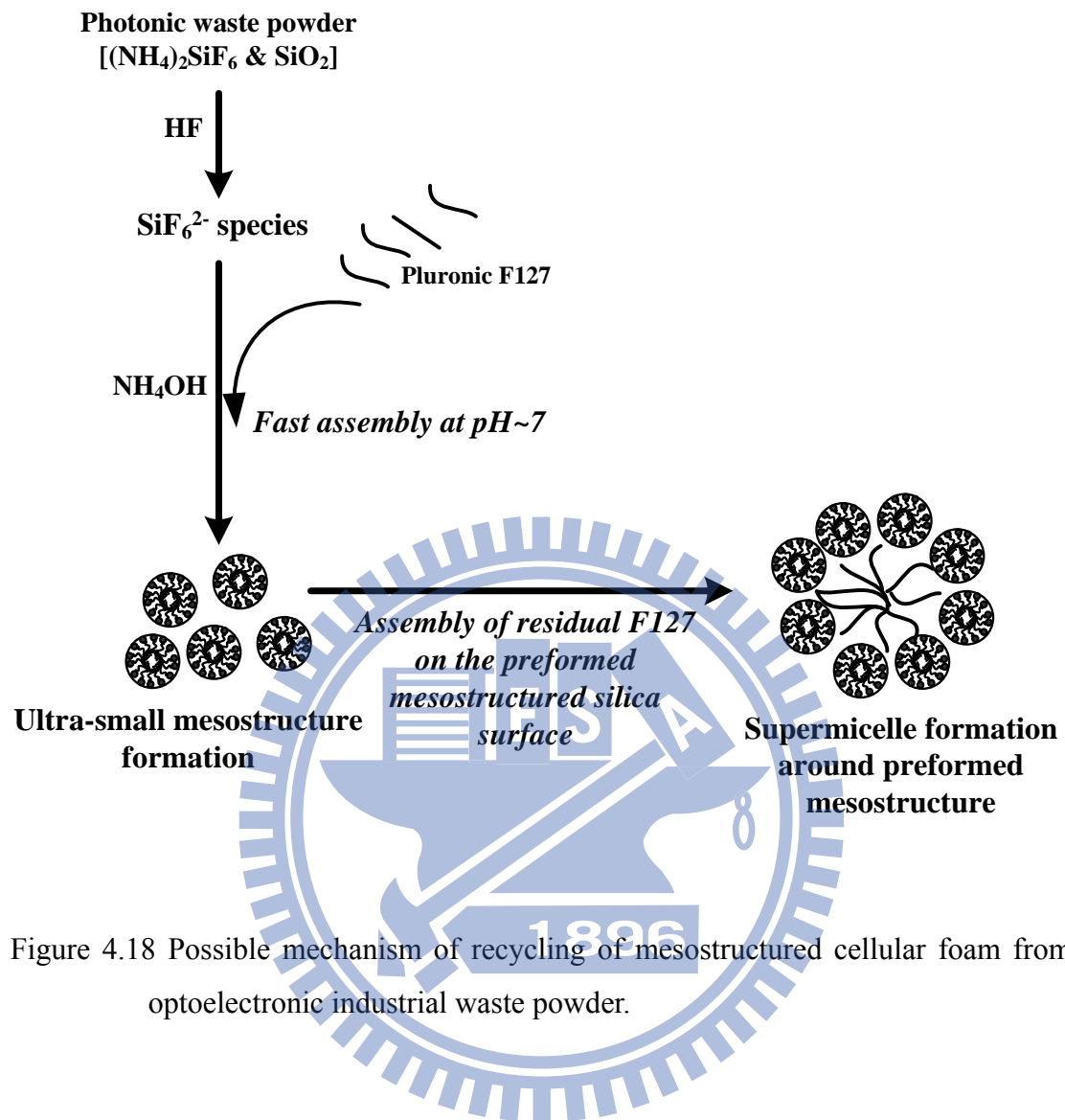


Figure 4.18 Possible mechanism of recycling of mesostructured cellular foam from optoelectronic industrial waste powder.

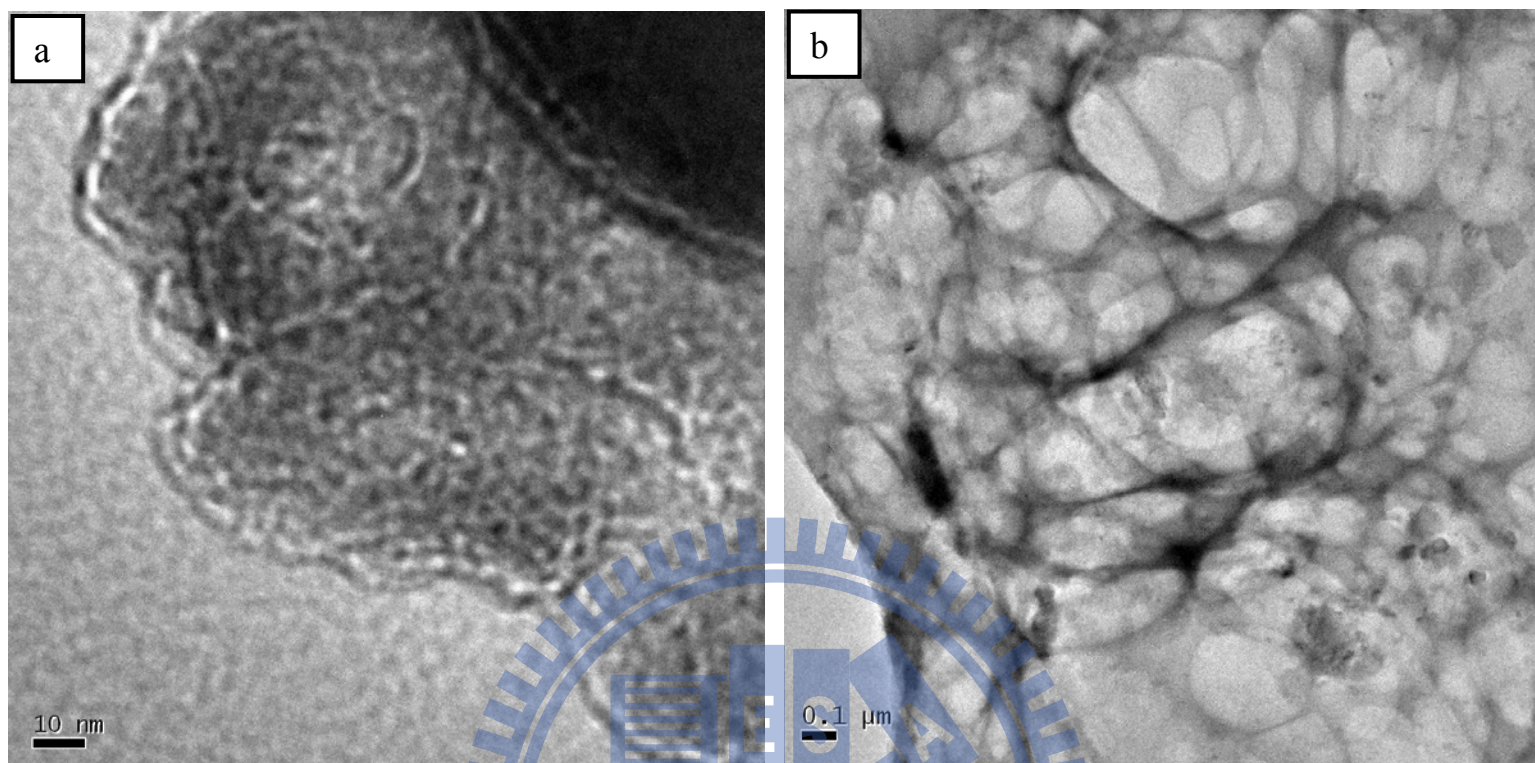


Figure 4.19 TEM images of the recycled mesoporous silica samples synthesized by using different amounts of F127. a) MS(0.001), b) MS(0.01)

Table 4.2 Physical parameters of the optoelectronic waste powder and the recycled mesoporous silica samples prepared at different n_{F127}/n_{Si} ratio.

Sample name	n_{F127}/n_{Si}	n_{HF}/n_{Si}	$^a S_{BET}$ (m^2/g)	$^b D_p$ (nm)	$^c V_p$ (cm^3/g)
Waste powder	-	-	30	-	0.07
MS(0.001)	0.001	6	596	3.87	0.62
MS(0.0023)	0.0023	6	716	14.2	1.75
MS (0.003)	0.003	6	773	7.7	1.28
MS (0.01)	0.01	6	757	5.9	1.07

NOTE: a BET surface area; b Pore diameter calculated by BJH theory; c Pore volume was estimated at a relative pressure P/P_0 of 0.995

Table 4.3 Physical parameters of the recycled mesoporous silica samples prepared at different n_{HF}/n_{Si} ratio.

Sample name	n_{F127}/n_{Si}	n_{HF}/n_{Si}	$^a S_{BET}$ (m^2/g)	$^b D_p$ (nm)	$^c V_p$ (cm^3/g)
MS(0F)	0.0023	0	239	3.87	0.33
MS(4F)	0.0023	4	596	13.5	1.14
MS (6F)	0.0023	6	716	14.2	1.75
MS (8F)	0.0023	8	865	8.3	1.50
MS (10F)	0.0023	10	938	5.0	1.13

NOTE: a BET surface area; b Pore diameter calculated by BJH theory; c Pore volume was estimated at a relative pressure P/P_0 of 0.995

CHAPTER V AEROSOL-ASSISTED SYNTHESIS OF MESOPOROUS SILICA PARTICLES VIA THE USE OF SODIUM METASILICATE PRECURSOR

5.1 Motivation

Up to date, most researches on the manufacture of mesoporous materials were focused on solution precipitation method which belongs to aqueous route [125,126]. Typically, these materials are synthesized via either conventional sol-gel or hydrothermal treatment. The aqueous methods are usually tedious and time-consuming. For example, the MCM-41 material is one of the mesoporous products made by the hydrothermal method which commonly proceeds at 100~150°C for several days [126]. On the other hand, the aerosol processing of materials, which belongs to the gas phase production method, has become one of the facile processes because of its rapid synthesis and simplicity for scaling up as compared to the traditional aqueous routes.

In the aerosol-assisted process, TEOS is commonly utilized to synthesize silica-based materials because of its characteristic of easy preparation of homogeneous sol solution and controllable condensation rate in precursor solution. However, the need of an expensive organic silica precursor would limit its industrial applications, especially for the environmental protection applications which require massive quantity of adsorbents or catalysts. Considering the prices of organic silica precursors, the use of inexpensive inorganic silica sources such as colloidal silica or sodium silicate solution seem to be good candidates as the starting precursors. If the materials could be fabricated from inexpensive sources, the costs would be significantly reduced and the application fields of the materials would be widened. For example, one of the applications is the capture of CO₂ greenhouse gas using amine-modified mesoporous silica as the adsorbent [127].

Sodium metasilicate nanohydrate (Na₂SiO₃ · 9H₂O) which is widely used in the synthesis of silica-based materials in conventional aqueous route is much less expensive as compared to TEOS [111]. It has been verified that sodium silicate can act as both a silica source and inorganic salt in the formation of mesoporous silica via

the aqueous approaches [128,129]. However, to our knowledge there is still no report on the synthesis of MSPs via aerosol-assisted EISA approach using Na_2SiO_3 precursor. In this study, Na_2SiO_3 is driven to replace TEOS as the silicon precursor for synthesizing MSPs by the aerosol-assisted EISA route for the first time.

5.2 Preparation of the mesoporous silica spherical particles (MSP)

Figure 5.1 depicts the experimental setup of the reactor for continuously synthesizing the MSP via aerosol-assisted EISA method. For the precursor solution, sodium metasilicate nanohydrate ($\text{Na}_2\text{SiO}_3 \cdot 9\text{H}_2\text{O}$) was employed as the silica source and cetyltrimethylammonium bromide (CTAB) was used as the structure-directing surfactant template in the synthesis. The molar composition of the gel mixture was $1\text{SiO}_2: x \text{CTAB}: 20 \text{C}_2\text{H}_5\text{OH}: 667 \text{H}_2\text{O}: 6.47 \text{HCl}$ (x varies from 0.1 to 0.36). The precursor mixture was mixed and nebulized by an ultrasonic atomizer and carried by a high pressure, clean and dry air flow. The reagent flow was then passed through a high-temperature tubular reactor which consists of two heating zones with the temperatures of 150°C and 550°C , respectively. The total flow rate in this study was fixed at $2000 \text{ cm}^3/\text{min}$ (25°C , 1atm) which corresponded to a residence time of 4 seconds. After the heating process, the synthesized MSPs were collected downstream of the reactor by a high-efficiency filter. It was then recovered by washing and filtration with DI water followed by drying in an oven at 110°C . Finally, the complete removal of all bromine and carbon residues was removed by using a muffle furnace at 550°C in air for 4 hours.

For comparison purpose, the MSP sample was also obtained from TEOS precursor following a procedure reported by Hung and Bai [110,130]. The molar composition of the gel mixture was $1\text{SiO}_2: 0.18 \text{CTAB}: 10 \text{C}_2\text{H}_5\text{OH}: 40 \text{H}_2\text{O}: 0.008 \text{HCl}$, which has been proved to be the optimal precursor molar ratio in our prior studies. The collected solid products were further calcined in air at 550°C for 4 hours to remove the organic template residues.

The MSP samples synthesized from Na_2SiO_3 are denoted as MSP(NaSi)-X, where X indicated the precursor molar ratio of CTAB surfactant to Na_2SiO_3 (Surf/Si). For example, MSP(NaSi)-18 indicated that the MSP sample was prepared from Na_2SiO_3 under Surf/Si molar ratio of 0.18. The MSP sample derived from TEOS was given the

name of MSP(TEOS).

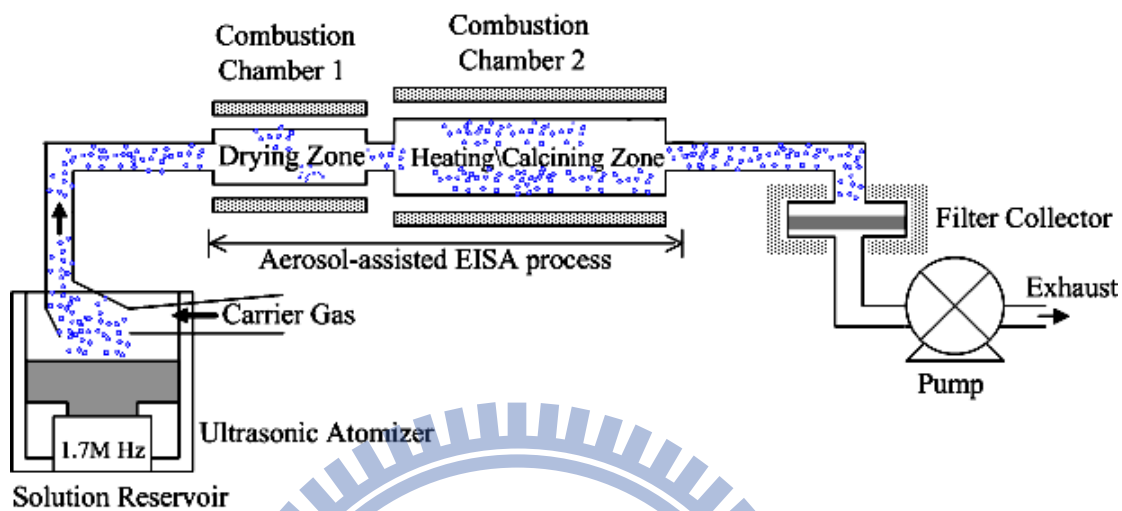


Figure 5.1 Experimental setup for the generation of mesoporous silica spherical particles (MSPs) through aerosol-assisted evaporation induced self-assembly (EISA) process.

5.3 Results and discussion

Powder XRD patterns of the calcined MSP samples prepared from Na_2SiO_3 and TEOS through aerosol-assisted EISA procedure are shown in Figure 5.2. Upon calcination, the MSP(TEOS) sample exhibits a well-resolved diffraction peak located at 2θ of $2.3\text{-}2.8^\circ$ which is indexed to the (100) reflection and corresponds to a hexagonal lattice of mesoporous silica materials [111,131]. Similar observation was also seen for the MSP(NaSi) samples at Surf/Si molar ratios of 0.10-0.22, indicating that the hexagonal mesostructure was also obtained using Na_2SiO_3 as the silica precursor through aerosol-assisted EISA procedure.

In addition, it can also be found from Figure 5.2 that the (100) diffraction peaks are shifted to higher angles with increasing the Surf/Si molar ratios, this leads to decreases in their d-spacing values. It was verified that a shorter inter-micellar distance is caused by a larger surfactant volume fraction via increasing the Surf/Si ratio [112]. The intensity of (100) peak is diminished and becomes broader for the MSP(NaSi) samples with Surf/Si molar ratio of higher than 0.22. This suggests the collapse of long range crystallographic order due to an excessive amount of surfactant [112].

Generally, mesoporous material of MCM-41 synthesized via conventional aqueous route shows unidirectional pore orientation; therefore high-degree diffraction intensity of (110) as well as (210) peaks, which are typical diffraction peaks of hexagonal lattice with $p6mm$ space group, are observed. In contrary, the materials of either MSP(TEOS) or MSP(NaSi) synthesized from aerosol-assisted process have multiple pore orientations within individual particles which would lead to less degree of (110) and (210) peaks in XRD pattern.

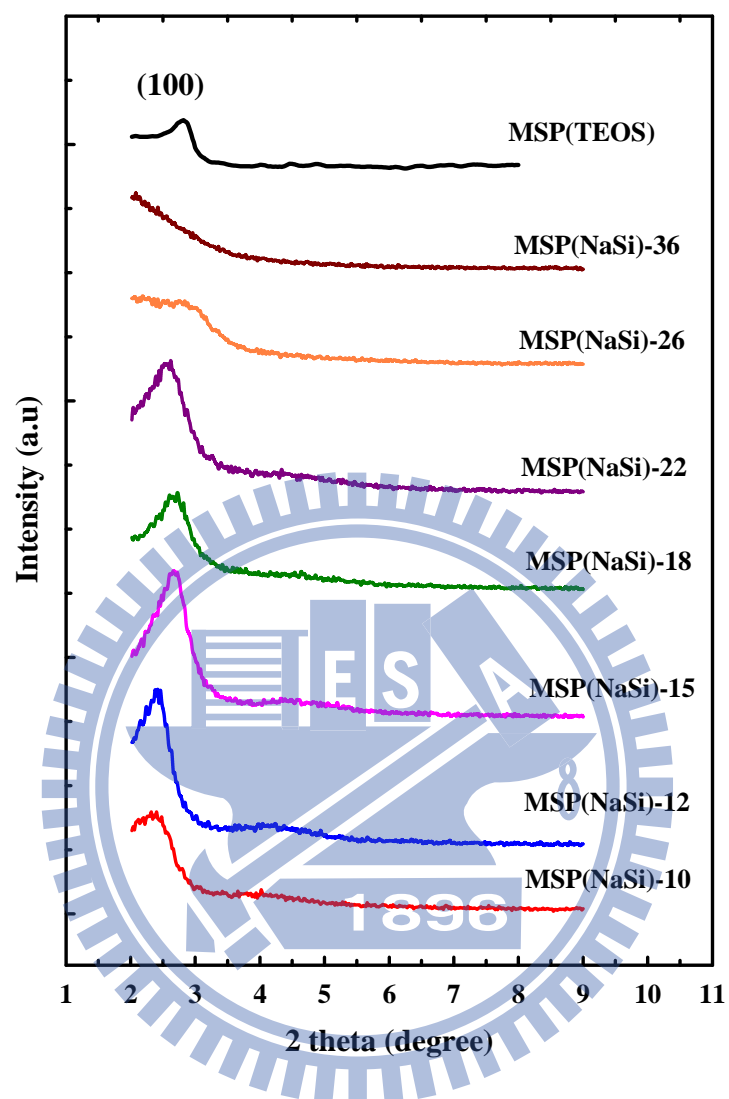


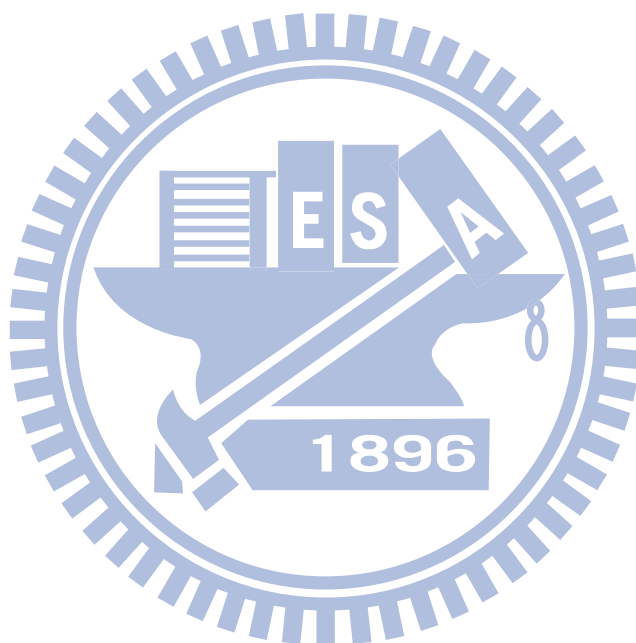
Figure 5.2 XRD patterns of calcined MSPs prepared from Na_2SiO_3 (denoted as MSP(NaSi)) and TEOS (denoted as MSP(TEOS)), respectively.

The N₂ adsorption-desorption isotherms of all calcined samples are shown in [Figure 5.3](#). The nitrogen adsorption-desorption isotherms for MSP(TEOS) and MSP(NaSi) samples with Surf/Si molar ratios from 0.10 to 0.22 exhibit a type IV isotherm of typical mesoporous materials according to the IUPAC classification, which feature a narrow step due to capillary condensation of N₂ within the primary mesopores [132]. As compared to that of the MSP(TEOS) sample, the MSP(NaSi) samples with Surf/Si ratios from 0.10 to 0.22 shows no hysteresis loop at $p/p_0 = 0.2$ to 0.4. The less steep condensation step for MSP(NaSi) samples indicates a less degree of uniform mesostructure as compared to that of MSP(TEOS) sample. By increasing the Surf/Si molar ratios to above 0.26, the MSP(NaSi)-26 and MSP(NaSi)-36 samples show different adsorption-desorption isotherms which belong to the type I with H4 hysteresis loop, it can be indexed to the microporous materials based on the IUPAC classification [132].

[Figure 5.4](#) displays the BJH pore size distribution of MSP(TEOS) and MSP(NaSi) samples with Surf/Si molar ratios from 0.10 to 0.22. It is obvious that all samples show narrow pore size distribution, suggesting the uniform porosity of the obtained materials. MSP(TEOS) exhibits the highest intensity of the pore size distribution, which indicates that the uniformity of mesostructure of MSP(TEOS) is superior to those samples prepared from Na₂SiO₃. This is consistent with the N₂ adsorption-desorption isotherms that MSP(TEOS) displays a sharper condensation step and hysteresis loop. This may probably due to the presence of sodium salts on the framework causing deterioration in the order arrangement of the mesostructure. The MSP(NaSi)-18 presents the highest intensity of the pore size distribution as compared to other samples prepared from Na₂SiO₃, this implies that MSP(NaSi)-18 has the most uniform mesostructure. On the other hand, the BJH pore size distributions of MSP(NaSi)-26 and MSP(NaSi)-36 shifted to microporous region (< 2 nm) and thus it could not be detected in this study. The result is in agreement with the N₂ adsorption-desorption isotherms shown in [Figure 5.3](#).

The textural properties of BET specific surface area, specific pore volume and average pore diameter derived from nitrogen adsorption-desorption measurements are summarized in [Table 5.1](#). One can see that the specific surface areas of the MSP(NaSi) samples with mesoporous structure (Surf/Si ratios from 0.10 to 0.22) are in the range of 823 to 1058 m²/g. The pore diameters of MSP(NaSi), 2.4-2.8 nm, are higher than

that of MSP(TEOS), 2.3 nm. It is believed that sodium silicate can act as both a silica source and inorganic salt in the formation of mesoporous silica. Addition of inorganic salts can increase the aggregate number of the micelles, which can further enhance the pore diameter of the micelles. A similar observation was seen for the synthesis of mesoporous silica using sodium silicate as the precursor over conventional aqueous route [129].



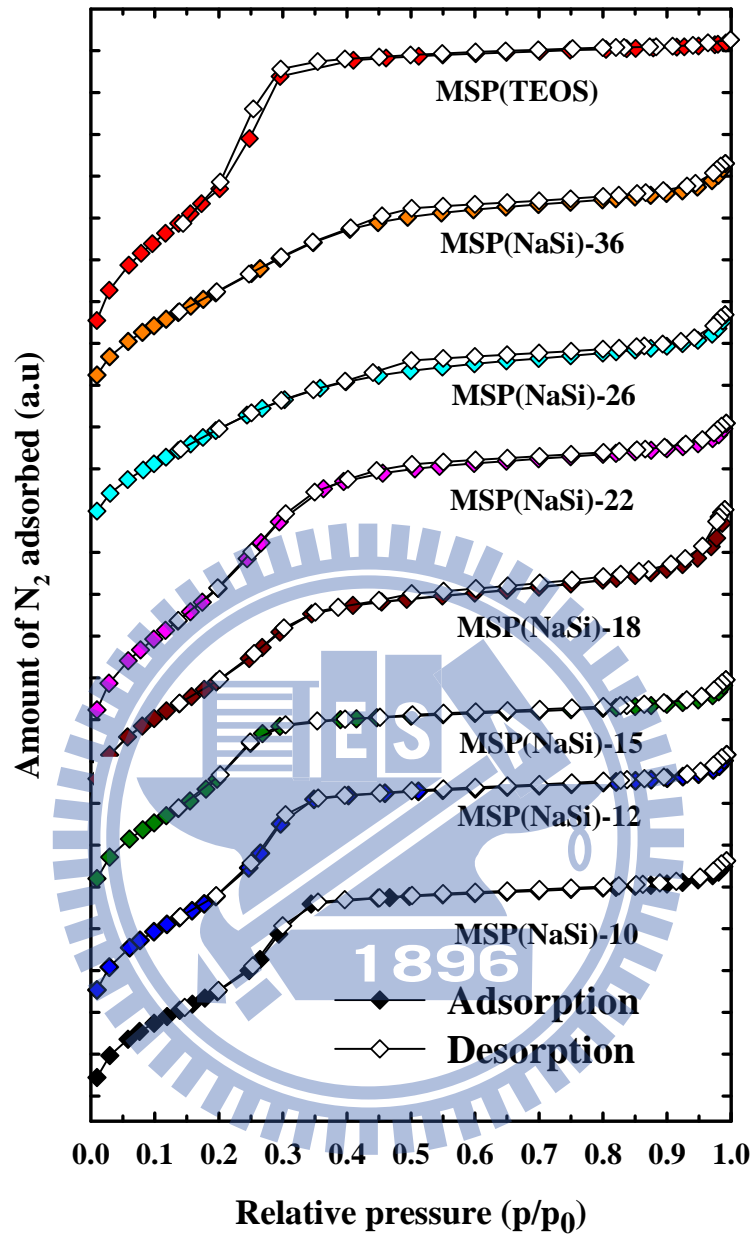


Figure 5.3 Nitrogen adsorption-desorption isotherms of calcined MSP(NaSi) and MSP(TEOS), respectively.

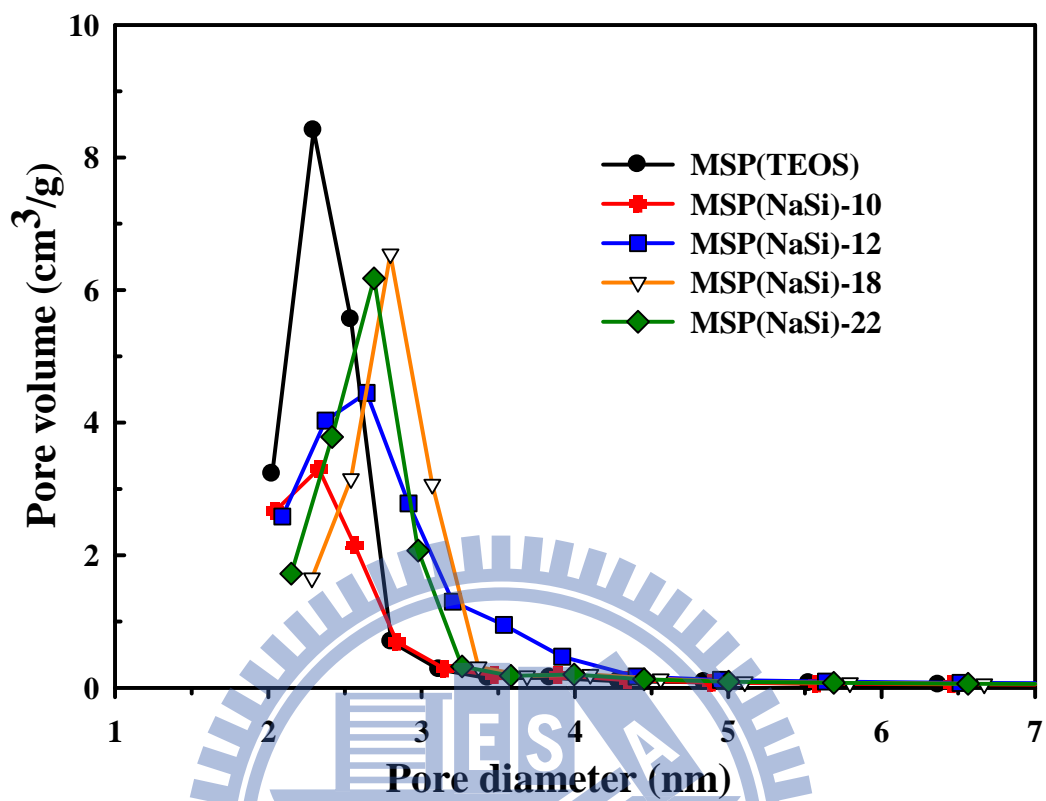


Figure 5.4 BJH pore diameter distribution of calcined MSP(NaSi) and MSP(TEOS), respectively.

Figure 5.5 presents the SEM images of MSP(TEOS) and MSP(NaSi)-18 samples. It can be clearly observed that MSP(TEOS) was in spherical shape. On the contrary, some hollow and fractured particles were formed in addition to the near spherical particles for the MSP(NaSi)-18. Similar observations have been reported by Bruinsma et al. [133] who synthesized mesoporous silica with hollow morphology using TEOS as the silica source. They claimed that the operating conditions and solution/slurry characteristics had great influence on the particle morphology so that it could be from spherical particles to hollow and fractured particles.

Since the operating conditions for the fabrication of MSP(TEOS) and MSP(NaSi) samples were the same, therefore the solution/slurry characteristics should play a crucial role in determining the particle morphology. It was proposed that hollow structure was formed at low slurry concentration because the time required to homogenize the droplet is longer than the solvent evaporation time during the quick-drying process of the droplets [134]. In this study, MSP(NaSi) samples were synthesized at relatively lower slurry concentration as compared to that of MSP(TEOS). The MSP(TEOS) with much higher solution concentration could be homogenized prior to the completion of drying the droplets. Consequently, spherical particles were much more easily formed with well-defined morphology. On the other hand, MSP(NaSi)-18 with relatively lower solution concentration might result in higher possibility for the formation of hollow and fractured particles, the solid shell formed in the beginning where the concentration is the highest, the internal pressure increases because the moisture cannot be released immediately.

The particle size distributions of the MSP(NaSi) and MSP(TEOS) were also compared. They were determined based on averaging over 80 particles from the SEM images. Values of the geometric mean diameter (D_{pg}) and geometric standard deviation (σ_g) are listed in Table 5.1. One can see that the particle sizes of MSP(NaSi) samples gradually decreased with the increasing of Surf/Si molar ratio. This may be due to that many smaller clusters were formed at lower CTAB concentrations and they had weaker dispersion potential and lower chemical activity toward self-assembly [135]. Consequently, these small clusters or primary particles were able to aggregate due to their significant numbers and led to larger particle sizes before evaporation process began in the heating ovens. On the other hand, larger cluster sizes were formed at higher concentrations of CTAB and led to lower cluster or primary particle

numbers, thus the low flocculation tendency at lower cluster (primary particle) number concentrations resulted in smaller final particle sizes.

It is also interesting to note that the MSP(NaSi) samples resulted in smaller particle sizes ($D_{pg}=0.79\sim 2.82\ \mu\text{m}$) as compared to that of MSP(TEOS) ($D_{pg}=3.86\ \mu\text{m}$). It is well known that sodium silicate exhibited rapid hydrolysis and condensation rates which would lead to larger cluster size. The less agglomeration of larger clusters resulted in smaller particle sizes when using sodium silicate as the silica source. In addition, the MSP(NaSi) samples presented small degree of particle size distribution ($\sigma_g=1.8\sim 4.0$) as compared to that of MSP(TEOS) ($\sigma_g=5.0$). Similar observations were found using sodium silicate and TEOS, respectively, as the silica precursor via liquid route [129].

The textural mesostructure of the MSP(TEOS) and MSP(NaSi) samples with various Surf/Si molar ratios was characterized by TEM images and the results are shown in Figure 5.6. The TEM image of MSP(TEOS) material (Figure 5.6(a)) clearly shows a well ordered long range hexagonal array of mesopores and these long range crystallographic features are consistent with the results of XRD and BET analyses. The hexagonal structure can also be observed in MSP(NaSi) samples. The uniform porosities of obtained materials revealed by TEM analysis are also consistent with the narrow pore size distribution (BJH) determined by N_2 adsorption-desorption measurements for all the calcined materials. The mesostructure is composed of tubular pores either perpendicular or parallel to the particle surface, which is the characteristic of spherical MSPs fabricated through EISA route, while MCM-41 synthesized via conventional aqueous route exhibits unidirectional pore orientation within rod- or flake-shaped particles [110].

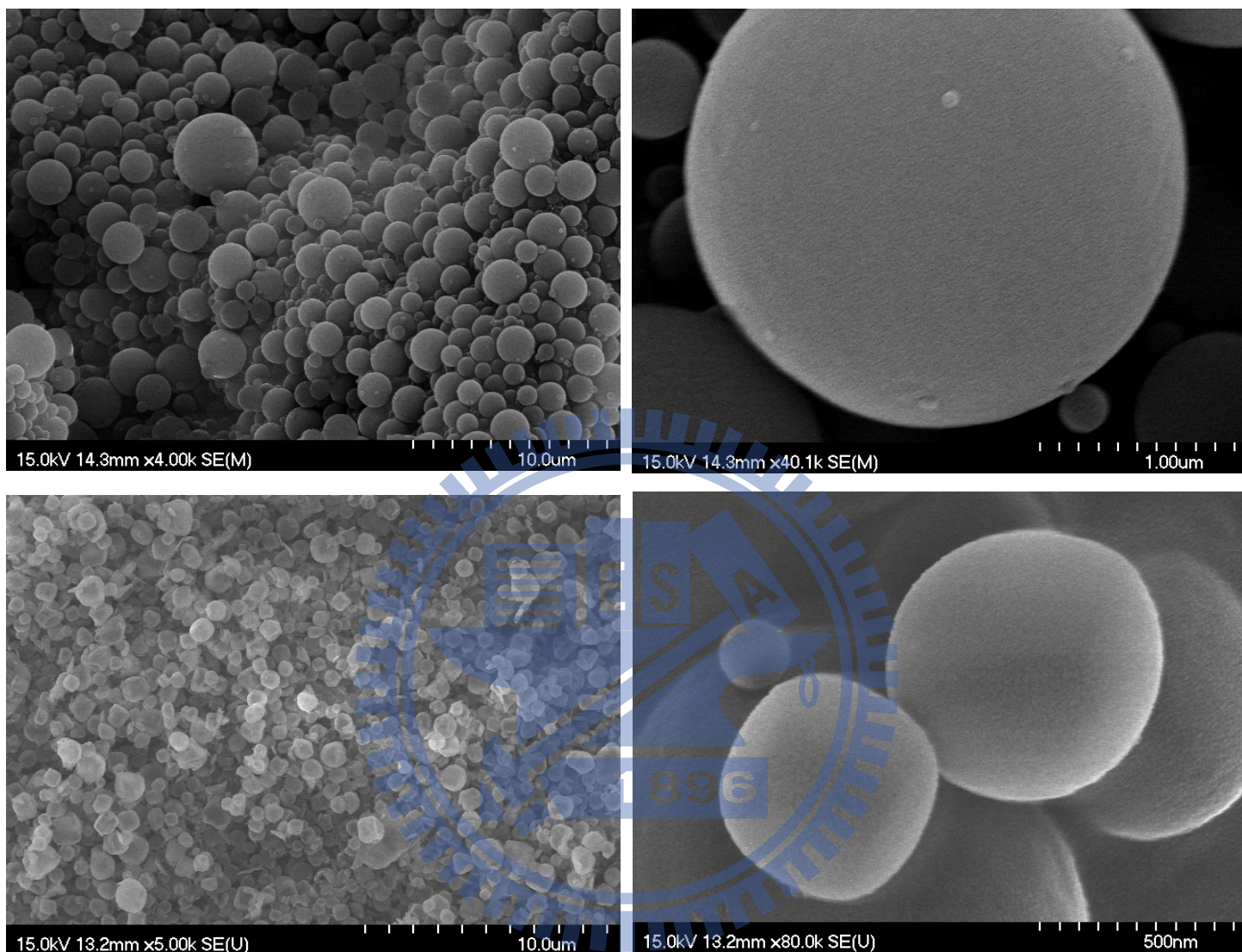


Figure 5.5 SEM images of calcined MSPs. (a1) MSP(TEOS) with scale bar of 10 μm , (a2) MSP(TEOS) with scale bar of 1 μm (b1) MSP(NaSi)-18 with scale bar of 10 μm , and (b2) MSP(NaSi)-18 with scale bar of 500 nm.

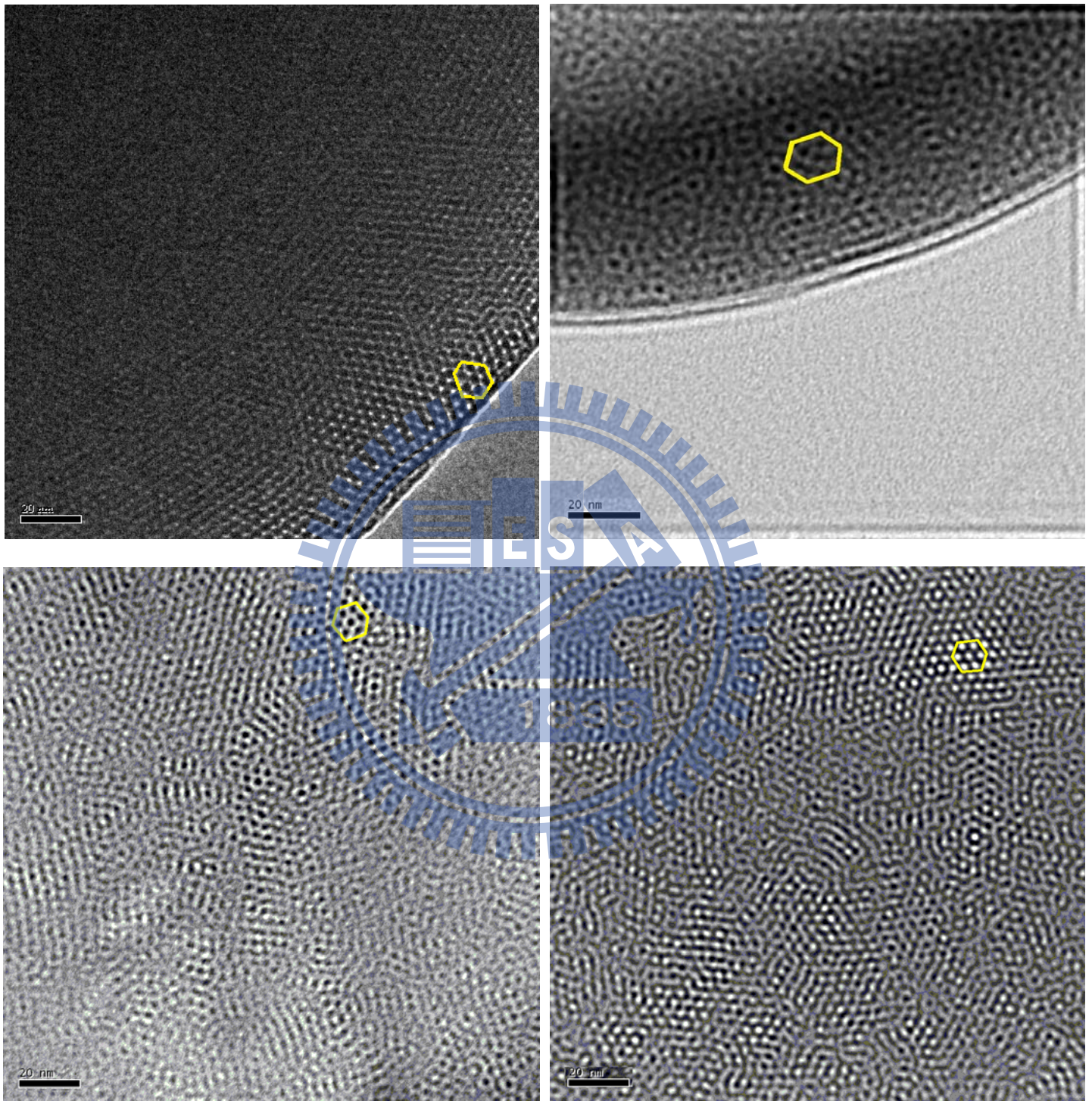


Figure 5.6 TEM images of calcined MSPs. (a) MSP(TEOS), (b) MSP(NaSi)-10, (c) MSP(NaSi)-18 and (d) MSP(NaSi)-22. (The scale bar is 20 nm)

Table 5.1 Physical properties of the mesoporous adsorbents

Sample	$n_{\text{CTAB}}/n_{\text{Si}}$	$^a S_{\text{BET}}$ (m^2/g)	$^b d_{\text{BJH}}$ (nm)	$^c V_p$ (cm^3/g)	$^d d_{100}$ (nm)	$^e a_o$ (nm)	$^f T_w$ (nm)	$^g D_p$ (μm)/ σ_g
MSP (TEOS)	0.18	1153	2.3	0.75	3.4	3.9	1.6	3.86/5.0
MSP(NaSi)-10	0.10	823	2.8	0.69	3.7	4.3	1.5	2.82/1.8
MSP(NaSi)-12	0.12	866	2.7	0.71	3.6	4.2	1.5	2.03/2.0
MSP(NaSi)-15	0.15	881	2.5	0.70	3.3	3.8	1.2	1.40/2.4
MSP(NaSi)-18	0.18	908	2.6	0.75	3.3	3.8	1.2	1.04/2.5
MSP(NaSi)-22	0.22	1058	2.4	0.88	3.4	3.9	1.6	1.00/2.8
MSP(NaSi)-26	0.26	710	-	0.60	-	-	-	0.91/3.0
MSP(NaSi)-36	0.36	696	-	0.61	-	-	-	0.79/4.0

NOTE: a BET surface area. b Pore diameter calculated by BJH theory. c Pore volume. d d-spacing between (100) planes. e Hexagonal unit cell ($a_o = 2 d_{100} / \sqrt{3}$). f Pore wall thickness ($T_w = a_o - d_{\text{BJH}}$). $^g D_p$ is the geometric mean diameter and σ_g is the geometric standard deviation.

CHAPTER VI AEROCESSING OF MESOPOROUS SILICA PARTICLES USING WASTE-DERIVED SILICATE

6.1 Salt-assisted synthesis of mesoporous silica particles using waste-derived silicate

6.1.1 Motivation

Our prior study investigated the feasibility of extracting silicate supernatant from the optoelectronic industrial waste powder, which is one of the major by-products in semiconductor and optoelectronic industries. It was demonstrated that the optoelectronic waste powder could be an alternative resource for producing silica-based materials.

Up to date, most researches on the synthesis of mesoporous silica materials from siliceous wastes has been processed through solution precipitation methods using batch reactors, which require complex preparation steps and long contact times. To overcome the disadvantages of traditional batch processes, vapor-phase synthesis of the mesoporous silica materials has been recently developed and become one of the facile processes for particles engineering purposes due to its rapid and continuous synthesis as well as simplicity of scaling up [136–142]. However, to our knowledge, there is no report yet concerning the synthesis of mesoporous silica materials via aerosol approach using industrial solid wastes as the starting material.

6.1.2 Synthesis of MSP (AS)

The sodium silicate solution was prepared by mixing optoelectronic waste powder with 6 M NaOH solution at room temperature for 12 h. [Table 6.1](#) shows the elemental analysis of the raw waste powder and the silicate supernatant after extraction with NaOH solution. The molar composition of the precursor mixture was 1SiO_2 : $3(\text{NH}_4)_2\text{SO}_4$: $359\text{H}_2\text{O}$: 7.32HCl . The precursor mixture was mixed and nebulized by an ultrasonic atomizer and carried by a high pressure, clean and dry air flow. The reagent flow was then passed through a high-temperature tubular reactor with the temperature of $400\text{ }^\circ\text{C}$. The total flow rate in this study was fixed at $2000\text{ cm}^3/\text{min}$ ($25\text{ }^\circ\text{C}$, 1 atm), which corresponded to a residence time of 4 seconds. After the heating

process, the as-synthesized MSP samples were collected downstream of the reactor by a high-efficiency filter. Finally, they were recovered by washing and filtration with DI water followed by drying in an oven at 110 °C. The aerosol processing of mesoporous silica sample from the waste powder in the presence of (NH₄)₂SO₄ template was denoted as MSP (AS), while the mesoporous silica sample from the waste powder in the absence of (NH₄)₂SO₄ template was named as MSP.

To investigate the effect of the support on the adsorption capacity of the adsorbent, mesoporous silica materials including MCM-41 and SBA-15 were synthesized as well. The synthesis of MCM-41 was performed using pure chemicals of sodium metasilicate nanohydrate (Na₂SiO₃·9H₂O) and cetyltrimethylammonium bromide (CTAB) as the silica source and template, respectively. The molar composition of the gel mixture was 1SiO₂: 0.2 CTAB: 120 H₂O: 0.89 H₂SO₄. The resulting gel mixture was transferred into a Teflon coated autoclave and kept in an oven at 145 °C for 36 h. After cooling to room temperature, the resultant solid was recovered by filtration, washed with DI water and dried in an oven at 100 °C. Finally, the organic template was removed by using a muffle furnace in air at 550 °C for 6 h.

Mesoporous SBA-15 was synthesized using a tri-block copolymer, EO₂₀-PO₇₀-EO₂₀ (Pluronic P123, BASF) as the template and sodium silicate solution (~14% NaOH, ~27% SiO₂, Aldrich) as the silica source. The molar composition of the gel mixture was 1SiO₂: 0.01 P123: 286 H₂O: 0.7 H₂SO₄. For a typical synthesis, 2.01 g of P123 (dissolved in 20 g of DI water) was added to 100 g of 6 M H₂SO₄. After stirring for 1 h, 8 g of sodium silicate solution (dissolved in 50 g of DI water) was added to the above solution with continuous stirring for 15 min. The resultant mixture was aged at 100 °C for 24 h. The obtained solid product was filtered and washed with DI water, followed by drying in an oven at 60 °C. Finally, the complete removal of residual surfactants was carried out by using a muffle furnace at 500 °C in air for 6 h.

6.1.3 CO₂ adsorption measurement

The CO₂ adsorption tests were conducted by a thermo-gravimetric analyzer (TGA, Netzsch TG209 F1, Germany). Typically, approximately 10 mg of adsorbents were loaded on the TGA sample holder and purged with nitrogen gas at the temperature of 110 °C with a flow rate of 120 cm³/min for 30 min until the weight is not changed,

suggesting that the evaporation of water on the adsorbents was complete. The mass change of the adsorbents during CO₂ adsorption was then measured under isothermal condition of 60 °C. The inlet CO₂ concentration was 10% (v/v in N₂) which was obtained from a certified gas cylinder and introduced at a flow rate of 40 cm³/min (25 °C, 1atm) for 60 min of adsorption time until the weight was not changed to ensure that the adsorbents were completely saturated. The moisture in the CO₂ gas cylinder was measured to be 5% relative humidity, which corresponded to an absolute moisture content of only 0.16% (v/v). This was much lower than the CO₂ concentration and thus the moisture impact on the CO₂ adsorption is negligible.



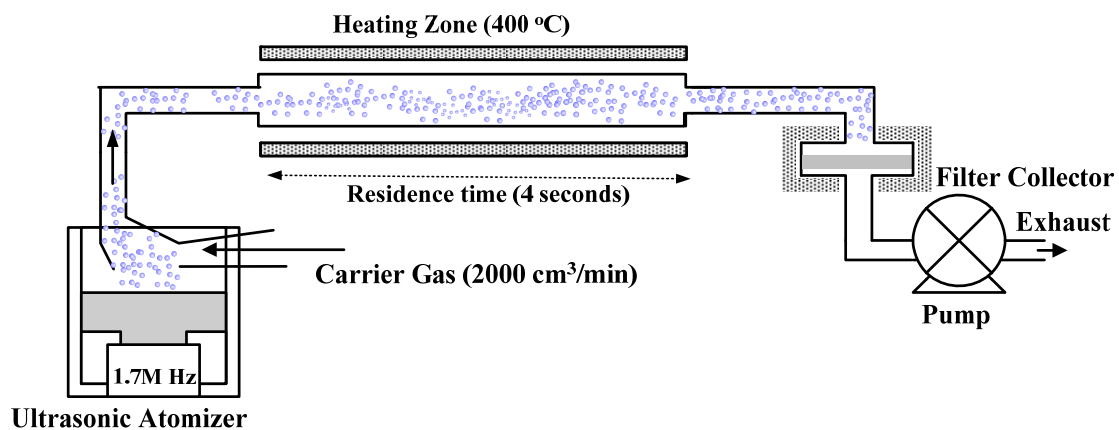


Figure 6.1 Experimental setup for the generation of mesoporous silica spherical particles (MSPs) through aerosol spray process.

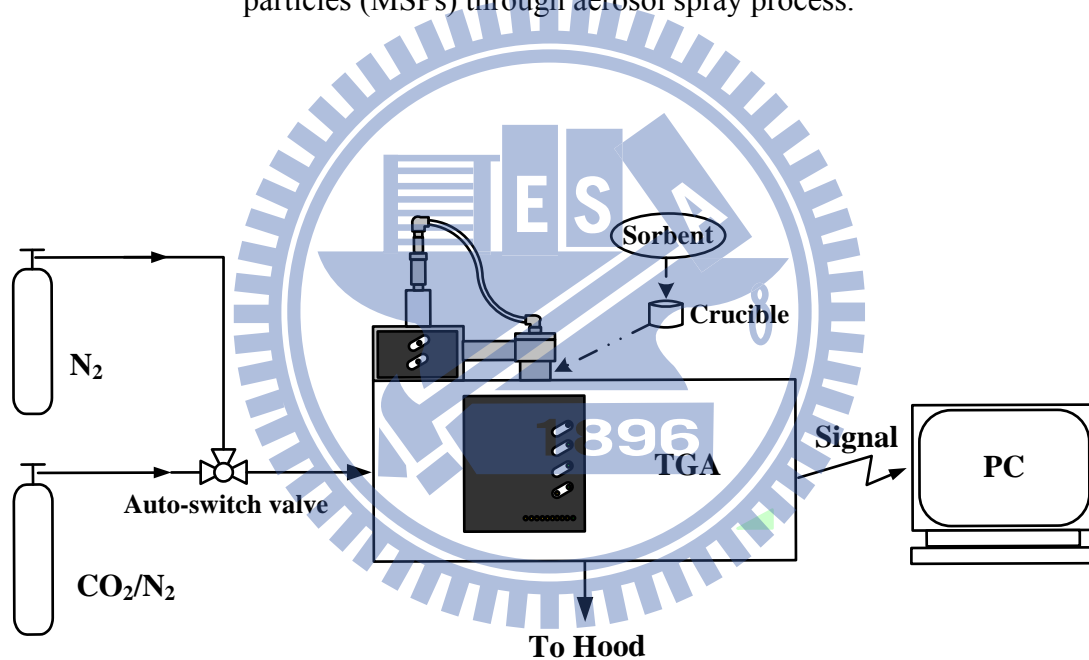


Figure 6.2 TGA system for the CO₂ adsorption.

6.1.4 Results and discussion

Powder XRD patterns of the as-synthesized and washed MSP samples prepared using sodium silicate precursor from optoelectronic waste powder through aerosol spray process are shown in Figure 6.3. As can be seen from the results, the as-synthesized MSP sample prepared without $(\text{NH}_4)_2\text{SO}_4$ salt shows significant diffraction peaks at 2θ of 22° , 27° , 32° , 45° , 56° , 66° and 75° . The reflection peak centered at 22° can be assigned to the silica in amorphous phase and the other peaks are indexed on the NaCl crystallite [143]. Since NaCl exhibits stronger crystallinity than that of amorphous silica, the NaCl crystallites are expected to show higher diffraction intensity as depicted in Figure 6.3(a). To elucidate the above findings, the general theory of silica polymerization must be addressed. In the preparation of silica precursors, two reactions took place simultaneously, i.e., condensation and sodium silicate acidification. The silica condensation process, which is the formation of a siloxane linkage between surface silanol groups, can be represented as [144]:



And the reaction of sodium silicate solution with hydrochloric acid during acidification process can be written as:

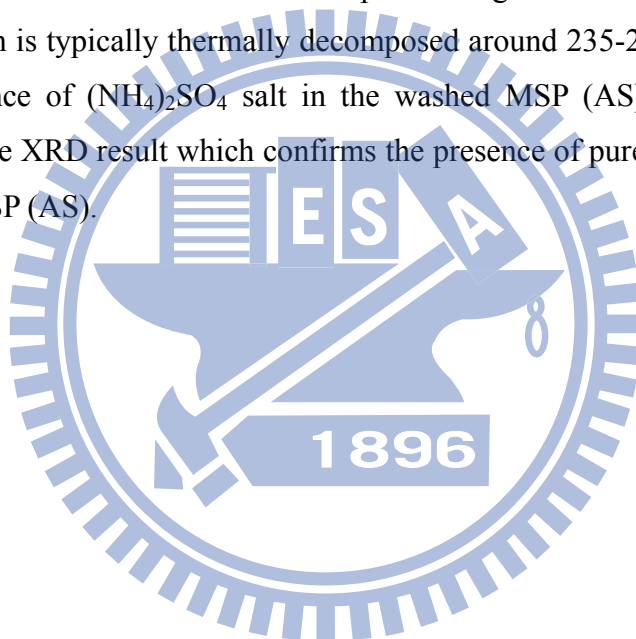


When the sodium silicate precursor is added to hydrochloric acid solution, fine crystallites of NaCl are formed and embedded in the silica particles during aerosol spray process. Consequently, the co-existence of amorphous silica and NaCl is observed in the as-synthesized MSP sample.

On the other hand, as the $(\text{NH}_4)_2\text{SO}_4$ salt is used in the starting precursors, the as-synthesized-MSP (AS) sample contains a large amount of crystalline $(\text{NH}_4)_2\text{SO}_4$ as the main component [145]. Meanwhile, the intensities of reflection peaks assigned to crystalline NaCl are decreased and become insignificant in the as-synthesized MSP (AS). This suggests that $(\text{NH}_4)_2\text{SO}_4$ is present with relatively higher loadings as compared to that of NaCl in the as-synthesized-MSP (AS) sample. After aqueous washing procedure, there is only one broad diffraction peak observed in the washed MSP (AS) material, which is indicative of amorphous silica [105]. This implies that pure siliceous material can be obtained after the removal of salt template by aqueous

washing process.

To understand the thermal stability of the washed MSP (AS) material, the TGA and DTG analyses were carried out and shown in [Figure 6.4\(a\)](#) and [Figure 6.4\(b\)](#), respectively. One can see from [Figure 6.4\(a\)](#) that the washed MSP (AS) shows an initial weight loss at $<100\text{ }^{\circ}\text{C}$, which can be ascribed to the evaporation of the physically adsorbed water on the surface of the material. Besides, it is found from [Figure 6.4\(b\)](#) that the DTG curve showed two weak peaks from 200 to $900\text{ }^{\circ}\text{C}$. The first step ($200\text{-}600^{\circ}\text{C}$) is due to the loss of chemically adsorbed water bonded to Si-OH through hydrogen bond. From 600 to 900°C , the weight loss is expected to be associated with the further condensation of the Si-OH groups from the amorphous SiO_2 [107]. It is noticeable that there are no peaks assigned to the decomposition of $(\text{NH}_4)_2\text{SO}_4$, which is typically thermally decomposed around $235\text{-}280^{\circ}\text{C}$. This clearly reveals the absence of $(\text{NH}_4)_2\text{SO}_4$ salt in the washed MSP (AS) material. This is consistent with the XRD result which confirms the presence of pure siliceous material of the washed MSP (AS).



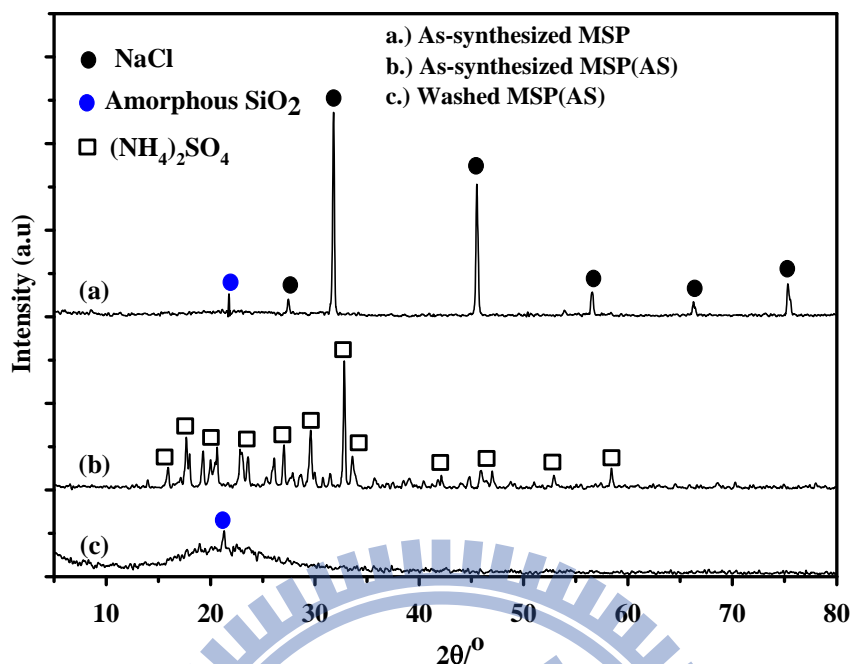


Figure 6.3 XRD patterns of as-synthesized MSP, as-synthesized MSP (AS) and washed MSP (AS) samples.

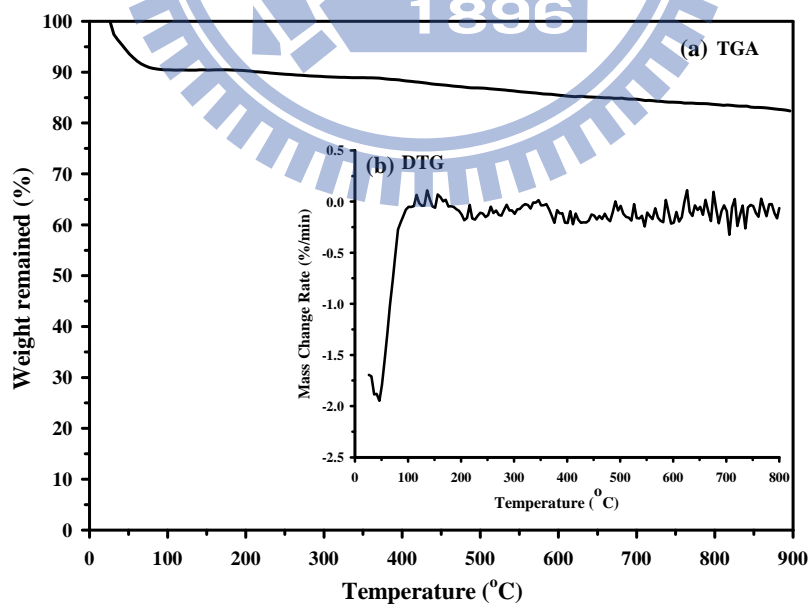


Figure 6.4 (a) TGA and (b) DTG analyses of the washed MSP (AS).

The N₂ adsorption-desorption isotherms of the washed MSP and MSP (AS) are presented in [Figure 6.5\(a\)](#). Both the washed samples show type IV isotherms of mesoporous material according to the IUPAC classification, featuring a narrow step due to capillary condensation of N₂ within the primary mesopores [146]. Furthermore, the isotherm of the washed MSP (AS) also shows the type H1 hysteresis loop, which is associated with the uniform pore channels [147]. [Figure 6.5\(b\)](#) displays the BJH pore size distribution of the washed MSP and MSP (AS) samples, where a significant pore enlargement is observed for washed MSP (AS) sample.

The effect of the salt templating medium on the physical properties such as BET specific surface area, total pore volume and BJH pore diameter derived from N₂ adsorption-desorption measurements are summarized in [Table 6.1](#). Apparently, the as-synthesized MSP (AS) exhibits low surface area and tiny pore voids due to the occluded salt template. After the removal of salt matrix by aqueous washing, the specific surface area and the total pore volume of the washed MSP (AS) are drastically enhanced. In addition, the washed MSP (AS) shows higher surface area and larger pores as compared to those of the washed MSP, which was prepared without the addition of (NH₄)₂SO₄. These results are quite conclusive in demonstrating that (NH₄)₂SO₄ salt can be employed as an effective template to support the mesostructure.

Table 6.1 Elemental analysis of optoelectronic waste powder and silicate supernatant analyzed by the SEM-EDS and ICP-MS analysis

Element	Si	F	O	N	Na
^a Optoelectronic waste powder (wt%)	28.82	47.82	17.54	5.82	-
^b Supernatant (ppm)	31420	-	- ^c	-	69670

NOTE: a: sample analyzed by the SEM-EDS analysis

b: sample analyzed by the ICP-MS analysis

c: non-detected.

Table 6.2 Structural parameters of the materials

Sample name	^a S _{BET} (m ² /g)	^b d _{BJH} (nm)	^c V _p (cm ³ /g)
As-synthesized MSP (AS)	26	16.8	0.08
Washed MSP (AS)	585	9.1	1.24
Washed MSP	480	5.7	0.7
MCM-41	1101	3.0	0.99
SBA-15	745	6.5	1.10
Zeolite NaY	712	-	0.35
TEPA-MSP (AS)	54	8.7	0.22
TEPA-MCM-41	36	-	0.07
TEPA-SBA-15	40	6.0	0.11
TEPA-NaY	2.5	-	0.001

NOTE: ^aBET surface area; ^bPore diameter calculated by BJH theory; ^cPore volume calculated by BJH theory

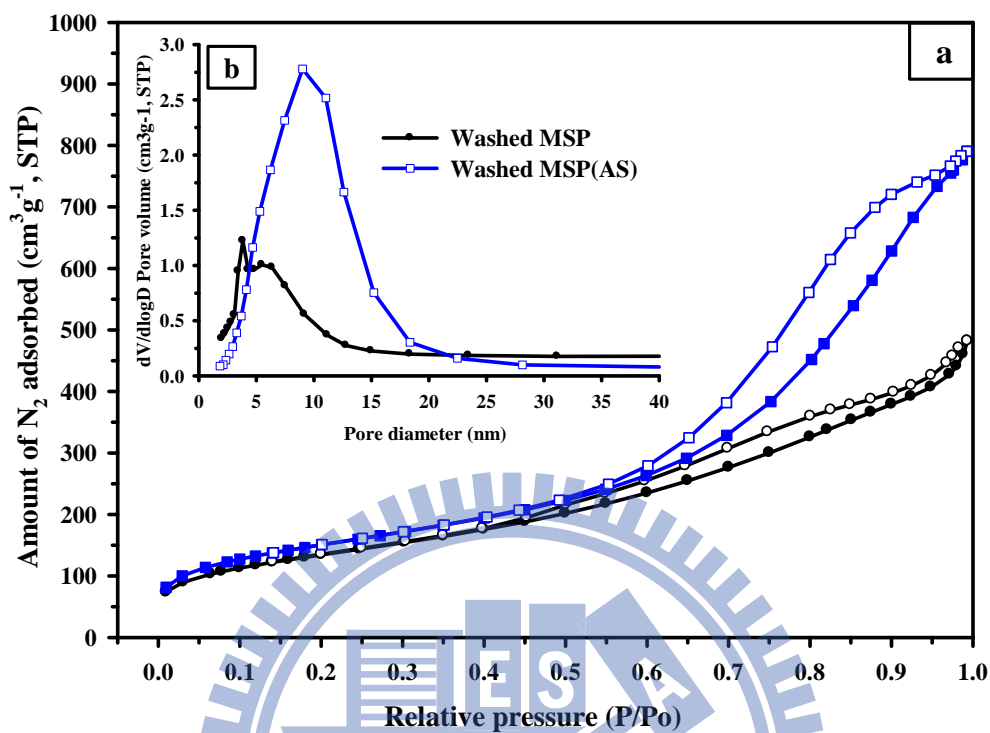
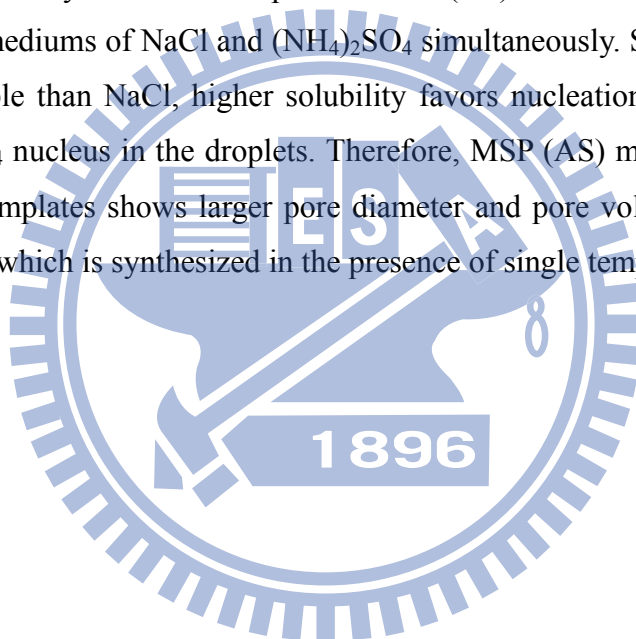


Figure 6.5 (a) N_2 adsorption-desorption isotherms and (b) BJH pore diameter distributions of the washed MSP and MSP(AS) samples.

The possible pathway of formation of MSP and MSP (AS) materials via aerosol spray process is illustrated in [Figure 6.6](#). In the present study, sodium silicate solution extracted from optoelectronic industrial waste powder is firstly acidified with the aid of hydrochloric acid to form polymeric silica sol. The NaCl crystallites are formed during sodium silicate acidification and embedded into MSP particles on aerosol process. As the precursor solution is aerosolized, the rapid evaporation of water drastically enhanced the silica polymerization and solidification of the salt to act as a template matrix to support the formation of porous structure. Finally, mesoporous silica particles with three-dimensional network can be obtained by subsequent aqueous washing process to completely remove the salt templates.

It is noteworthy that the mesoporous MSP (AS) is fabricated by employing dual templating mediums of NaCl and $(\text{NH}_4)_2\text{SO}_4$ simultaneously. Since $(\text{NH}_4)_2\text{SO}_4$ is more water soluble than NaCl, higher solubility favors nucleation and formation of bigger $(\text{NH}_4)_2\text{SO}_4$ nucleus in the droplets. Therefore, MSP (AS) material synthesized using dual salt templates shows larger pore diameter and pore volume than those of the MSP sample, which is synthesized in the presence of single template of NaCl.



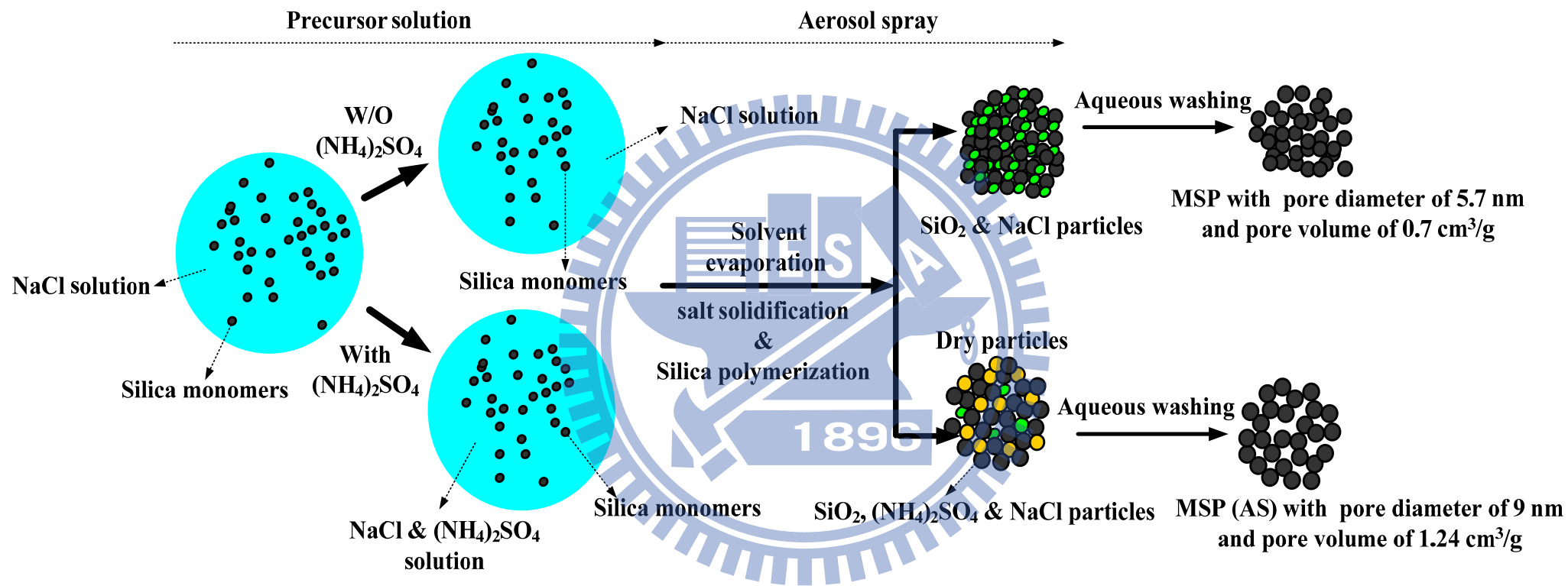
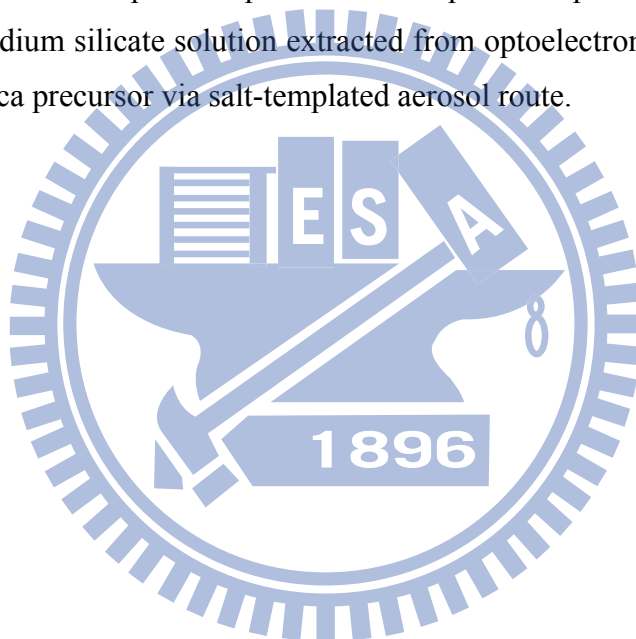


Figure 6.6 Possible pathway for the formation of MSP and MSP (AS) samples through aerosol spray process.

The morphology of the washed MSP (AS) was revealed by SEM analysis depicted in [Figure 6.7\(a\)](#). It is observed that the washed MSP (AS) material is in spherical shape with particle size of ca. 1-1.5 μm . SEM image with higher magnification ([Figure 6.7\(b\)](#)) further reveals that the washed MSP (AS) shows rough surface, which are assembled from primary nanoparticles with average size of ca. 25 nm. TEM image in [Figure 6.7\(c\)](#) proves that the washed MSP (AS) particles are porous, appears to consist of interconnected network. Furthermore, the chemical composition of the washed MSP (AS) was analyzed by EDX analysis ([Figure 6.7\(d\)](#)), where there are only Si and O elements observed (Cu peak from the TEM grid). This is in agreement with the XRD result, which confirms the presence of amorphous silica. Consequently, it can conclude that silica spherical particles with open mesoporous structure can be prepared using sodium silicate solution extracted from optoelectronic industrial waste powder as the silica precursor via salt-templated aerosol route.



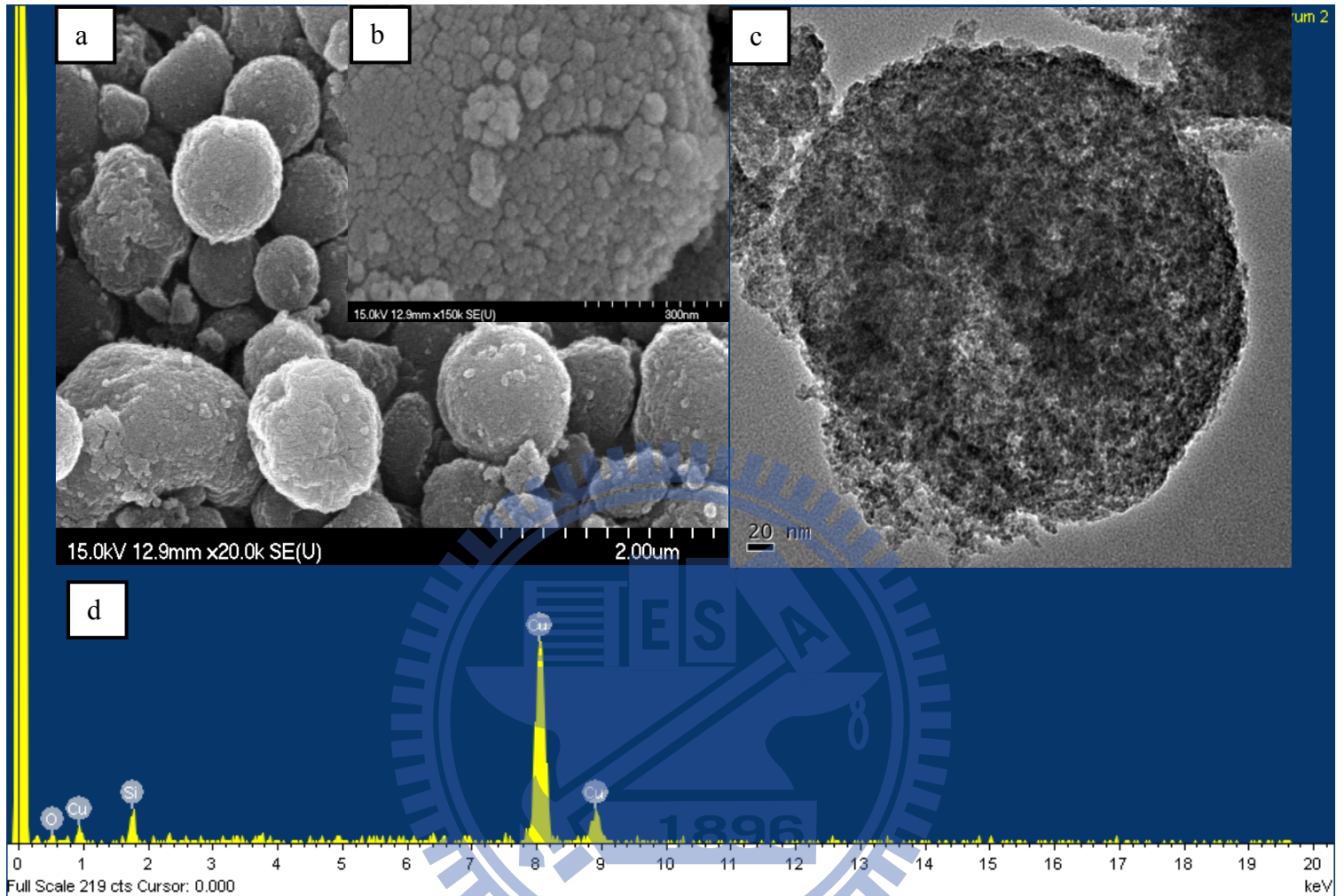


Figure 6.7 SEM images (a) low-magnification, (b) high-magnification of the washed MSP (AS). (c) TEM image and (d) EDS spectrum of the washed MSP (AS).

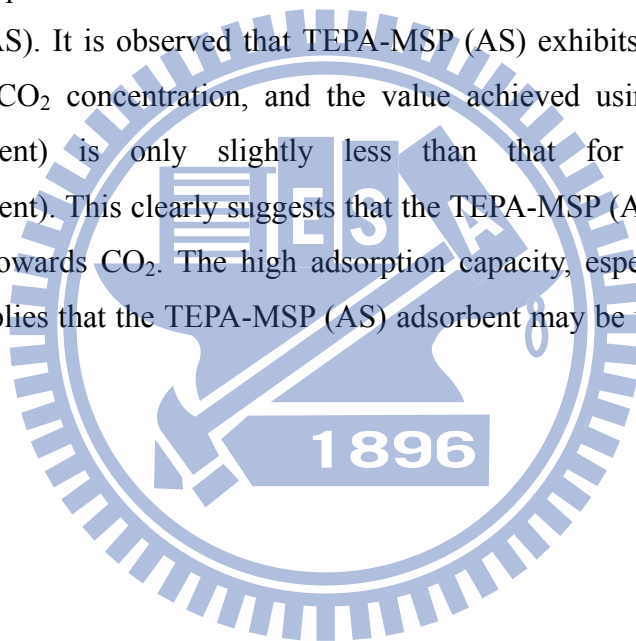
Figure 6.8 shows the time dependence of CO₂ uptake in the presence of 10% CO₂ at 60 °C for TEPA-functionalized MCM-41, SBA-15, MSP (AS) as well as zeolite NaY adsorbents. It can be found that the CO₂ uptake increased rapidly to more than 90% of the maximum uptake within the first five minutes of adsorption before reaching a constant equilibrium value for all adsorbents. The TEPA-MSP (AS) exhibits the highest CO₂ adsorption capacity, which could achieve 127 mg-CO₂/g-adsorbent, followed by the TEPA-SBA-15 (117 mg-CO₂/g-adsorbent), TEPA-MCM-41 (112 mg-CO₂/g-adsorbent) and TEPA-NaY (96 mg-CO₂/g-adsorbent). It is noteworthy that the adsorption capacity sequence coincides with the order of pore diameter and total pore volume of the parent silica supports.

The difference in the CO₂ uptake between TEPA-MSP (AS), TEPA-SBA-15, TEPA-MCM-41 and TEPA-NaY can be elucidated by their N₂ adsorption-desorption isotherms as shown in Figure 6.9(a) and Figure 6.9(b) as well as their pore structure data listed in Table 6.2. As shown in Figure 6.9(a), the parent MCM-41, SBA-15 and MSP (AS) all show type IV isotherms of mesoporous materials, while type I isotherm of microporous material is observed for raw NaY. After functionalized with TEPA, it was found from Figure 6.9(b) that both TEPA-MCM-41 and TEPA-NaY adsorbents exhibit type II isotherm, which is a typical indication of non-porous material. This implies that both MCM-41 and NaY supports were fully filled with 50 wt% of TEPA reagents. On the other hand, both TEPA-MSP (AS) and TEPA-SBA-15 samples show sharp capillary condensation steps with well-resolved hysteresis loops, suggesting that the intrinsic mesostructures of the MSP (AS) and SBA-15 were still partially retained after TEPA loading.

Because the density of TEPA is about 0.99 cm³/g and the total pore volumes of parent MSP (AS), SBA-15, MCM-41 and NaY are 1.24 cm³/g, 1.10 cm³/g, 0.99 cm³/g and 0.35 cm³/g, the maximum TEPA loading expected to load inside the channels of MSP (AS), SBA-15, MCM-41 and NaY is 56%, 53%, 50% and 26%, respectively. It is reported that more efficient contact between the CO₂ gas and the impregnated TEPA could be achieved when a small space is still left inside the pores of the mesoporous silica after TEPA loading [23]. As a result, the MCM-41 and NaY had lower CO₂ adsorption capacities due to the fact that they had smaller pore volumes, which may result in more constricted or blocked pores in the adsorbents.

Furthermore, since both the pores of MSP (AS) and SBA-15 were not completely filled by TEPA, there are enough accessible spaces in TEPA-MSP (AS) and TEPA-SBA-15 samples. Therefore, it could be speculated that the pore volume was not a main parameter which affected the CO₂ capturing performance. Very recently, Yan et al. [76] demonstrated that the CO₂ uptake increased with the increasing pore size of mesoporous substrates. Thus, the MSP (AS) with larger pore diameter could facilitate more TEPA into the pore channels more easily, which would lead to higher CO₂ adsorption performance than that of SBA-15 with smaller pore diameter. Therefore, it could be concluded that the large pore diameter and pore volume of MSP (AS) resulted in the highest CO₂ adsorption capacity among all adsorbents.

Figure 6.10 depicts the effect of CO₂ concentration on the adsorption performance of TEPA-MSP (AS). It is observed that TEPA-MSP (AS) exhibits a high adsorption capacity at low CO₂ concentration, and the value achieved using 10% CO₂ (127 mg-CO₂/g-adsorbent) is only slightly less than that for pure CO₂ (138 mg-CO₂/g-adsorbent). This clearly suggests that the TEPA-MSP (AS) adsorbent has a high selectivity towards CO₂. The high adsorption capacity, especially at low CO₂ concentration implies that the TEPA-MSP (AS) adsorbent may be useful for practical applications.



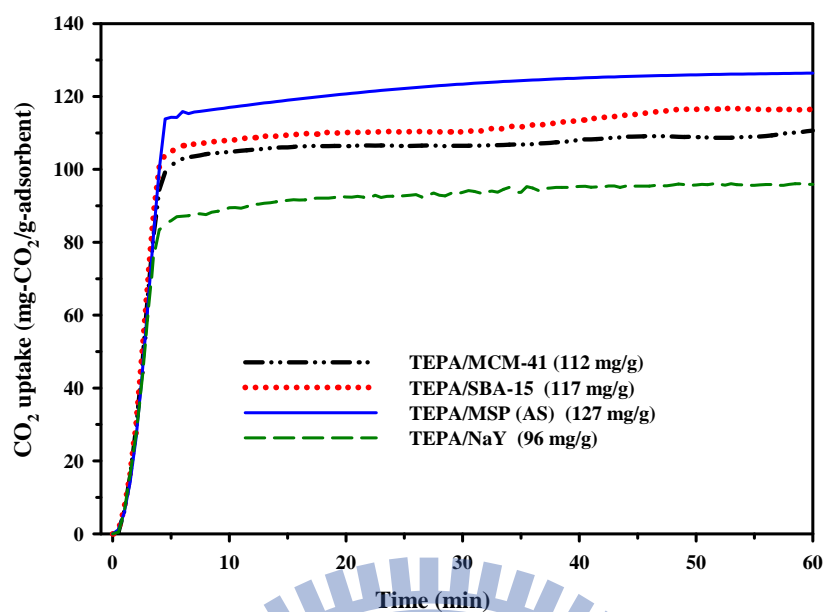


Figure 6.8 Comparison on CO₂ uptakes of TEPA loaded on MCM-41, SBA-15, MSP (AS) and NaY zeolite samples.

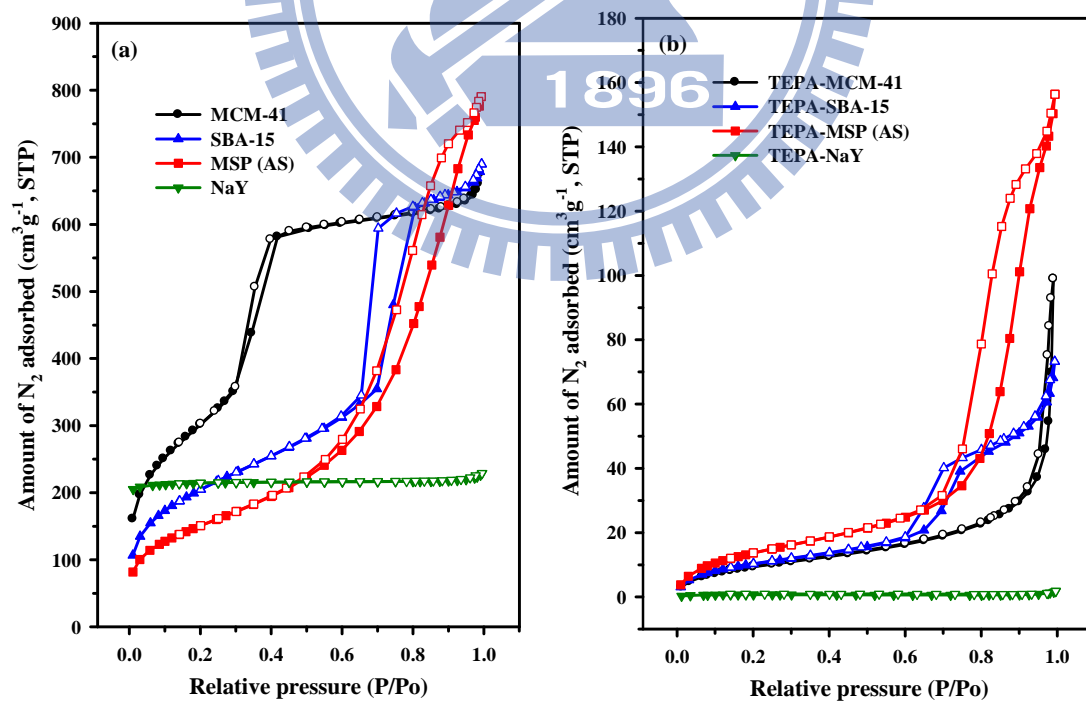


Figure 6.9 N₂ adsorption-desorption isotherms (a) parent MCM-41, SBA-15, MSP (AS) and NaY zeolite and (b) TEPA loaded on MCM-41, SBA-15, MSP (AS) and NaY zeolite samples.

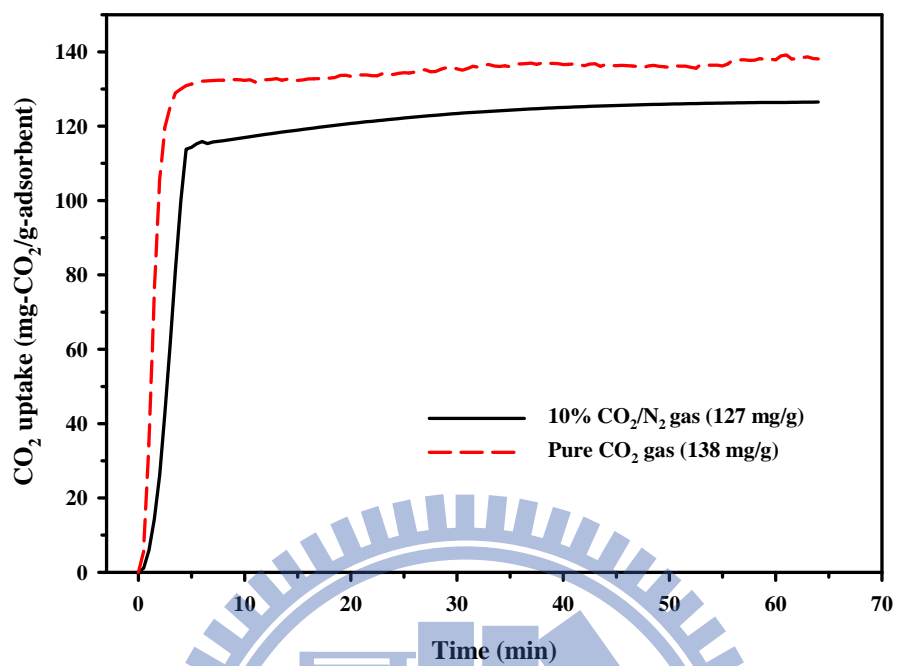


Figure 6.10 CO₂ adsorption performance of TEPA-MSP (AS) with 10% and pure CO₂ feed gas at 60°C.

6.2 Acid-directed synthesis of mesoporous silica spheres from waste-derived silicate

6.2.1 Motivation

In the prior section, it is demonstrated that silica particles with mesoporous framework can be easily prepared by neutralizing the basic silicate supernatant from waste powder with hydrochloric acid through aerosol spray process. Herein, three kinds of inorganic acids including hydrochloric acid, sulfuric acid as well as nitric acid were employed. The pore structures of the obtained spray-dried silica particles using different acids were studied.

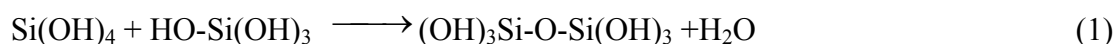
6.2.2 Synthesis of MSS

The sodium silicate solution was prepared by mixing optoelectronic waste powder with 6 M NaOH solution at room temperature for 12 h. The obtained silicate supernatant of 240g was then acidified by adding 11g of hydrochloric acid, 5.5g of sulfuric acid as well as 8.7g of nitric acid, respectively, with moderate stirring. The precursor mixture was mixed and nebulized by an ultrasonic atomizer and carried by a high pressure, clean and dry air flow. The reagent flow was then passed through a high-temperature tubular reactor with the temperature of 400 °C. The total flow rate in this study was fixed at 2000 cm³/min (25 °C, 1atm), which corresponded to a residence time of 4 seconds. After the heating process, the as-synthesized MSP samples were collected downstream of the reactor by a high-efficiency filter. Finally, they were recovered by washing and filtration with DI water followed by drying in an oven at 110 °C. The spray-dried samples from the waste silicate supernatant with the aid of sulfuric acid was denoted as MSS (H₂SO₄), while the sample from the waste silicate supernatant with the aid of nitric acid was named as MSS (HNO₃).

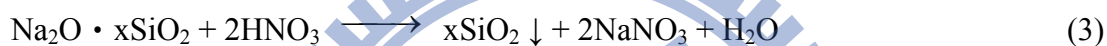
6.2.3 Results and discussion

Powder XRD patterns of the as-synthesized MSS samples prepared using sodium silicate precursor from optoelectronic waste powder with different acids through aerosol spray process are shown in [Figure 6.11](#). It was confirmed that the as-synthesized MSS(H₂SO₄) sample contains NaHSO₄ as the main component whereas NaNO₃ crystallites exists predominately in the as-synthesized MSS(HNO₃)

sample. Furthermore, spray-dried MSS(HCl) sample also includes crystalline materials, mainly sodium chlorides [143]. To elucidate the above findings, the general theory of silica polymerization must be addressed. In the preparation of silica precursors, two reactions took place simultaneously, i.e., condensation and sodium silicate acidification. The silica condensation process, which is the formation of a siloxane linkage between surface silanol groups, can be represented as [144]:



And the reaction of sodium silicate solution with hydrochloric acid during acidification process can be written as [148]:



When the sodium silicate precursor is added to different acid solutions, fine crystalline materials of NaHSO₄, NaNO₃ and NaCl are formed and embedded in the silica particles during aerosol spray process. Consequently, the co-existence of amorphous silica and sodium salt crystallites are observed in the as-synthesized MSS samples. After aqueous washing procedure, there is only one broad diffraction peak observed for all washed MSS materials, which is indicative of amorphous silica [105]. This implies that pure siliceous material can be obtained after the removal of salt template by aqueous washing process.

Figure 6.12 shows the N₂ adsorption-desorption isotherms for the washed MSS samples. All samples exhibit typical type IV isotherms with a well-defined capillary step, which are indicative of mesoporous materials. The MSS(HCl) sample shows the H3-type hysteresis loop attributed the interconnected mesoporous system with slit-like shapes [146]. In contract, the MSS(HNO₃) and MSS(H₂SO₄) show significant higher adsorption capacity. It is interesting to see that the sorption isotherms for the MSS(HNO₃) and MSS(H₂SO₄) samples have H1-like hysteresis loop, which are remarkable different from the MSS(HCl) sample. Besides, the hysteresis loop of MSS(H₂SO₄) tends to shift toward higher values of relative pressure as compared to

other samples, which implies that $\text{MSS}(\text{H}_2\text{SO}_4)$ exhibits larger pore diameter. This result is further confirmed by the BJH pore size distribution shown in [Figure 6.13](#). It is clear to see that the sequence of pore diameter is in the order of $\text{MSS}(\text{H}_2\text{SO}_4) > \text{MSS}(\text{HNO}_3) > \text{MSS}(\text{HCl})$. The physical properties such as BET specific surface area, total pore volume and BJH pore diameter of the spray-dried samples derived from N_2 adsorption-desorption measurements are summarized in [Table 6.4](#). Apparently, the washed $\text{MSS}(\text{HNO}_3)$ shows the highest surface area whereas the washed $\text{MSS}(\text{H}_2\text{SO}_4)$ sample exhibits the largest mesopores. These results are quite conclusive in demonstrating that the difference in the features of the pore geometry seems to be correlated to different occluded salt templates.

SEM images of the spray-dried MSS samples, as depicted in [Figure 6.14](#), show that there are spherical particles observed for the $\text{MSS}(\text{H}_2\text{SO}_4)$ and $\text{MSS}(\text{HNO}_3)$ samples. It is noted that the $\text{MSS}(\text{HCl})$ mainly consists of single crystal with hollow and fractured structures. TEM image in [Figure 6.14](#) proves that the washed $\text{MSS}(\text{H}_2\text{SO}_4)$ and $\text{MSS}(\text{HNO}_3)$ particles are porous, appears to consist of interconnected network. In contrast, the internal void insides $\text{MSS}(\text{HCl})$ seems to be strongly associated with NaCl crystals.

When the precursor solution is nebulized and heated, water would evaporate and result in an increased concentration of salt. As this process continues, salt would precipitate out of the droplet at the air interface, forming a crust. Therefore, it is expected that the nature of the embedded salts would strongly affect the structural properties of the spray-dried materials. In the present investigation, the main crystallites embedded in $\text{MSS}(\text{HCl})$ sample are NaCl, which has a high melting point of 800°C . The melting point of the NaNO_3 and NaHSO_4 is 308°C and 315°C , respectively. Since the melting points of NaNO_3 and NaHSO_4 were lower than the furnace temperature (400°C). When water evaporation occurs at temperatures near the melting point of the salts, the salt mixture becomes molten and serves as a solvent, diffusing back into the core in response to the concentration gradient. Thus, larger porous SiO_2 particles are produced as the product.

In contrary, the $\text{MSS}(\text{HCl})$ shows the crystal-like pore networks. This is probably due to that the preformed NaCl crystallites embedded in the $\text{MSS}(\text{HCl})$ samples. Since NaCl crystallites with melting point of 800°C are thermally stable in the spray-drying process, they could be easily solidified as the occluded templates. When

the salt templates were subsequently washed by aqueous process, the obtained MSS(HCl) shows the crystal-like pore networks. In addition, the formation of fractured particles with hollow structures in MSS(HCl) sample might be ascribed to the relatively lower slurry concentration of the starting precursors. Generally, hollow structure was formed at low slurry concentration because the time required to homogenize the droplet is longer than the solvent evaporation time during the quick-drying process of the droplets [134]. As the water evaporates rapidly, the solid shell formed in the beginning where the concentration is the highest and the internal pressure increases because the moisture cannot be released immediately, which would lead to the formation of fractured and hollow particles.

Figure 6.15 shows the time dependence of CO₂ uptake in the presence of 10% CO₂ at 60 °C for TEPA-functionalized MCM-41, SBA-15, MSS(H₂SO₄), MSS(HNO₃) as well as MSS(HCl) adsorbents. It can be found that the CO₂ uptake increased rapidly to more than 90% of the maximum uptake within the first five minutes of adsorption before reaching a constant equilibrium value for all adsorbents. The TEPA-MSS(H₂SO₄) exhibits the highest CO₂ adsorption capacity, which could achieve 125 mg-CO₂/g-adsorbent, followed by the TEPA-MSS(HNO₃) (122 mg-CO₂/g-adsorbent), TEPA-SBA-15 (117 mg-CO₂/g-adsorbent), TEPA-MCM-41 (113 mg-CO₂/g-adsorbent) and TEPA-MSS(HCl) (107 mg-CO₂/g-adsorbent). The sequence of the adsorption capacities of these sorbents is in agreement with the order of the pore volume and pore diameter of the supports. This observation is in line with the previous discussion in which pore volume of the support was found to play a vital role determining the adsorption performance.

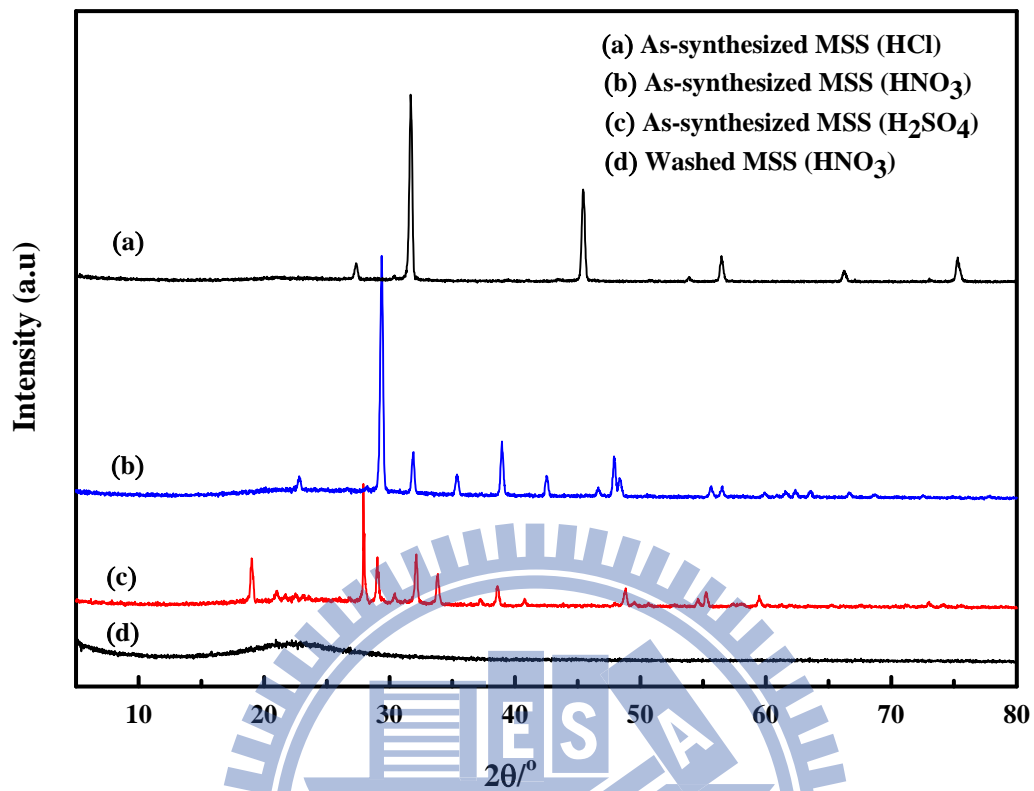


Figure 6.11 XRD patterns of the as-synthesized MSS samples.

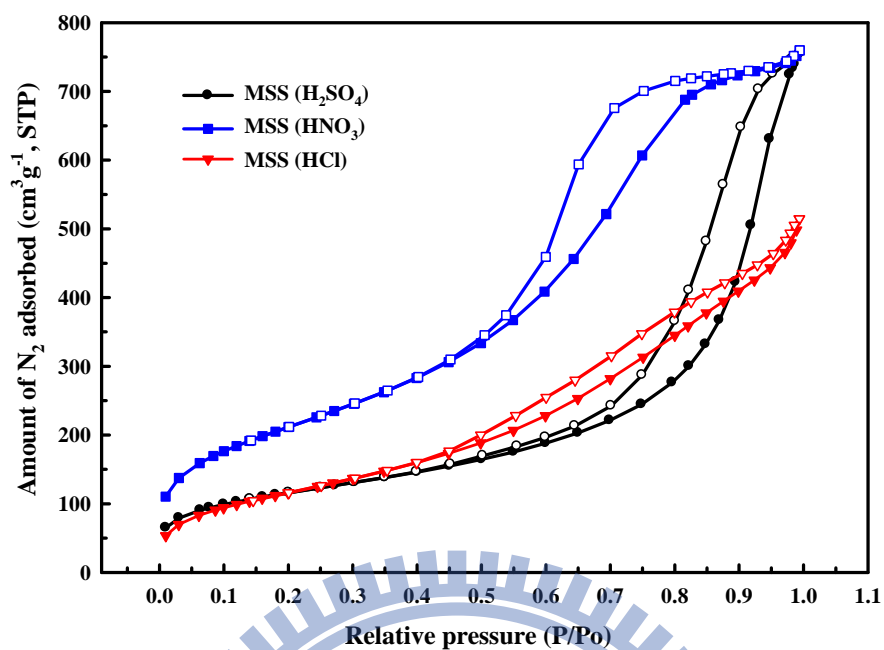


Figure 6.12 N₂ adsorption-desorption isotherms of the washed MSS samples.

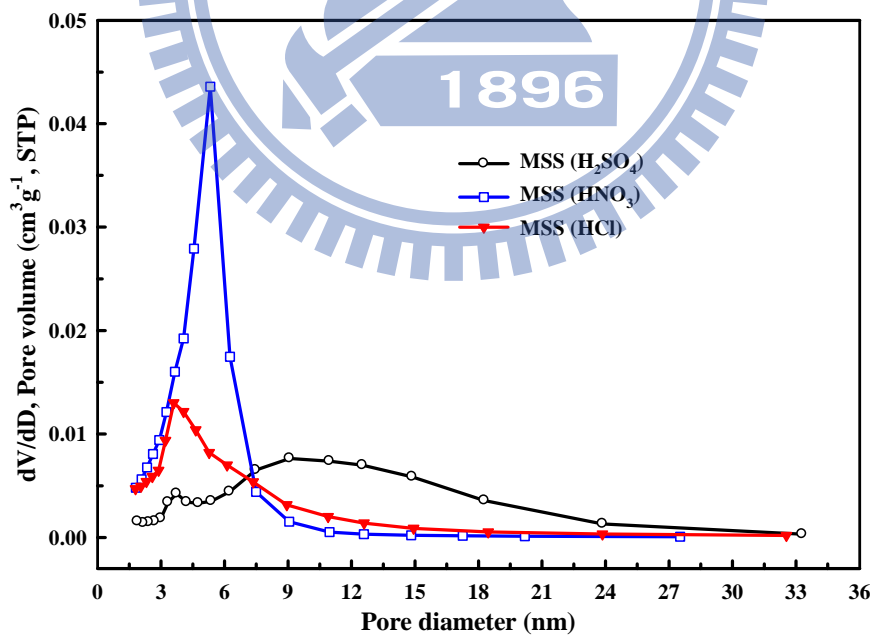


Figure 6.13 Pore size distribution of the washed MSS samples.

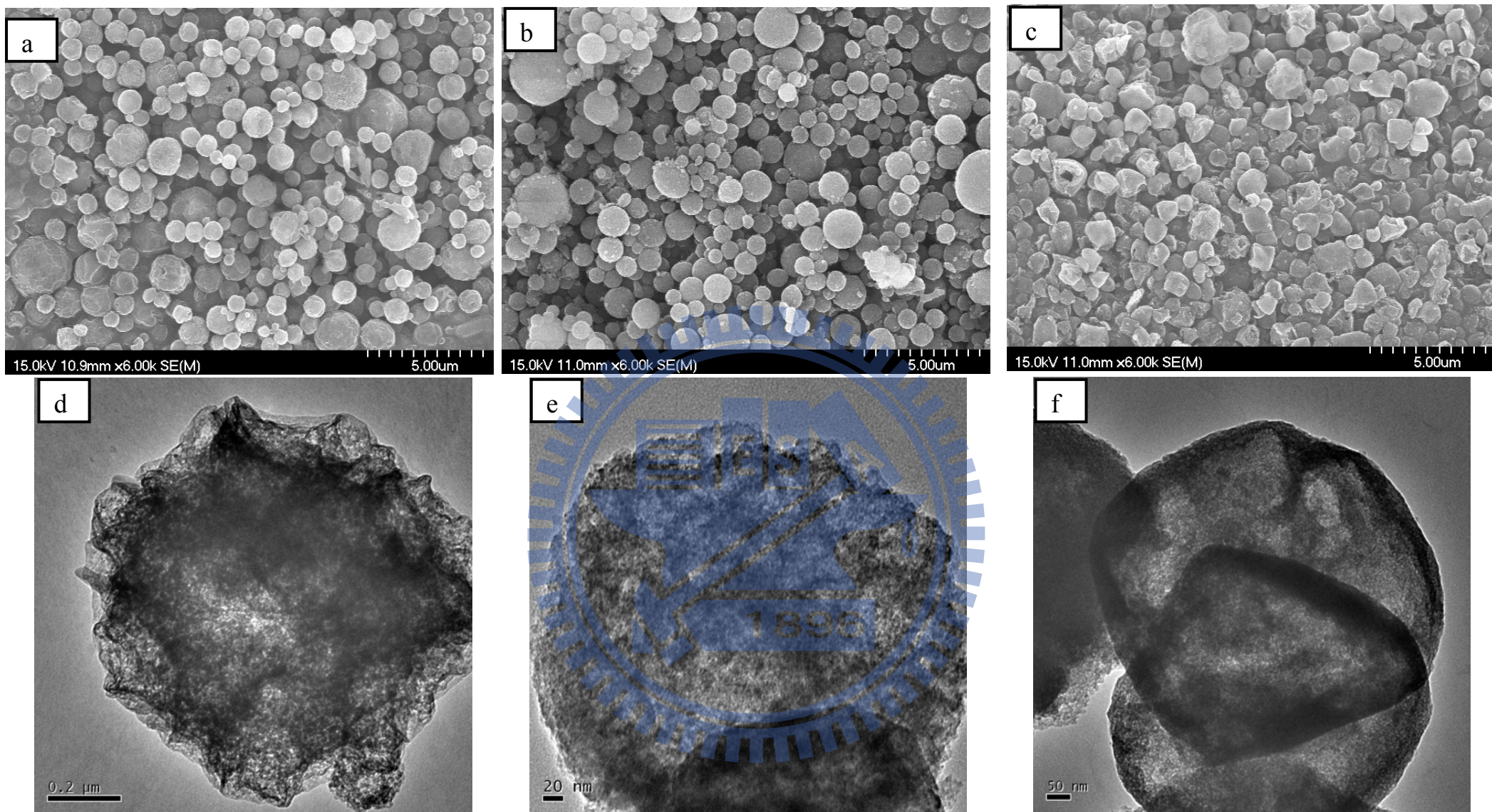


Figure 6.14 SEM images of the washed (a) MSS (H₂SO₄), (b) MSS (HNO₃) and MSS (HCl) samples; TEM images of the washed (d) MSS (H₂SO₄), (e) MSS (HNO₃) and (f) MSS (HCl) samples

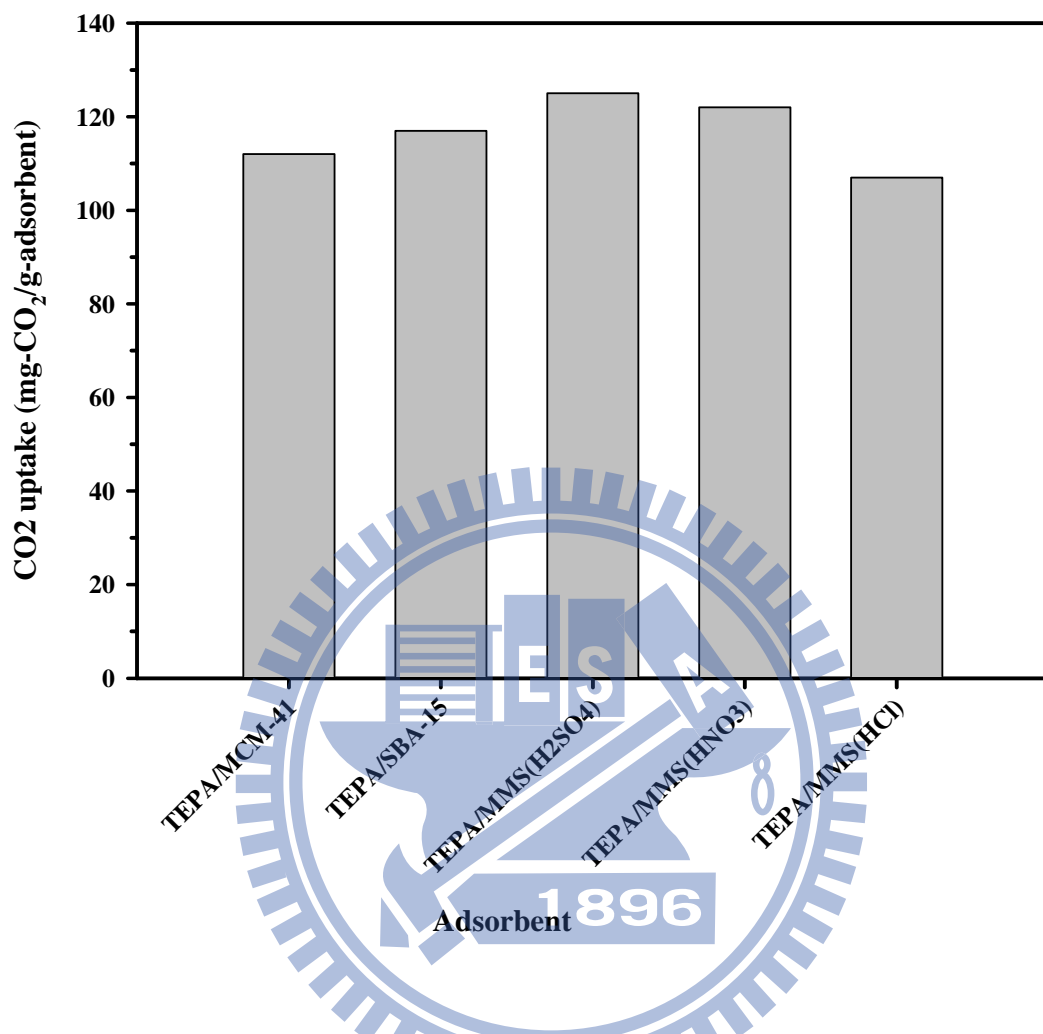
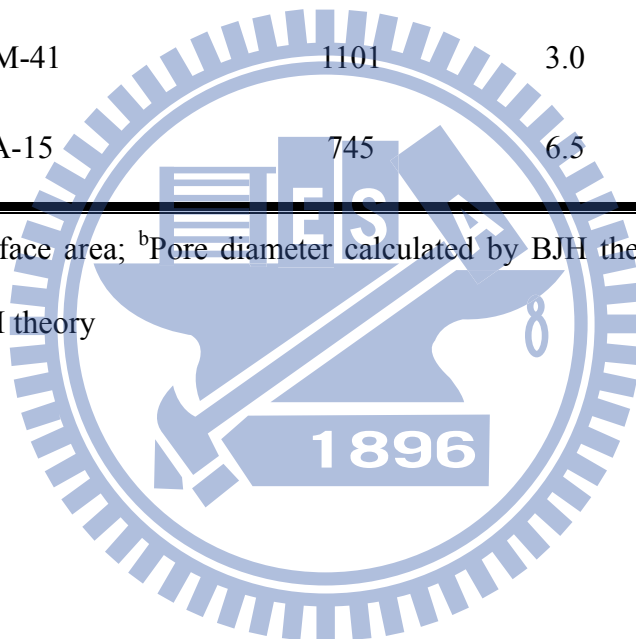


Figure 6.15 Comparison on CO₂ uptakes of TEPA loaded on MCM-41, SBA-15, MSS (H₂SO₄), MSS (HNO₃) and MSS (HCl) samples.

Table 6.3 Structural parameters of mesoporous and microporous adsorbents

Sample name	^a S _{BET} (m ² /g)	^b D _p (nm)	^c V _p (cm ³ /g)
Optoelectronic waste powder	30	-	0.07
MSS(H ₂ SO ₄)	419	10.2	1.21
MSS(HNO ₃)	776	4.9	1.17
MSS(HCl)	435	5.8	0.8
MCM-41	1101	3.0	0.99
SBA-15	745	6.5	1.10

NOTE: ^aBET surface area; ^bPore diameter calculated by BJH theory; ^cPore volume calculated by BJH theory



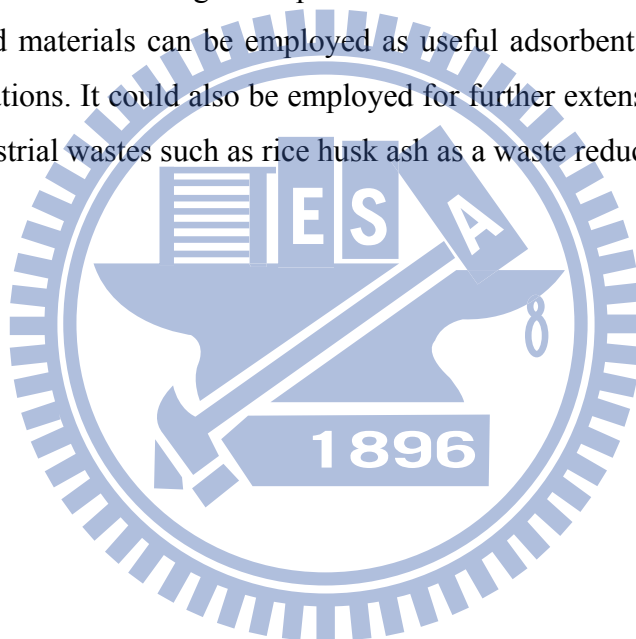
CHAPTER VII COMPARISON OF WASTE-BASED ADSORBENTS FOR THEIR CO₂ CAPTURE PERFORMANCE

Figure 7.1 to Figure 7.3 display the correlation coefficients (R^2) between the CO₂ adsorption capacities and the structural properties of the waste-derived mesoporous silica materials. It can be clear to observe that pore volume of the supports plays a vital role in the performance of CO₂ adsorption with the strongest linear correlation ($R^2 > 0.9$). The tests were performed for all materials of MCM-41(NaSi), MCM-41(AF), MCM-41(DU), MCM-41(DU)-F, SBA-15, MSP(AS), MSS(HNO₃), MSS(H₂SO₄) as well as MSS(HCl). It is possible that more efficient contact between the CO₂ gas and the impregnated TEPA could be achieved when a small space is still left inside the pores of the mesoporous silica after TEPA loading, leading to higher adsorption performance. The present study clearly demonstrates the relationships between the CO₂ adsorption performances and the mesoporous materials of either the same mesoporous substrate with different surface area, pore size as well as pore volume as supports or various substrates with different textural properties. This could be expected to provide better understandings inside the relationship between the CO₂ adsorption performances and the textural properties of supported substrates.

Table 7.1 lists the summary on the comparison of TEPA-related materials used for CO₂ adsorption in terms of their starting precursors, manufacture process as well as CO₂ adsorption performance. It is observed that under the same conditions, TEPA-MSS(HNO₃) adsorbent has an excellent adsorption performance at low CO₂ concentration with the lowest manufacturing costs as compared to other adsorbents. To date, research works on the preparation of mesoporous silica materials including MCM-41, SBA-15, KIT-6, HMS and silica monolith, etc are generally manufactured via conventional hydrothermal process, which require long and tedious batch process time of several days. A subsequent thermal process is also required to remove the organic surfactants from the silica/surfactant hybrids, which would further increase the manufacturing costs and energy penalty. Furthermore, it has been reported that conventional MCM-41 and SBA-15 materials with rod- or flake-shaped particles tend to have low bulk density, which would lead to higher pressure drop for obtaining the same mass adsorption capacity of adsorbent [110]. The use of spherical silica spheres either MSP(AS) or MSS materials with higher volume-based adsorption capacity as

supports of adsorbents can significantly reduce the adsorber volume of CO₂, and this has been another important issue that needs to be considered for field application.

Taking into account the potential scale involved in the production of porous silica for CO₂ capture, the manufacture of these materials using waste materials through an easy method would seem highly desirable. In this work, the recycled MSS(HNO₃) material shows several important advantages as compared to other materials in terms of cost, availability, low energy-consumed synthetic process and superior CO₂ adsorption capacity (122 mg/g-adsorbent). It can not only reduce the CO₂ greenhouse gas emission but also produce less waste after CO₂ adsorption since the adsorbent itself was made from the waste material. Therefore, this process will offer novel solutions not only to waste management problems but also to environmental problems since the recycled materials can be employed as useful adsorbent for environmental protection applications. It could also be employed for further extensible to other kinds of Si-related industrial wastes such as rice husk ash as a waste reduction strategy.



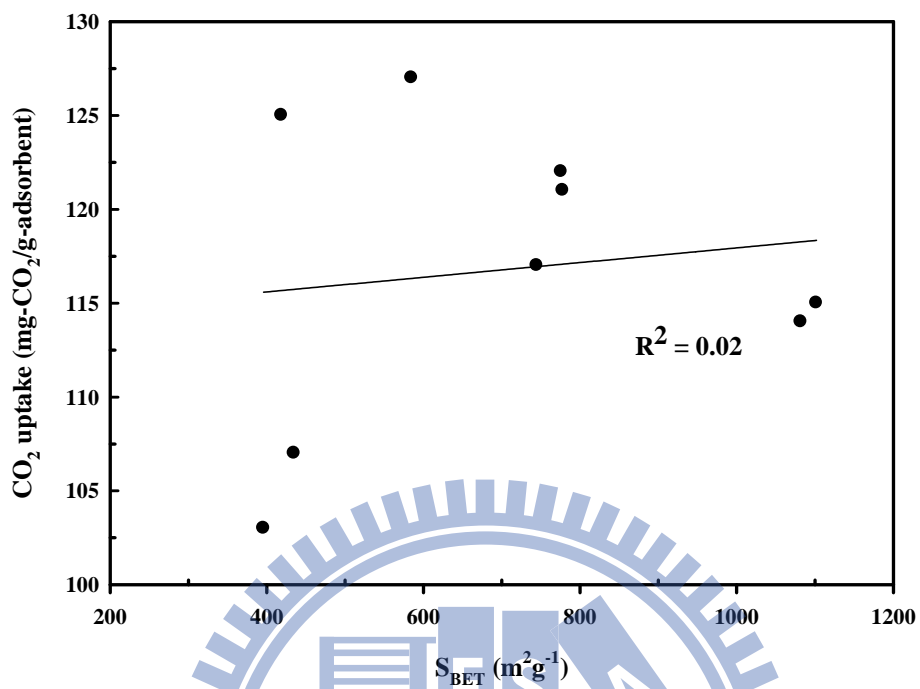


Figure 7.1 Correlation of the surface area of the mesoporous substrates and the CO_2 uptake.

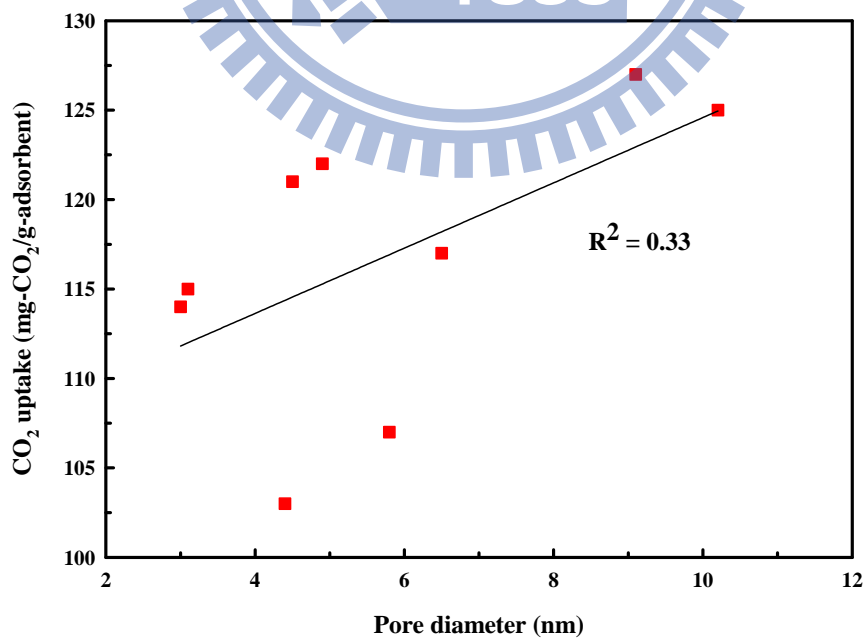


Figure 7.2 Correlation of the pore diameter of the mesoporous substrates and the CO_2 uptake.

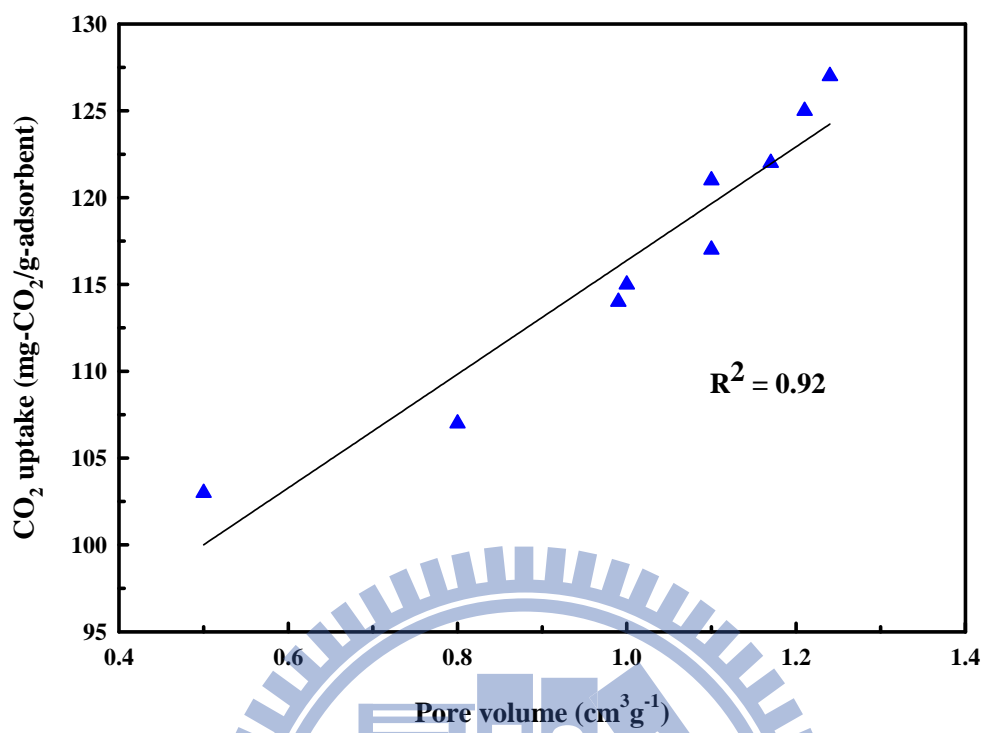


Figure 7.3 Correlation of total pore volume of the mesoporous substrates and the CO₂ uptake.

Table 7.1 TEPA-related adsorbents for CO₂ capture in this work.

Support	Precursor	Synthesis Process	Process time	^a S _{BET} (m ² /g)	Capacity (mg/g)	^d Manufacturing cost index
				^b d _{BJH} (nm)		
				^c V _p (cm ³ /g)		
MCM-41(NaSi)	Sodium silicate + CTAB	Batch process	36 h process + 6 h calcination	^a 1102 ^b 3.1 ^c 1.0	115	1.00
MCM-41(AF)	Waste powder + CTAB	Batch process	24h extraction + 36 h process + 6 h calcination	^a 1082 ^b 3.0 ^c 0.99	114	0.97
MCM-41(DU)-F	Waste powder + CTAB	Batch process	8 h process + 6 h calcination	^a 778 ^b 4.5 ^c 1.1	121	0.72
SBA-15	Sodium silicate + P123	Batch process	24 h process + 6 h calcination	^a 745 ^b 6.5 ^c 1.10	117	0.41

Support	Precursor	Synthesis Process	Process time	^a S _{BET} (m ² /g)	Capacity (mg/g)	^d Manufacturing cost index
				^b d _{BJH} (nm)		
				^c V _p (cm ³ /g)		
MS(0.0023)	Waste powder + F127	Batch process	1.5 h process + 6 h calcination	^a 716 ^b 14.2 ^c 1.75	-	0.28
MSP(AS)	Waste powder + (NH ₄) ₂ SO ₄	Continuous process	12 h extraction + 4 s process + washing	^a 585 ^b 9.1 ^c 1.24	127	0.3
MSS(HNO ₃)	Waste powder	Continuous process	12 h extraction + 4 s process + washing	^a 776 ^b 5.0 ^c 1.21	122	0.02

NOTE: ^aBET surface area; ^bPore diameter calculated by BJH theory; ^cPore volume calculated by BJH theory; ^dManufacturing cost index: The relative prices of chemicals were calculated based on the ratio of the purchase price of chemicals used for manufacturing the adsorbents to that for manufacturing the MCM-41. The treatment and disposal costs of the optoelectronic waste powder were not included, which should further reduce the manufacture costs of the mesoporous materials when using the waste powder as the precursor.

CHAPTER VIII CONCLUSIONS AND RECOMMENDATION

8.1 Conclusions

This study successfully explored the feasibility of utilization of optoelectronic industrial waste powder as the sustainable resource for the production of silica-based sorbents as supports of adsorbents for the removal of CO₂. Recycling of solid wastes from optoelectronic industry, which can improve cost effectiveness for the mass production of valuable mesoporous silica materials from cheap and abundant resources through convenient processes, is truly beneficial from the viewpoint of economical use of optoelectronic industrial waste powder.

The conclusions of this study are given below:

1. Optoelectronic industrial waste powder is mainly composed of 85% of (NH₄)₂SiF₆ and 15% of SiO₂ from the results of TGA, FTIR and SEM-EDS analyses and the total Si mass fraction (from (NH₄)₂SiF₆ and SiO₂) detected by ICP-MS analysis is 22.4%. Alkali extraction process was confirmed to effectively separate silicate supernatant and the sediment. The obtained sediment contains purified NaF (>90%), which provides further reuse possibility since NaF is widely applied in chemical industry. The waste supernatant is a valuable silicate source for synthesizing silica-based materials.
2. Optoelectronic industrial waste powder can be directly converted into mesoporous MCM-41 (DU)-F materials with hexagonal pore arrangement in the presence of hydrofluoric acid, CTAB and ammonium hydroxide at ambient temperature. Through similar pathway, silica materials with either cage-like or cellular foam-like mesophase can be prepared from the waste powder with the aid of triblock copolymer F127. Moreover, the structural properties of the recycled silica materials can be facilely controlled by altering the n_{F127}/n_{Si} and n_{HF}/n_{Si} ratios of the starting precursors.
3. Fast synthesis of ordered spherical mesoporous silica materials with hexagonal pore

arrangement using the inorganic silica source of sodium metasilicate ($\text{Na}_2\text{SiO}_3 \cdot 9\text{H}_2\text{O}$) via aerosol spray of evaporation induced self assembly method is demonstrated in the present study. Furthermore, it has been conducted the spray-dried mesoporous silica particles can be rapidly fabricated by using TFT-LCD waste powder derived silicate supernatant as the precursor. The addition of inorganic salts of $(\text{NH}_4)_2\text{SO}_4$ could further enlarge the mesopores of the materials.

4. The waste derived mesoporous silica materials including MCM-41(NaSi), MCM-41(AF), MCM-41(DU), MCM-41(DU)-F, SBA-15, MSP(AS), MSS(HNO_3), MSS(H_2SO_4) as well as MSS(HCl) were functionalized with amines and evaluated as CO_2 sorbents. It was demonstrated that pore volume of the supports plays a vital role in the performance of CO_2 adsorption with the strongest linear correlation ($R^2 > 0.90$).
5. Considering the potential of mass production of mesoporous silica supports for field application, the MSS material fabricated from waste products shows several important advantages in terms of low-cost synthetic process, fast production rate and high CO_2 adsorption capacity. It could be considered as a potential and competitive adsorbent for the CO_2 capture from flue gas.

8.2 Recommendation for future work

1. In the present study, although the fast synthesis of spherical mesoporous silica materials using the waste silicate supernatant via salt-templated aerosol spray method has been suggested, further works might be still necessary since the salt templates occluded insides the spray-dried particles significantly determine the pore geometry of the obtained materials. Therefore, the effects of the pH value of the starting precursors and the drying temperatures on the obtained mesoporous silica materials need to be addressed.

2. It would be interesting to utilize the recycled mesoporous silica materials such as MS and MSS materials which possess high specific surface area, large pore diameter and large pore volume, along with three-dimensional interconnected pore structure as the catalyst support. They might offer more accessible internal volume for better mass transfer for large molecules.



REFERENCES

- [1] J.D. Figueroa, T. Fout, S. Plasynski, H. McIlvried, R.D. Srivastava, Advances in CO₂ capture technology--The U.S. Department of Energy's Carbon Sequestration Program, *International Journal of Greenhouse Gas Control*. 2 (2008) 9–20.
- [2] D. Aaron, C. Tsouris, Separation of CO₂ from Flue Gas: A Review, *Separation Science and Technology*. 40 (2005) 321.
- [3] M.M. Abu-Khader, Recent Progress in CO₂ Capture/Sequestration: A Review, *Energy Sources, Part A: Recovery, Utilization, and Environmental Effects*. 28 (2006) 1261.
- [4] J.C. Chow, R. Berglund, P. Biswas, D. Eatough, P.K. Mueller, J.G. Watson, Separation and capture of CO₂ from large stationary sources and sequestration in geological formations, *J Air Waste Manag Assoc*. 53 (2003) 643–644.
- [5] S.-W. Hung, J.-M. Tsai, M.-J. Cheng, P.-C. Chen, Analysis of the development strategy of late-entrants in Taiwan and Korea's TFT-LCD industry, *Technology in Society*. 34 (2012) 9–22.
- [6] K.S. Hui, C.Y.H. Chao, Synthesis of MCM-41 from coal fly ash by a green approach: Influence of synthesis pH, *Journal of Hazardous Materials*. 137 (2006) 1135–1148.
- [7] M. Bhagiyalakshmi, L.J. Yun, R. Anuradha, H.T. Jang, Utilization of rice husk ash as silica source for the synthesis of mesoporous silicas and their application to CO₂ adsorption through TREN/TEPA grafting, *Journal of Hazardous Materials*. 175 (2010) 928–938.
- [8] C.L. Choi, M. Park, D.H. Lee, J.-E. Kim, B.-Y. Park, J. Choi, Salt-Thermal Zeolitization of Fly Ash, *Environmental Science & Technology*. 35 (2001) 2812–2816.
- [9] M. Bhagiyalakshmi, J.Y. Lee, H.T. Jang, Synthesis of mesoporous magnesium oxide: Its application to CO₂ chemisorption, *International Journal of Greenhouse Gas Control*. 4 (2010) 51–56.
- [10] D. Trong On, D. Desplandier-Giscard, C. Danumah, S. Kaliaguine,

- Perspectives in catalytic applications of mesostructured materials, *Applied Catalysis A: General*. 253 (2003) 545–602.
- [11] A. Taguchi, F. Schüth, Ordered mesoporous materials in catalysis, *Microporous and Mesoporous Materials*. 77 (2005) 1–45.
- [12] A. Sayari, Catalysis by Crystalline Mesoporous Molecular Sieves, *Chemistry of Materials*. 8 (1996) 1840–1852.
- [13] X.S. Zhao, G.Q. (Max) Lu, G.J. Millar, Advances in Mesoporous Molecular Sieve MCM-41, *Industrial & Engineering Chemistry Research*. 35 (1996) 2075–2090.
- [14] M. Vallet-Regi, A. Ramila, R.P. del Real, J. Perez-Pariente, A New Property of MCM-41: Drug Delivery System, *Chemistry of Materials*. 13 (2001) 308–311.
- [15] D. Zhao, J. Feng, Q. Huo, N. Melosh, G.H. Fredrickson, B.F. Chmelka, Triblock Copolymer Syntheses of Mesoporous Silica with Periodic 50 to 300 Angstrom Pores, *Science*. 279 (1998) 548–552.
- [16] J.-S. Lee, J.-H. Kim, J.-T. Kim, J.-K. Suh, J.-M. Lee, C.-H. Lee, Adsorption Equilibria of CO₂ on Zeolite 13X and Zeolite X/Activated Carbon Composite, *Journal of Chemical & Engineering Data*. 47 (2002) 1237–1242.
- [17] D.M. Ruthven, B.K. Kaul, Adsorption of aromatic hydrocarbons in NaX zeolite. 2. Kinetics, *Industrial & Engineering Chemistry Research*. 32 (1993) 2053–2057.
- [18] P.J.E. Harlick, F.H. Tezel, Adsorption of carbon dioxide, methane, and nitrogen: pure and binary mixture adsorption by ZSM-5 with SiO₂/Al₂O₃ ratio of 30, *Separation Science and Technology*. 37 (2002) 33.
- [19] M.P. Mokhonoana, N.J. Coville, Synthesis of [Si]-MCM-41 from TEOS and water glass: the water glass-enhanced condensation of TEOS under alkaline conditions, *J Sol-Gel Sci Technol*. 54 (2010) 83–92.
- [20] L. Wang, Y. Shao, J. Zhang, M. Anpo, Improvement of the hydrothermal stability of MCM-48 mesoporous molecular sieves, *Res Chem Intermed*. 34 (2008) 267–286.

- [21] E.M. Johansson, M.A. Ballem, J.M. Córdoba, M. Odén, Rapid Synthesis of SBA-15 Rods with Variable Lengths, Widths, and Tunable Large Pores, *Langmuir*. 27 (2011) 4994–4999.
- [22] T.-W. Kim, R. Ryoo, K.P. Gierszal, M. Jaroniec, L.A. Solovyov, Y. Sakamoto, Characterization of mesoporous carbons synthesized with SBA-16 silica template, *J. Mater. Chem.* 15 (2005) 1560.
- [23] C. Chen, W.-J. Son, K.-S. You, J.-W. Ahn, W.-S. Ahn, Carbon dioxide capture using amine-impregnated HMS having textural mesoporosity, *Chemical Engineering Journal*. 161 (2010) 46–52.
- [24] Y. Liu, T.J. Pinnavaia, Assembly of Hydrothermally Stable Aluminosilicate Foams and Large-Pore Hexagonal Mesostructures from Zeolite Seeds under Strongly Acidic Conditions, *Chemistry of Materials*. 14 (2002) 3–5.
- [25] W.W. Lukens, P. Yang, G.D. Stucky, Synthesis of Mesocellular Silica Foams with Tunable Window and Cell Dimensions, *Chem. Mater.* 13 (2001) 28–34.
- [26] C. Yu, B. Tian, J. Fan, G.D. Stucky, D. Zhao, Synthesis of Siliceous Hollow Spheres with Ultra Large Mesopore Wall Structures by Reverse Emulsion Templating, *Chemistry Letters*. 31 (2002) 62–63.
- [27] Y. Liu, J. Shi, J. Chen, Q. Ye, H. Pan, Z. Shao, Dynamic performance of CO₂ adsorption with tetraethylenepentamine-loaded KIT-6, *Microporous and Mesoporous Materials*. 134 (2010) 16–21.
- [28] Y. Liu, Q. Ye, M. Shen, J. Shi, J. Chen, H. Pan, Carbon Dioxide Capture by Functionalized Solid Amine Sorbents with Simulated Flue Gas Conditions, *Environ. Sci. Technol.* 45 (2011) 5710–5716.
- [29] C.T. Kresge, M.E. Leonowicz, W.J. Roth, J.C. Vartuli, J.S. Beck, Ordered mesoporous molecular sieves synthesized by a liquid-crystal template mechanism, *Nature*. 359 (1992) 710–712.
- [30] C.-T. Hung, H. Bai, Adsorption behaviors of organic vapors using mesoporous silica particles made by evaporation induced self-assembly method, *Chemical Engineering Science*. 63 (2008) 1997–2005.
- [31] M. Karthik, L.-Y. Lin, H. Bai, Bifunctional mesoporous Cu–Al–MCM-41 materials for the simultaneous catalytic abatement of NO_x and VOCs,

- Microporous and Mesoporous Materials. 117 (2009) 153–160.
- [32] C. Hung, H. Bai, M. Karthik, Ordered mesoporous silica particles and Si-MCM-41 for the adsorption of acetone: A comparative study, *Separation and Purification Technology*. 64 (2009) 265–272.
- [33] M. Kruk, M. Jaroniec, A. Sayari, A Unified Interpretation of High-Temperature Pore Size Expansion Processes in MCM-41 Mesoporous Silicas, *The Journal of Physical Chemistry B*. 103 (1999) 4590–4598.
- [34] A. Sayari, M. Kruk, M. Jaroniec, I.L. Moudrakovski, New Approaches to Pore Size Engineering of Mesoporous Silicates, *Adv. Mater.* 10 (1998) 1376–1379.
- [35] V. Meynen, P. Cool, E.F. Vansant, Verified syntheses of mesoporous materials, *Microporous and Mesoporous Materials*. 125 (2009) 170–223.
- [36] H. Jin, Q. Wu, C. Chen, D. Zhang, W. Pang, Facile synthesis of crystal like shape mesoporous silica SBA-16, *Microporous and Mesoporous Materials*. 97 (2006) 141–144.
- [37] Z. Jin, X. Wang, X. Cui, A two-step route to synthesis of small-pored and thick-walled SBA-16-type mesoporous silica under mildly acidic conditions, *Journal of Colloid and Interface Science*. 307 (2007) 158–165.
- [38] J. Wei, J. Shi, H. Pan, Q. Su, J. Zhu, Y. Shi, Thermal and hydrothermal stability of amino-functionalized SBA-16 and promotion of hydrophobicity by silylation, *Microporous and Mesoporous Materials*. 117 (2009) 596–602.
- [39] C. Lin, Synthesis of SBA-16 and SBA-15 mesoporous silica crystals templated with neutral block copolymer surfactants, *Journal of Physics and Chemistry of Solids*. 69 (2008) 415–419.
- [40] S.-Y. Chen, S. Cheng, Acid-Free Synthesis of Mesoporous Silica Using Triblock Copolymer as Template with the Aid of Salt and Alcohol, *Chemistry of Materials*. 19 (2007) 3041–3051.
- [41] P. Van Der Voort, M. Benjelloun, E.F. Vansant, Rationalization of the Synthesis of SBA-16: Controlling the Micro- and Mesoporosity, *The Journal of Physical Chemistry B*. 106 (2002) 9027–9032.
- [42] S.-E. Park, J.-S. Chang, Y.K. Hwang, D.S. Kim, S.H. Jung, J.S. Hwang,

Supramolecular Interactions and Morphology Control in Microwave Synthesis of Nanoporous Materials, *Catalysis Surveys from Asia*. 8 (2004) 91–110.

- [43] Z. Jin, X. Wang, X. Cui, Synthesis and morphological investigation of ordered SBA-15-type mesoporous silica with an amphiphilic triblock copolymer template under various conditions, *Colloids and Surfaces A: Physicochemical and Engineering Aspects*. 316 (2008) 27–36.
- [44] J.R. Matos, L.P. Mercuri, M. Kruk, M. Jaroniec, Toward the Synthesis of Extra-Large-Pore MCM-41 Analogues, *Chemistry of Materials*. 13 (2001) 1726–1731.
- [45] Y. Sakamoto, M. Kaneda, O. Terasaki, D.Y. Zhao, J.M. Kim, G. Stucky, Direct imaging of the pores and cages of three-dimensional mesoporous materials, *Nature*. 408 (2000) 449–453.
- [46] J.S. Lettow, Y.J. Han, P. Schmidt-Winkel, P. Yang, D. Zhao, G.D. Stucky, Hexagonal to Mesocellular Foam Phase Transition in Polymer-Templated Mesoporous Silicas, *Langmuir*. 16 (2000) 8291–8295.
- [47] P. Schmidt-Winkel, Lukens, P. Yang, D.I. Margolese, J.S. Lettow, J.Y. Ying, Microemulsion Templating of Siliceous Mesostructured Cellular Foams with Well-Defined Ultralarge Mesopores, *Chem. Mater*. 12 (2000) 686–696.
- [48] P. Schmidt-Winkel, Lukens, D. Zhao, P. Yang, B.F. Chmelka, G.D. Stucky, Mesocellular Siliceous Foams with Uniformly Sized Cells and Windows, *Journal of the American Chemical Society*. 121 (1999) 254–255.
- [49] X.-Y. Yang, A. Léonard, A. Lemaire, G. Tian, B.-L. Su, Self-formation phenomenon to hierarchically structured porous materials: design, synthesis, formation mechanism and applications, *Chem. Commun.* 47 (2011) 2763–2786.
- [50] Z.-Y. Yuan, B.-L. Su, Insights into hierarchically meso–macroporous structured materials, *J. Mater. Chem.* 16 (2005) 663–677.
- [51] D.M. D'Alessandro, B. Smit, J.R. Long, Carbon Dioxide Capture: Prospects for New Materials, *Angewandte Chemie International Edition*. 49 (2010) 6058–6082.
- [52] A. Sayari, Y. Belmabkhout, R. Serna-Guerrero, Flue gas treatment via CO₂

- adsorption, *Chemical Engineering Journal*. 171 (2011) 760–774.
- [53] A.C. Yeh, H. Bai, Comparison of ammonia and monoethanolamine solvents to reduce CO₂ greenhouse gas emissions, *Science of The Total Environment*. 228 (1999) 121–133.
- [54] H. Bai, A.C. Yeh, Removal of CO₂ Greenhouse Gas by Ammonia Scrubbing, *Ind. Eng. Chem. Res.* 36 (1997) 2490–2493.
- [55] J.C. Fisher, J. Tanthana, S.S.C. Chuang, Oxide-supported tetraethylenepentamine for CO₂ capture, *Environmental Progress & Sustainable Energy*. 28 (2009) 589–598.
- [56] F. Su, C. Lu, W. Chen, H. Bai, J.F. Hwang, Capture of CO₂ from flue gas via multiwalled carbon nanotubes, *Science of The Total Environment*. 407 (2009) 3017–3023.
- [57] F. Su, C. Lu, S.-C. Kuo, W. Zeng, Adsorption of CO₂ on Amine-Functionalized Y-Type Zeolites, *Energy & Fuels*. 24 (2010) 1441–1448.
- [58] P.D. Jadhav, R.V. Chatti, R.B. Biniwale, N.K. Labhsetwar, S. Devotta, S.S. Rayalu, Monoethanol Amine Modified Zeolite 13X for CO₂ Adsorption at Different Temperatures, *Energy & Fuels*. 21 (2007) 3555–3559.
- [59] R.V. Siriwardane, M.-S. Shen, E.P. Fisher, J.A. Poston, Adsorption of CO₂ on Molecular Sieves and Activated Carbon, *Energy & Fuels*. 15 (2001) 279–284.
- [60] R. Chatti, A.K. Bansiwale, J.A. Thote, V. Kumar, P. Jadhav, S.K. Lokhande, Amine loaded zeolites for carbon dioxide capture: Amine loading and adsorption studies, *Microporous and Mesoporous Materials*. 121 (2009) 84–89.
- [61] M.B. Yue, Y. Chun, Y. Cao, X. Dong, J.H. Zhu, CO₂ Capture by As-Prepared SBA-15 with an Occluded Organic Template, *Advanced Functional Materials*. 16 (2006) 1717–1722.
- [62] M.B. Yue, L.B. Sun, Y. Cao, Y. Wang, Z.J. Wang, J.H. Zhu, Efficient CO₂ Capturer Derived from As-Synthesized MCM-41 Modified with Amine, *Chemistry - A European Journal*. 14 (2008) 3442–3451.
- [63] M.B. Yue, L.B. Sun, Y. Cao, Z.J. Wang, Y. Wang, Q. Yu, Promoting the CO₂

- adsorption in the amine-containing SBA-15 by hydroxyl group, *Microporous and Mesoporous Materials*. 114 (2008) 74–81.
- [64] G. Qi, Y. Wang, L. Estevez, X. Duan, N. Anako, A.-H.A. Park, High efficiency nanocomposite sorbents for CO₂ capture based on amine-functionalized mesoporous capsules, *Energy Environ. Sci.* 4 (2011) 444.
- [65] F. Zheng, D.N. Tran, B.J. Busche, G.E. Fryxell, R.S. Addleman, T.S. Zemanian, Ethylenediamine-Modified SBA-15 as Regenerable CO₂ Sorbent, *Industrial & Engineering Chemistry Research*. 44 (2005) 3099–3105.
- [66] W.-J. Son, J.-S. Choi, W.-S. Ahn, Adsorptive removal of carbon dioxide using polyethyleneimine-loaded mesoporous silica materials, *Microporous and Mesoporous Materials*. 113 (2008) 31–40.
- [67] P.J.E. Harlick, A. Sayari, Applications of Pore-Expanded Mesoporous Silicas. 3. Triamine Silane Grafting for Enhanced CO₂ Adsorption, *Industrial & Engineering Chemistry Research*. 45 (2006) 3248–3255.
- [68] R. Sanz, G. Calleja, A. Arencibia, E.S. Sanz-Pérez, CO₂ adsorption on branched polyethyleneimine-impregnated mesoporous silica SBA-15, *Applied Surface Science*. 256 (2010) 5323–5328.
- [69] X. Xu, C. Song, J.M. Andresen, B.G. Miller, A.W. Scaroni, Novel Polyethylenimine-Modified Mesoporous Molecular Sieve of MCM-41 Type as High-Capacity Adsorbent for CO₂ Capture, *Energy Fuels*. 16 (2002) 1463–1469.
- [70] X. Xu, C. Song, J.M. Andrésen, B.G. Miller, A.W. Scaroni, Preparation and characterization of novel CO₂ “molecular basket” adsorbents based on polymer-modified mesoporous molecular sieve MCM-41, *Microporous and Mesoporous Materials*. 62 (2003) 29–45.
- [71] M. Bhagiyalakshmi, L.J. Yun, R. Anuradha, H.T. Jang, Synthesis of chloropropylamine grafted mesoporous MCM-41, MCM-48 and SBA-15 from rice husk ash: their application to CO₂ chemisorption, *J Porous Mater.* 17 (2009) 475–484.
- [72] M. Bhagiyalakshmi, S.D. Park, W.S. Cha, H.T. Jang, Development of TREN dendrimers over mesoporous SBA-15 for CO₂ adsorption, *Applied Surface*

- Science. 256 (2010) 6660–6666.
- [73] J. Wei, J. Shi, H. Pan, W. Zhao, Q. Ye, Y. Shi, Adsorption of carbon dioxide on organically functionalized SBA-16, *Microporous and Mesoporous Materials*. 116 (2008) 394–399.
- [74] H.Y. Huang, R.T. Yang, D. Chinn, C.L. Munson, Amine-Grafted MCM-48 and Silica Xerogel as Superior Sorbents for Acidic Gas Removal from Natural Gas, *Ind. Eng. Chem. Res.* 42 (2002) 2427–2433.
- [75] C. Chen, S.-T. Yang, W.-S. Ahn, R. Ryoo, Amine-impregnated silica monolith with a hierarchical pore structure: enhancement of CO₂ capture capacity, *Chemical Communications*. (2009) 3627.
- [76] X. Yan, L. Zhang, Y. Zhang, K. Qiao, Z. Yan, S. Komarneni, Amine-modified mesocellular silica foams for CO₂ capture, *Chemical Engineering Journal*. 168 (2011) 918–924.
- [77] D.M. D'Alessandro, B. Smit, J.R. Long, Carbon Dioxide Capture: Prospects for New Materials, *Angewandte Chemie International Edition*. 49 (2010) 6058–6082.
- [78] H.T. Jang, Y. Park, Y.S. Ko, J.Y. Lee, B. Margandan, Highly siliceous MCM-48 from rice husk ash for CO₂ adsorption, *International Journal of Greenhouse Gas Control*. 3 (2009) 545–549.
- [79] R.S. Franchi, P.J.E. Harlick, A. Sayari, Applications of Pore-Expanded Mesoporous Silica. 2. Development of a High-Capacity, Water-Tolerant Adsorbent for CO₂, *Industrial & Engineering Chemistry Research*. 44 (2005) 8007–8013.
- [80] X. Yan, L. Zhang, Y. Zhang, G. Yang, Z. Yan, Amine-Modified SBA-15: Effect of Pore Structure on the Performance for CO₂ Capture, *Ind. Eng. Chem. Res.* 50 (2011) 3220–3226.
- [81] X. Wang, H. Li, H. Liu, X. Hou, AS-synthesized mesoporous silica MSU-1 modified with tetraethylenepentamine for CO₂ adsorption, *Microporous and Mesoporous Materials*. 142 (2011) 564–569.
- [82] D.J.N. Subagyono, Z. Liang, G.P. Knowles, A.L. Chaffee, Amine modified mesocellular siliceous foam (MCF) as a sorbent for CO₂, *Chemical Engineering*

- Research and Design. 89 (2011) 1647–1657.
- [83] G. Qi, L. Fu, B.H. Choi, E.P. Giannelis, Efficient CO₂ sorbents based on silica foam with ultra-large mesopores, *Energy & Environmental Science*. (2012).
- [84] X. Xu, C. Song, B.G. Miller, A.W. Scaroni, Adsorption separation of carbon dioxide from flue gas of natural gas-fired boiler by a novel nanoporous “molecular basket” adsorbent, *Fuel Processing Technology*. 86 (2005) 1457–1472.
- [85] V. Zelenák, M. Badanicová, D. Halamová, J. Cejka, A. Zukal, N. Murafa, et al., Amine-modified ordered mesoporous silica: Effect of pore size on carbon dioxide capture, *Chemical Engineering Journal*. 144 (2008) 336–342.
- [86] W.-J. Son, J.-S. Choi, W.-S. Ahn, Adsorptive removal of carbon dioxide using polyethyleneimine-loaded mesoporous silica materials, *Microporous and Mesoporous Materials*. 113 (2008) 31–40.
- [87] R. Franchi, P.J.E. Harlick, A. Sayari, A high capacity, water tolerant adsorbent for CO₂: diethanolamine supported on pore-expanded MCM-41, in: *Nanoporous Materials IV Proceedings of the 4th International Symposium on Nanoporous Materials*, Elsevier, 2005: pp. 879–886.
- [88] P.J.E. Harlick, A. Sayari, Applications of Pore-Expanded Mesoporous Silicas. 3. Triamine Silane Grafting for Enhanced CO₂ Adsorption, *Ind. Eng. Chem. Res.* 45 (2006) 3248–3255.
- [89] V. Zelenák, M. Badanicová, D. Halamová, J. Cejka, A. Zukal, N. Murafa, et al., Amine-modified ordered mesoporous silica: Effect of pore size on carbon dioxide capture, *Chemical Engineering Journal*. 144 (2008) 336–342.
- [90] J. Matos, M. Rosales, A. García, C. Nieto-Delgado, J.R. Rangel-Mendez, Hybrid photoactive materials from municipal sewage sludge for the photocatalytic degradation of methylene blue, *Green Chem.* (2011).
- [91] H. Misran, R. Singh, S. Begum, M.A. Yarmo, Processing of mesoporous silica materials (MCM-41) from coal fly ash, *Journal of Materials Processing Technology*. 186 (2007) 8–13.
- [92] Y. Kuwahara, T. Ohmichi, T. Kamegawa, K. Mori, H. Yamashita, A novel conversion process for waste slag: synthesis of a hydrotalcite-like compound

- and zeolite from blast furnace slag and evaluation of adsorption capacities, *J. Mater. Chem.* 20 (2010) 5052–5062.
- [93] C.-T. Hsiao, P.-L. Chang, C.-W. Chen, H.-H. Huang, A systems view for the high-tech industry development: a case study of large-area TFT-LCD industry in Taiwan, *Asian Journal of Technology Innovation*. 19 (2011) 117–132.
- [94] I. Majchrzak-Kuceba, W. Nowak, Development of Fly Ash-Based Sorbent to Capture CO₂ from Flue Gas, in: G. Yue, H. Zhang, C. Zhao, Z. Luo (Eds.), *Proceedings of the 20th International Conference on Fluidized Bed Combustion*, Springer Berlin Heidelberg, 2010: pp. 596–602.
- [95] G. Chandrasekar, W. Son, W. Ahn, Synthesis of mesoporous materials SBA-15 and CMK-3 from fly ash and their application for CO₂ adsorption, *Journal of Porous Materials*. 16 (2009) 545–551.
- [96] J.-E. Park, H.-K. Youn, S.-T. Yang, W.-S. Ahn, CO₂ capture and MWCNTs synthesis using mesoporous silica and zeolite 13X collectively prepared from bottom ash, *Catalysis Today*. (n.d.).
- [97] C. Chen, K.-S. You, J.-W. Ahn, W.-S. Ahn, Synthesis of mesoporous silica from bottom ash and its application for CO₂ sorption, *Korean Journal of Chemical Engineering*. 27 (2010) 1010–1014.
- [98] M. Bhagiyalakshmi, L.J. Yun, R. Anuradha, H.T. Jang, Utilization of rice husk ash as silica source for the synthesis of mesoporous silicas and their application to CO₂ adsorption through TREN/TEPA grafting, *Journal of Hazardous Materials*. 175 (2010) 928–938.
- [99] H.-L. Chang, C.-M. Chun, I.A. Aksay, W.-H. Shih, Conversion of Fly Ash into Mesoporous Aluminosilicate, *Industrial & Engineering Chemistry Research*. 38 (1999) 973–977.
- [100] M. Saadoun, B. Bessaïs, N. Mliki, M. Ferid, H. Ezzaouia, R. Bennaceur, Formation of luminescent (NH₄)₂SiF₆ phase from vapour etching-based porous silicon, *Applied Surface Science*. 210 (2003) 240–248.
- [101] C. Lu, H. Bai, B. Wu, F. Su, J.F. Hwang, Comparative Study of CO₂ Capture by Carbon Nanotubes, Activated Carbons, and Zeolites, *Energy Fuel*. 22 (2008) 3050–3056.

- [102] H.S. Yu, K.-I. Rhee, C.K. Lee, D.-H. Yang, Two-step ammoniation of by-product fluosilicic acid to produce high quality amorphous silica, *Korean J. Chem. Eng.* 17 (2000) 401–408.
- [103] E.I. Mel'nichenko, G.F. Krysenko, $(\text{NH}_4)_2\text{SiF}_6$ evaporation in the presence of SiO_2 , *Russ. J. Inorg. Chem.* 51 (2006) 27–31.
- [104] T. Cardinal, O. Efimov, H. Francois-Saint-Cyr, L. Glebov, L. Glebova, V. Smirnov, Comparative study of photo-induced variations of X-ray diffraction and refractive index in photo-thermo-refractive glass, *Journal of Non-crystalline Solids.* 325 (2003) 275–281.
- [105] P.B. Sarawade, J.-K. Kim, A. Hilonga, H.T. Kim, Recovery of high surface area mesoporous silica from waste hexafluorosilicic acid (H_2SiF_6) of fertilizer industry, *Journal of Hazardous Materials.* 173 (2010) 576–580.
- [106] L. Wang, A. Lu, C. Wang, X. Zheng, D. Zhao, R. Liu, Nano-fibriform production of silica from natural chrysotile, *J. Colloid Interface Sci.* 295 (2006) 436–439.
- [107] K. Liu, Q. Feng, Y. Yang, G. Zhang, L. Ou, Y. Lu, Preparation and characterization of amorphous silica nanowires from natural chrysotile, *J. Non-Cryst. Solids.* 353 (2007) 1534–1539.
- [108] H.-L. Chang, C.-M. Chun, I.A. Aksay, W.-H. Shih, Conversion of Fly Ash into Mesoporous Aluminosilicate, *Industrial & Engineering Chemistry Research.* 38 (1999) 973–977.
- [109] L.-Y. Lin, H. Bai, Continuous generation of mesoporous silica particles via the use of sodium metasilicate precursor and their potential for CO_2 capture, *Microporous and Mesoporous Materials.* 136 (2010) 25–32.
- [110] C. Hung, H. Bai, M. Karthik, Ordered mesoporous silica particles and Si-MCM-41 for the adsorption of acetone: A comparative study, *Sep Purif Technol.* 64 (2009) 265–272.
- [111] M. Karthik, L.-Y. Lin, H. Bai, Bifunctional mesoporous Cu-Al-MCM-41 materials for the simultaneous catalytic abatement of NO_x and VOCs, *Microporous Mesoporous Mater.* 117 (2009) 153–160.
- [112] N. Baccile, D. Grosso, C. Sanchez, Aerosol generated mesoporous silica

- particles, *J. Mater. Chem.* 13 (2003) 3011–3016.
- [113] M.T. Bore, S.B. Rathod, T.L. Ward, A.K. Datye, Hexagonal Mesostructure in Powders Produced by Evaporation-Induced Self-Assembly of Aerosols from Aqueous Tetraethoxysilane Solutions, *Langmuir*. 19 (2003) 256–264.
- [114] G. Chandrasekar, K.-S. You, J.-W. Ahn, W.-S. Ahn, Synthesis of hexagonal and cubic mesoporous silica using power plant bottom ash, *Microporous and Mesoporous Materials*. 111 (2008) 455–462.
- [115] L.-Y. Lin, J.-T. Kuo, H. Bai, Silica materials recovered from photonic industrial waste powder: Its extraction, modification, characterization and application, *Journal of Hazardous Materials*. 192 (2011) 255–262.
- [116] S.-Y. Chen, S. Cheng, Acid-Free Synthesis of Mesoporous Silica Using Triblock Copolymer as Template with the Aid of Salt and Alcohol, *Chemistry of Materials*. 19 (2007) 3041–3051.
- [117] S. Jun, J.M. Kim, R. Ryoo, Y.-S. Ahn, M.-H. Han, Hydrothermal stability of MCM-48 improved by post-synthesis restructuring in salt solution, *Microporous and Mesoporous Materials*. 41 (2000) 119–127.
- [118] L. Wang, Y. Shao, J. Zhang, M. Anpo, Cooperative effect of crystallization temperature and NaF addition in the formation process and hydrothermal stability of MCM-48 mesoporous molecular sieve, *Microporous and Mesoporous Materials*. 100 (2007) 241–249.
- [119] J. Lee, J. Kim, J. Kim, H. Jia, M.I. Kim, J.H. Kwak, et al., Simple Synthesis of Hierarchically Ordered Mesocellular Mesoporous Silica Materials Hosting Crosslinked Enzyme Aggregates, *Small*. 1 (2005) 744–753.
- [120] P. Zhang, Z. Wu, N. Xiao, L. Ren, X. Meng, C. Wang, et al., Ordered Cubic Mesoporous Silicas with Large Pore Sizes Synthesized via High-Temperature Route, *Langmuir*. 25 (2009) 13169–13175.
- [121] M. Choi, W. Heo, F. Kleitz, R. Ryoo, Facile synthesis of high quality mesoporous SBA-15 with enhanced control of the porous network connectivity and wall thickness, *Chemical Communications*. (2003) 1340.
- [122] L. Wang, J. Zhang, F. Chen, M. Anpo, Fluoride-Induced Reduction of CTAB Template Amount for the Formation of MCM-48 Mesoporous Molecular Sieve,

- J. Phys. Chem. C. 111 (2007) 13648–13651.
- [123] Y. Hsu, Y. Chang, C. Yang, Swelling-Agent-Free Synthesis of Siliceous and Functional Mesocellular Foam-Like Mesophases by Using a Carboxy-Terminated Triblock Copolymer, *Advanced Functional Materials*. 18 (2008) 1799–1808.
- [124] S. An, J. Joo, J. Lee, Ultra-low-cost route to mesocellular siliceous foam from steel slag and mesocellular carbon foam as catalyst support in fuel cell, *Microporous and Mesoporous Materials*.
- [125] D. Zhao, Q. Huo, J. Feng, B. Chmelka, G. Stucky, Nonionic Triblock and Star Diblock Copolymer and Oligomeric Surfactant Syntheses of Highly Ordered, Hydrothermally Stable, Mesoporous Silica Structures, *J. Am. Chem. Soc.* 120 (1998) 6036, 6024.
- [126] C.T. Kresge, M.E. Leonowicz, W.J. Roth, J.C. Vartuli, J.S. Beck, Ordered mesoporous molecular sieves synthesized by a liquid-crystal template mechanism, *Nature*. 359 (1992) 710–712.
- [127] X. Xu, C. Song, J.M. Andrésen, B.G. Miller, A.W. Scaroni, Preparation and characterization of novel CO₂ “molecular basket” adsorbents based on polymer-modified mesoporous molecular sieve MCM-41, *Microporous Mesoporous Mater.* 62 (2003) 29–45.
- [128] K. Kosuge, T. Sato, N. Kikukawa, M. Takemori, Morphological Control of Rod- and Fiberlike SBA-15 Type Mesoporous Silica Using Water-Soluble Sodium Silicate, *Chem. Mater.* 16 (2004) 899–905.
- [129] X. Pang, F. Tang, Morphological control of mesoporous materials using inexpensive silica sources, *Microporous Mesoporous Mater.* 85 (2005) 1–6.
- [130] C.-T. Hung, H. Bai, Adsorption behaviors of organic vapors using mesoporous silica particles made by evaporation induced self-assembly method, *Chem. Eng. Sci.* 63 (2008) 1997–2005.
- [131] P.T. Tanev, T.J. Pinnavaia, Mesoporous Silica Molecular Sieves Prepared by Ionic and Neutral Surfactant Templating: A Comparison of Physical Properties, *Chem. Mater.* 8 (1996) 2068–2079.

- [132] M.D. Donohue, G.L. Aranovich, Adsorption Hysteresis in Porous Solids, *J. Colloid Interface Sci.* 205 (1998) 121–130.
- [133] P.J. Bruinsma, A.Y. Kim, J. Liu, S. Baskaran, Mesoporous Silica Synthesized by Solvent Evaporation: Spun Fibers and Spray-Dried Hollow Spheres, *Chem. Mater.* 9 (1997) 2507–2512.
- [134] A.-J. Wang, Y.-P. Lu, R.-X. Sun, Recent progress on the fabrication of hollow microspheres, *Mater. Sci. Eng., A.* 460-461 (2007) 1–6.
- [135] R.I. Nooney, D. Thirunavukkarasu, Y. Chen, R. Josephs, A.E. Ostafin, Self-Assembly of Mesoporous Nanoscale Silica/Gold Composites, *Langmuir.* 19 (2003) 7628–7637.
- [136] C. Boissiere, D. Grosso, A. Chaumonot, L. Nicole, C. Sanchez, Aerosol Route to Functional Nanostructured Inorganic and Hybrid Porous Materials, *Advanced Materials.* 23 (2011) 599–623.
- [137] J.H. Bang, K.S. Suslick, Applications of Ultrasound to the Synthesis of Nanostructured Materials, *Advanced Materials.* 22 (2010) 1039–1059.
- [138] S.H. Kim, B.Y.H. Liu, M.R. Zachariah, Ultrahigh Surface Area Nanoporous Silica Particles via an Aero-Sol-Gel Process, *Langmuir.* 20 (2004) 2523–2526.
- [139] T. Kimura, K. Kato, Y. Yamauchi, Temperature-controlled and aerosol-assisted synthesis of aluminium organophosphonate spherical particles with uniform mesopores, *Chemical Communications.* (2009) 4938.
- [140] Y. Lu, H. Fan, A. Stump, T.L. Ward, T. Rieker, C.J. Brinker, Aerosol-assisted self-assembly of mesostructured spherical nanoparticles, *Nature.* 398 (1999) 223–226.
- [141] Y. Lu, H. Fan, N. Doke, D.A. Loy, R.A. Assink, D.A. LaVan, et al., Evaporation-Induced Self-Assembly of Hybrid Bridged Silsesquioxane Film and Particulate Mesophases with Integral Organic Functionality, *J. Am. Chem. Soc.* 122 (2000) 5258–5261.
- [142] C. Urata, Y. Yamauchi, Y. Aoyama, J. Imasu, S. Todoroki, Y. Sakka, et al., Fabrication of Hierarchically Porous Spherical Particles by Assembling Mesoporous Silica Nanoparticles via Spray Drying, *Journal of Nanoscience and Nanotechnology.* 8 (2008) 3101–3105.

- [143] S.H. Kim, B.Y.H. Liu, M.R. Zachariah, Synthesis of Nanoporous Metal Oxide Particles by a New Inorganic Matrix Spray Pyrolysis Method, *Chemistry of Materials*. 14 (2002) 2889–2899.
- [144] C. Jo, K. Kim, R. Ryoo, Syntheses of high quality KIT-6 and SBA-15 mesoporous silicas using low-cost water glass, through rapid quenching of silicate structure in acidic solution, *Microporous and Mesoporous Materials*. 124 (2009) 45–51.
- [145] R. Kiyoura, K. Urano, Mechanism, Kinetics, and Equilibrium of Thermal Decomposition of Ammonium Sulfate, *Ind. Eng. Chem. Proc. Des. Dev.* 9 (1970) 489–494.
- [146] L.-Y. Lin, H. Bai, Continuous generation of mesoporous silica particles via the use of sodium metasilicate precursor and their potential for CO₂ capture, *Microporous and Mesoporous Materials*. 136 (2010) 25–32.
- [147] S.H. Kim, B.Y.H. Liu, M.R. Zachariah, Ultrahigh Surface Area Nanoporous Silica Particles via an Aero-Sol-Gel Process, *Langmuir*. 20 (2004) 2523–2526.
- [148] H. Isobe, S. Utsumi, K. Yamamoto, H. Kanoh, K. Kaneko, Micropore to Macropore Structure-Designed Silicas with Regulated Condensation of Silicic Acid Nanoparticles, *Langmuir*. 21 (2005) 8042–8047.

APPENDIX

林亮毅 (Liang-Yi Lin)

(一) 主要學歷

2008/9-迄今 國立交通大學環境工程研究所博士生

2006/9-2008/6 國立交通大學環境工程研究所碩士

2002/9-2006/6 國立中央大學土木工程學系學士

(二) 榮譽

民國九十九年財團法人中興工程科技研究發展基金會獎助學金 (2010.7~2011.7)

(三) 著作:

A. SCI, EI 或具審查制度之國內外期刊

1. Karthik, M., Lin, L-Y., and Bai, H., (2009) “Bifunctional mesoporous Cu-Al-MCM-41 materials for simultaneous catalytic abatement of NO_x and VOCs”, *Microporous and Mesoporous Materials*, 117, p153-160. (SCI 2010 IF=3.220, Chem., App., 5/70; Mater. Sci., Multi. 37/225; Chem. Phys. 38/127, EI)
2. Jan, Y-H., Lin, L-Y., Karthik, M., and Bai, H., (2009) “Titanium dioxide/zeolite catalytic adsorbent for the simultaneous removals of NO and acetone vapors”, *J. Air & Waste Management Association*, 59, p1186-1193. (SCI 2010 IF=1.567, Eng., Env: 20/45; Env. Sci. 96/193, EI)
3. Lin, L-Y., Chen, C. C., and Bai, H., (2010) “Synthesis of adsorbents and catalysts via aerosol route and their applications for air pollution control”, *Japanese J. Aerosol Research*, 25(2), 121-133 (invited paper)
4. Lin, L-Y., and Bai, H. (2010) “Continuous generation of mesoporous silica particles via the use of sodium metasilicate precursor and their potential for CO₂ capture”, *Microporous and Mesoporous Materials*, 136, p25-32. (SCI 2010

- IF=3.220, Chem., App., 5/70; Mater. Sci., Multi. 37/225; Chem. Phys. 38/127, EI)
5. **Lin, L-Y.**, Kuo, J-T., and Bai, H., (2011) “Silica materials recovered from photonic industrial waste powder: Its extraction, modification, characterization and application”, *Journal of Hazardous Materials*, 192, p255-262. (SCI 2010 IF=3.723, Civil Eng., 2/115; Env.Sci., 18/193; Env. Eng., 6/45)
 6. **Lin, L-Y.**, and Bai, H. (2012) “Aerosol processing of low-cost mesoporous silica spherical particles from photonic industrial waste powder for CO₂ capture”, *Chemical Engineering Journal*. (Accepted, SCI 2010 IF=3.074; Chem. Eng.: 10/135; Env. Eng.: 8/45)
 7. **Lin, L-Y.**, and Bai, H. (2012) “An efficient method for recycling silica materials from waste powder of photonic industry”, *Environmental Science & Technology*. (1st revision, under review)
 8. **Lin, L-Y.**, Lin, C-W., and Bai, H. (2012) “Pore structure effect on the CO₂ capture using mesoporous silica adsorbents”, *Adsorption*. (to be submitted)
 9. **Lin, L-Y.**, and Bai, H. (2012) “Facile synthesis of siliceous foam-like materials with hierarchically mesocellular structure from industrial waste of display industry”, (Manuscript in preparation)
 10. **Lin, L-Y.**, and Bai, H. (2012) “Surfactant-free synthesis of mesoporous silica spheres from photonic industrial waste powder by spray pyrolysis method”, (Manuscript in preparation)
 11. **Lin, L-Y.**, and Bai, H. (2012) “Amine-modified as-synthesized mesocellular silica foam: Effect of surfactant concentration on the CO₂ capture”, (Manuscript in preparation)
 12. 白曠綾、陳祈緯、**林亮毅** (2010) “以可見光觸媒/中孔洞沸石複合材料同時處理 VOCs 與 NO_x 之可行性研究”, *工程科技通訊*, 106 期, p.66。
 13. **林亮毅**、白曠綾 (2010) “光電 TFT-LCD 廠廢棄物減量與資源化製成奈米孔洞材料”, *工業污染防治*, 115 期, p.145。
 14. **林亮毅**、白曠綾 (2012) “光電廢棄物粉末資源化製造技術”, *工業雜誌*, 350 期, p.150。

B: 研討會論文

國際研討會

1. Lin, L-Y. and Bai, H., (2012) “Aerosol synthesis of mesoporous silica particles from photonic industrial waste powder for CO₂ capture”, ZMPC 2012 International Symposium on Zeolites and Microporous Crystals, Hiroshima, Japan. (*presenter*)
2. Wan Ting Zeng, Liang-Yi Lin, Hsunling Bai., (2012) “Synthesis of mesoporous silica from rice husk ash for CO₂ capture”, ZMPC 2012 International Symposium on Zeolites and Microporous Crystals, Hiroshima, Japan.
3. Hsunling Bai, Chongwei Lin and Liang-Yi Lin., (2012) “Pore Structure Effect on the CO₂ Capture Using Mesoporous Silica Adsorbents”, The 6th Pacific Basin Conference on Adsorption Science and Technology, Taipei, Taiwan.
4. Lin, L-Y. and Bai, H., (2011) “A green approach for recovery of mesoporous silicas from photonic industrial waste powder for CO₂ capture”, IUMRS-ICA 2011, 12th International Conference in Asia, Nangang, Taipei, Taiwan. (*presenter*)
5. Lin, L-Y. and Bai, H., (2011) “CO₂ capture using a mesoporous silica adsorbent synthesized from photonic industrial waste powder”, 104th Air & Waste Management Association, Paper NO. 405, Orlando, Florida, USA (EI). (*presenter*)
6. Chia-Chi Li, Lin, L-Y., and Bai, H., (2011) “Recovery of photonic waste powder for the production of nano-porous silica material”, 104th Air & Waste Management Association, Paper NO. 406, Orlando, Florida, USA (EI). (*presenter*)
7. Lin, L-Y. and Bai, H., (2010) “CO₂ capture by amine-functionalized silica-based microporous and mesoporous materials”, 103th Air & Waste Management Association, Paper NO. 626, Calgary, Alberta, CANADA (EI). (*presenter*)
8. Karthik, M., Lin, L-Y., and Bai, H., (2008) “Using Waste Organic Solvent Vapors as the Reducing Agent of deNO_x Process”, 101th Air & Waste Management Association, Paper NO. 413, Portland, Oregon, USA (EI). (*presenter*)

國內研討會

1. Zeng, W-T., Lin, L-Y., Bai, H., (2012) “Preparation and characterization of mesoporous silica materials from rice husk ash for CO₂ capture”, 9th Environmental Protection and Nanotechnology. National Kaohsiung University. Kaohsiung.
2. Li, C-C., Lin, L-Y., Bai, H., (2011) “Recovery of photonic waste powder for the production of nano-porous silica material and the application of CO₂ capture”, 8th Environmental Protection and Nanotechnology. National Chung Hsing University. Taichung.
3. 林崇璋、林亮毅、白曠綾 (2011) “運用擴張劑合成不同孔洞大小之中孔洞吸附材料及其應用於二氧化碳捕獲之研究”，第八屆環境保護與奈米科技學術研討會論文集，國立中興大學。
4. Lin, L-Y., Bai, H. (2010) “Synthesis of mesoporous silica particles from sodium metasilicate precursor by aerosol method and their potential for CO₂ capture”, 17th International Conference on Aerosol Science and Technology. Taiwan University.
5. 郭建廷、林亮毅、白曠綾 (2010) “光電廢棄物資源化製成奈米材料”，第七屆環境保護與奈米科技學術研討會論文集，國立台灣大學。
6. Lin, L-Y., Bai, H., and Hung, C., (2009) “Synthesis of silica particles from inorganic precursor by aerosol method”, 16th International Conference on Aerosol Science and Technology. Chaoyang University of Technology.
7. 林亮毅、白曠綾 (2008) “V-Ti-MCM-41分子篩光觸媒同時處理VOC_S及NO_X之研究”，第五屆環境保護與奈米科技學術研討會論文集，國立中央大學。
8. 林亮毅、白曠綾 (2007) “Ti-MCM-41分子篩光觸媒同時處理VOC_S及NO_X之研究”，中華民國環境工程學會,空氣污染控制技術研討會,高雄大學。
9. Karthik, M., Lin, L-Y., and Bai, H., (2007) “Mesoporous Cu-MCM-41 and Cu-Al-MCM-41 Catalysts for the Simultaneous Abatement of NO_x and VOCs in Exhaust Gas Stream”, 4th Environmental Protection and Nanotechnology.

National Chung Hsing University. Taichung.

10. Hung, C., Bai, H., Karthik, M., Lin, L., (2007) “Comparison of mesoporous silica particles and MCM-41 as adsorbents for acetone removal”, 4th Environmental Protection and Nanotechnology. National Chung Hsing University. Taichung.

